HOFMEISTER SERIES AT THE LIQUID/LIQUID INTERFACE

by

XIANG GAO

A Dissertation submitted to the

Graduate School-New Brunswick

Rutgers, The State University of New Jersey

in partial fulfillment of the requirements

for the degree of

Doctor of Philosophy

Graduate Program in Chemistry and Chemical Biology

written under the direction of

Laurence S. Romsted

and approved by

_____

_____

_____

_____

New Brunswick, New Jersey

October, 2016

ABSTRACT OF THE DISSERTATION

HOFMEISTER SERIES AT THE LIQUID/LIQUID INTERFACE

by

XIANG GAO

Dissertation Director:

Laurence S. Romsted

This thesis is a study of the Hofmeister Series, or specific ion effects, at 3 interfaces: a zwitterionic emulsion interface, a gemini surfactant micelle interface and a neat tetradecane/water interface. The goal of this research is to provide new information such as local pH changes and local counterions concentrations to the specific ion effects research at liquid/liquid interfaces, which might help unveil the origin of specific ion effects.

This research utilized a unique chemical probe to study how different ions affect the physical chemical properties of the 3 interfaces. The probe molecule is a long chain amphiphilic arenediazonium ion. In micellar solutions, emulsions and oil/water mixture, the probe associates at the hydrophilic/hydrophobic interfacial region like other amphiphilic molecules do, and then reacts with water molecules and weak nucleophiles to produce corresponding organic products. The yields of products are analyzed by HPLC and used to calculate the interfacial concentrations of ions and water molecules. Using this method we can study the behavior of various ions and molecules at the interfacial region. The background of this method is introduced in Chapter 1.

Chapter 2 describes the specific ion effects on the interfacial pH of an emulsion prepared by a zwitterionic surfactant. The headgroup of SB3-14 has different affinities to different anions and cations, which changes ions density at the interfacial region and accordingly alters interface electronic property as well as the interfacial pH. The interfacial pH change was monitored through measuring the reaction rate between a long chain arenediazonium ion and *t*-butylhydroquinone.

Chapter 3 is a study of specific counterion effects on gemini surfactants (10-2-10 2X) physical properties such as cmc, aggregation number and interfacial counterion molarity. The ions affect micellar solutions properties in the order of Hofmeister Series. By combining physical characterization means and chemical trapping experiments, the correlation between bulky properties and interfacial properties were observed.

Chapter 4 describes the adsorption of different anions onto a neat alkane/water interface. The chemical trapping method was used to probe anions interfacial concentrations at tetradecane/water interface, which were proved to be higher than their

bulk concentrations, especially for hydrophobic ions I^-, SCN^-. Ions adsorption at the interface is supported by other types of experimental and simulation approaches in the literature.

DEDICATION

To my wonderful parents, Enli Gao and Shaozhen Chen, and to my love, Shangda Guo, for their endless love and support.

ACKNOWLEDGEMENTS

First and for most, I would like to thank my advisor Professor Larry S. Romsted for giving me the opportunity to join his group. I thank him for the guidance and mentorship, and the inspiration that he shared with me during my graduate career. It has been my great pleasure to work with and learn from him.

I would like to thank all my colleagues in the Romsted research group, especially Dr. Qing Gu, Yongliang Zhang, Dr. Changyao Liu, Dr. Gunaseelan Kanniguna, Dr. Tarek Awad, Dr. Aijaz Ahmad for their generous help and friendship. I really enjoyed working in this friendly environment.

I would like to thank Dr. Reiko Oda, Dr. Michel Laguerre, Dr. Dario Bassani at Institut Europ éen de Chimie et Biologie in Bordeaux, France for their instruction. I would also like to thank other collaborators such as Dr. Jiaji Cheng, Dr. Anne Cheng, Dr. Alla Mallinenko, Dr. Massimiliano Porrini, Dr. Sylvain Nlate.

I would like to thank my committee members, Prof. Ralf Warmuth, Prof. John Taylor and Prof. Qingrong Huang for their time, attention, and helpful discussions about my research. I would like to thank Prof Leslie Jimenez for her help during my IFRP and OFRP.

And last but not least, I would like to thank my girlfriend Shangda Guo, as well as my parents for their endless support and encouragement through the years of my graduate work and all my life.

TABLE OF CONTENTS

LIST OF FIGURES

LIST OF TABLES

Chapter 1 General Introduction

The chapter introduced the historical background of Hofmeister Series with special focus on liquid/liquid interfaces such as water/emulsion interface, water/micelle interface and neat water/oil interface. Surfactants are widely used interface active agents, and their properties are closely related to this research. Their fundamental properties will be introduced as well. The chemical trapping method is a powerful technique for probing the interfacial molarity of weak nucleophiles and water molecules in micellar solutions, emulsions and oil/water mixtures. The fundamentals of this method and the related pseudophase model will be introduced.

1.1 HOFMEISTER SERIES

1.1.1 Introduction

Specific ion effects were first reported by Franz Hofmeister in the 19th century when he studied the influence of different ions on protein solubility (salting-out and salting-in effects).[1] Since then the fact that different ions have different effects on systems properties has been discovered in many other research areas such as protein folding[2], micelles formation (1st cmc, sphere-to-rod transition, aggregation number, etc.)[3] and interface properties.[4, 5, 6, 7] To honor Dr. Hofmeister's exploratory contribution to this area, the order of ions that affects the egg white protein solubility discovered in his experiment was named as Hofmeister Series. Over the following one hundred years specific ion effects were found in other systems and they were amazingly similar to (but not necessarily the same as) the

original Hofmeister Series, so the term Hofmeister Series has become a general term to represent the ions order in specific ion effects phenomena in various systems.

Based on thousands of research papers on various systems, people have a widely accepted order of this anions Hofmeister Series when the cation stays unchanged:

$$F^- \approx SO_4^{2-} > HPO_4^{2-} > \text{acetate} > Cl^- > NO_3^- > Br^- > ClO_3^- > I^- > ClO_4^- > SCN^-$$

If the anion stays unchanged, the order of cations is:

$$Na^+ > K^+ > Li^+ > Ca^{2+} > Mg^{2+} > Fe^{2+} > Zn^{2+} > Cs^+ > Al^{3+} > NH_4^+ > H^+$$

The ions on the left side tend to decrease the solubility of egg white proteins, while those on the right side increase the solubility. Studies on Hofmeister Series dealt with anions more often than cations because in most of cases anions have stronger effects on the system.

The phenomena of specific ion effects are abundant in many systems. In aqueous salt solutions, specific ions affect viscosity, refractive index, activity coefficient, freezing and boiling point, etc.[8, 9, 10] In biological systems, many phenomena are ion specific, such as buffer salts effects,[11] proteins adsorption[12] and enzymes functions.[13, 14] In colloidal systems different ions can change the bubble coalescence,[15] microemulsion formation,[16] bilayer dispersion[17] and micelle morphology.[18] Overview of these topics can be found in some recent books.[19, 20]

The fundamental mechanisms which generate similar specific ions order in different phenomena of various systems have attracted people's attention since Dr. Hofmeister made his first discovery. People believed that the ions order in the Hofmeister Series is originated from some certain types of gradual changes in multiple intrinsic properties of those ions (for example, electron distribution, dipole orientation, polarity or other properties),

however, a complete molecular explanation for the Hofmeister Series is still lacking. Explaining the fundamentals of the universal Hofmeister Series in different systems is difficult. The difficulty is that classical theories were built on qualitative concepts such as hydration and hydrophobicity, and it is hard to use them to predict phenomena in new systems from known cases because the theoretical explanations based on these empirical conclusions are usually vague. Even though, it is still necessary to know about the evolution of related theories. Here are several examples of existing theories that are used to explain the Hofmeister Series order at different levels:

In *hydration theory*, people think water molecules are attracted and aligned surrounding the ions and target molecules (proteins, surfactants, etc., which are usually more hydrophobic than ions), forming a hydration shell. Since ions have greater capability to attract water molecules than target molecules, they compete with target molecules for water molecules.[21, 22] The hydration of target molecules is weakened and as a result the target molecules may precipitate or become unstable in solution. In this case the hydration number of ions is an important indicator of their hydration capabilities because usually the hydration number is proportional to the affinity between the ions and water molecules. The major limit of this model is the assumption that all types of ions compete hydration water molecules with target molecules. This assumption can not explain the fact that some ions have salting-in effect.[23]

Water dipole theory is a supplementary theory to *hydration theory*, focusing on the dipoles orientations of water molecules surrounding the surface of target molecules as well as ions. The theory states that when an ion or a target molecule is hydrated, the surrounding water molecules will be oriented by ion's or target molecule's electrostatic fields.[24, 25]

Negative charge attracts the hydrogen atoms of water molecules orientating to the ion or target molecule, while positive charge attracts the oxygen atoms of water molecules. Therefore those water molecules surrounding ions might have the same orientation as the water molecules surrounding target molecules, or the opposite orientations. When the orientations of ion's hydration water molecules align with that of target molecule's surrounding water molecules, the hydration of target molecules is strengthened. If the orientations of the two types of water molecules are opposite, then the hydration of target molecules is weakened. As a result the solubility and stability of target molecules are influenced. This theory remedies the disadvantage of *hydration theories* that the theory fails in explaining the salt-in phenomena. The limit of this theory is that in reality, interactions between molecules are many-body interactions, so the orientations of water molecules dipoles is not necessarily aligning to the hydrated ions.[4] Meanwhile the charge and hydrophobic interactions between ions and target molecules are ignored. Fundamentally this theory oversimplifies the system.

In addition, there are many other theories[4] but all of them only consider one or two factors involved in molecular interactions, and the descriptions in these theories are qualitative. However, specific interactions depend upon a number of factors including electrostatic interaction, hydration, hydrophobic interaction, polarizability, hydrogen bonding, π-ion interactions, van der Waals forces and steric interactions, which is way more complicated than the noted theories above can handle. Part of these factors can be quantified or partially quantified, and some other theories are built on the advantages of these quantitative approaches.

Van der Waals forces are an important part of molecular interactions in specific ion effects and have been researched extensively. The strength of the forces can be calculated by different empirical equations. The related theories are based on a fundamental molecular interaction: dipole-dipole interaction.[26] The van der Waals forces include 3 basic types of dipole-dipole interactions: orientation (Keesom force), induction (Debye force) and dispersion (London force). Orientation and induction interactions are derived from permanent and induced dipoles respectively, and dispersion interactions are from instantaneous dipoles. These interactions are closely related to polarizabilities and ionization potentials, which also contribute to specific interactions.[27, 28]

DLVO theory was developed to unite van der Waals forces and the electrostatic interactions by modeling the balance between repulsive electrostatic interactions and attractive van der Waals interactions between colloid particles[29] and has been used to explain the specific ion effects in colloidal systems. However, it does not fully explain the effects because ions are simplified to point charges which cannot consider the special properties of different ions such as size, polarizability, hydration properties, etc. As a result, different salts containing ions with the same number of charges behave in the same way according to the equation, which is definitely not true.[19]

Because no theory is currently available to explain and predict specific ions interactions based on previous noted properties, people have attempted to correlate specific ion effects with some difficult-to-quantify physical chemical parameters such as hydrophobicity,[30] waters affinity,[31] polarizability, ion radius,[32] partial molar volume [33] and viscosity coefficients,[34] etc. Water affinity is one of the most famous theories within them.

Collins introduced *law of matching water affinities* based on the fact that the interaction between two ions of similar sizes is usually stronger than that between two ions of different sizes.[35] In the theory, the capability of two oppositely charged ions to form ion pair is related to the difference of their hydration Gibbs free energy.[31] Ions with high hydration Gibbs free energy are called "kosmotropic"(k) and those with low hydration Gibbs free energy are called "chaotropic"(c). Kosmotropic ions are believed to stabilize and strengthen the interactions between water molecules, while chaotropic ions disturb and weaken the interactions between water molecules.

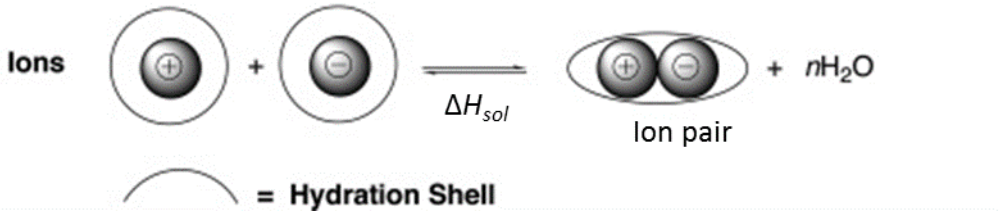

Cations and anions can have 4 combinations: k-c, c-k, c-c, k-k. When the cations and anions are both kosmotropic, their electrostatic interactions overpower the interactions between water and them, resulting an endothermic solution process ($\Delta H_{sol} > 0$). When they are both chaotropic, the solution process is also endothermic because water molecules favor to form hydrogen bonds with each other rather than to solvate 2 chaotropic ions. So if anions and cations have similar hydration Gibbs free energy, the ΔH_{sol} of their ion pair is above 0. If their hydration Gibbs free energy have big gap, then the ΔH_{sol} of the ion pair tends to be negative and solvation is favorable, as illustrated in Figure 1-1. In Hofmeister Series, hydrophobic ions are usually chaotropic and hydrophilic ions are usually kosmotropic. Collins' law is widely used to interpret specific ion effects. However, in Collins' model the entropy change (ΔS_{sol}) is not considered. The removal of water shells

from ions decreases entropy and cost the energy gain from electrostatic and van der Waals forces, which will affect the total energy change.[4] Collins' law is also focusing too much on the energy change of ions and ignores that solvation also includes the energy change of water molecules. In the case when one c-c ion pair is solvated, 2 hydrogen bonds between water molecules need to be broken and then the two chaotropic ions bind to water molecules, so the energy change will be: $\Delta H = 2*\text{Energy}(\text{c-}H_2O) - (\text{Energy}(\text{c-c}) + \text{Energy}(H_2O\text{-}H_2O))$. From the Collins' plot it is very hard to determine if the ΔH is negative or positive. The description is still not quantitative.

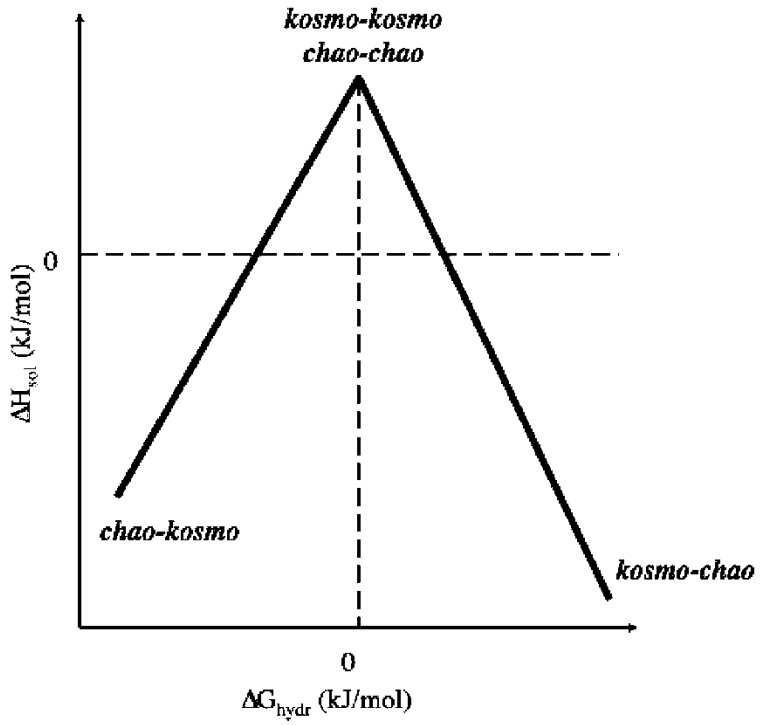

Figure 1-1 Plot of solvation energy of crystalline alkali halides at infinite dilution vs. the difference in hydration Gibbs free energy of the anions and cations, *ΔG* = G(anion)-G(cation), according to Collins. [35]

As concluded above, many attempts have been made to correlate a limited number of parameters to specific ions effects, but most of them only fit a specific system and they are hard to apply to other systems.[36, 37, 38] Ninham once declared that the key to the problem is that current theories lack elucidation from quantum mechanics perspectives that consider the contribution of dispersion forces to the ions interactions.[39, 40, 41, 42] However, people's understanding on quantum mechanics effects on the Hofmeister series is still limited. There is still a long way to go to fully understand the Hofmeister Series.

1.1.2 Specific ion effects on surfactant/water interface

Surfactant solutions are one of the most studied targets in the research of specific ion effects, because different combinations of type and concentration of salts and surfactants can bring dramatic changes to the surfactants physical properties such as cmc, aggregation number, solubility, phase transitions, morphology and viscosity. [17, 43, 44, 45, 46, 47, 48] Specific ion effects in surfactants solutions can be classified into two categories: effects of specific counterions (if the surfactant molecule has counterions) and effects of specific added ions. The two effects are closely related, because both rely on the specific interactions between headgroups and counterions in the surfactant/water interfacial region, which is mainly composed of headgroups, counterions and water molecules. When changing the type of counterions or added ions, the original subtle balance between water, headgroup and counterions at the interface will be shifted, producing measurable changes in bulk properties. In extreme cases, nonionic surfactants like poly(ethylene oxide)/ poly(propyleneoxide) (PEO/PPO) don't even have any counterions and their headgroup

has no strong electrostatic interaction with the added ions, but they still have specific ion effects that come from nonelectrostatic interaction between added ions and uncharged headgroups through hydrogen bonds, hydrophobic interactions and dipole-dipole interactions, which can change the hydration of headgroup and influence the balance of forces at the interface.[49, 50] So specific ion effects are ubiquitous in surfactant solutions, not only in micellar solutions, but in other related surfactants systems such as microemulsions and emulsions.[51, 52]

Our group has studied specific ion effects in surfactant systems extensively. For example, Dr. Yan Geng studied the NaBr salt effect onto the second cmc of 3 types of gemini surfactants N,N'-bis(dodecyldimethyl)-α,ω-alkanediammonium dibromide (12-n-12 2X) with different lengths of the linking chain (n). The result showed that for 12-2-12 2Br surfactant, adding NaBr will induce the micelles to transform from spherical to rod-like shape with a dramatic increment of interfacial Br^- concentration and decrement of interfacial water molarity, while 12-3-12 2Br and 12-4-12 2Br didn't show a similar trend.[53] Small variations on the headgroup structure bring big changes to the system bulky property, which again proves how sensitive the systems are to the change of interactions between counterions and headgroups.

Our collaborators in Prof. Reiko Oda's group has studied the specific counterion effects on 14-2-14 gemini surfactants properties.[3] Their results showed that when the counterions were replaced from hydrophilic to hydrophobic ions, the surfactants properties such as the critical micelle concentration (cmc), micellization free energy and ionization degree roughly change according to the Hofmeister Series. A more extreme case is from Dr. Oda's earlier paper,[54] in which she found that by changing the counterions of gemini

surfactants into chiral tartrate ions, the shape of the micelles transformed from spherical shape into an unusual chiral twisted ribbon. These examples are only few of the large amount of strong specific ion effects phenomena in surfactants solution systems.

In a word, specific ion effects in surfactants systems, no matter if it is from replacement of counterions, or addition of salts, originate from the specific ion interactions between counterions and headgroups at the surfactant/water interface.[55, 56]

1.1.3 Specific ion effect on neat oil/water interface

Besides surfactant/water interface, which is a partially-hydrophobic/water interface, the Hofmeister Series has also been studied at oil/water interfaces. Compared with surfactant/water interface, the oil/water interface has a bigger gap in polarity at the interfacial boundaries between two phases. In chemistry and biology the oil/water interface is a very important topic and related to many fundamental phenomena such as biomolecules solubility and stability,[57, 58] interfacial water molecules behavior,[59, 60] ions adsorption onto the interfaces[61] and proteins folding & unfolding,[59,62] because hydrophobic/water interface widely exists in these systems. However, direct studying the hydrophobic/water interface is not easy. Only in recent years the advancement in instrumentation is allowing scientists to study the hydrophobic/water interface from experimental[63,64] and computational approaches.[65,66] Previously only simpler systems such as air/water interface were studied and scientists tried to extrapolate the results to the oil/water interface.

Specific ion effects are frequently studied at the air/water. Experimentally the air/water interface is simpler because phenomena at the interface are easy to be detected by common

experimental approaches. Unlike oil/water interface that the boundary of two phases may raise various problems such as reflection and contamination, air/water interface is cleaner and easier to handle. As an example, in molecular dynamic simulation studies on air/water interface, the air phase can be directly represented by vacuum.[67, 68, 69, 70]

Experimentally, the air/water interface can be studied by a number of methods. Saykally's group used sum frequency generation (SFG) and second harmonic generation to study selective ions adsorption at water surfaces.[71] They found that thiocyanate shows an enhanced interfacial concentration at a water surface covered by a monolayer of dodecanol. Cremer's group used vibrational sum frequency spectroscopy and observed specific ions adsorption onto different polymer species that spread at the water interface.[64] They found the ions order of affecting water molecules vibration frequencies matches with Hofmeister Series. Ghosal et al. demonstrated strong Br^- and I^- adsorption at water-air interface by using x-ray photoelectron spectroscopy which is specially designed for the purpose.[72] The experimental result shows stronger ions adsorption than theoretically predicted. These powerful techniques clarify the specific ion effect on air/water interface.

On the other hand, few papers report research directly on neat oil/water interfaces. Richmond's group used SFG to study ions behavior on H_2O/CCl_4 interface[73, 74] and found that different ions change the hydrogen-bonding network strength of interfacial water molecules to different extents. Wick's group performed MD simulation on the same H_2O/CCl_4 interface and the results strengthen Richmond's conclusion that larger and more polarizable ions have higher concentration at this interface.[65] Jungwirth's group used nonpolarizable MD simulations with electronic continuum correction to simulate the behavior of Br^- and I^- at the water/decane interface and then predicted that both ions are

concentrating at the interface.[75] Most of related papers in literature are based on computational simulation and there are no experiments reported about specific ions adsorption onto neat oil/water interface except Richmond's CCl_4/H_2O interface. There is a great gap between simulation predictions and experimental evidences waiting for people to fill.

1.2 SURFACTANTS

1.2.1 Introduction

Surfactants are a category of molecules with both hydrophobic and hydrophilic functional groups in the structures (Figure 1-2). As a result it has affinity to both polar and nonpolar media. The polar part is called headgroup, while the nonpolar part is called tail. Surfactants self-assemble onto water/air, water/oil, and some water/solid interfaces, and also self-assemble in water. Aggregation of surfactants often leads to great changes in the system physical properties. Because of their amphiphility, surfactants have many applications such as cleaning, fracturing, oil recovery, lubricants, foaming agents, food preservation.[76, 77, 78]

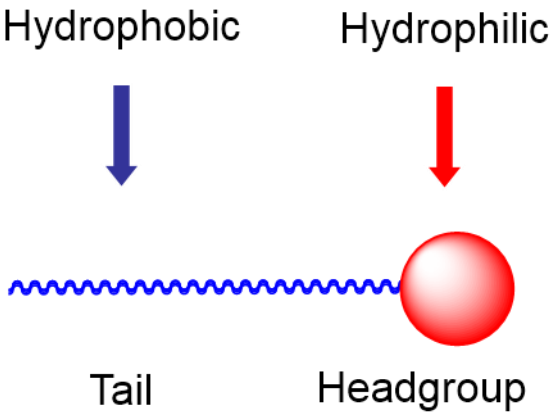

Figure 1-2 Surfactants molecular structure

The most common method for classifying surfactants is based on their headgroup charge type, including cationic, anionic, nonionic and zwitterioninc surfactants. Representative examples are shown below in Figure 1-3.

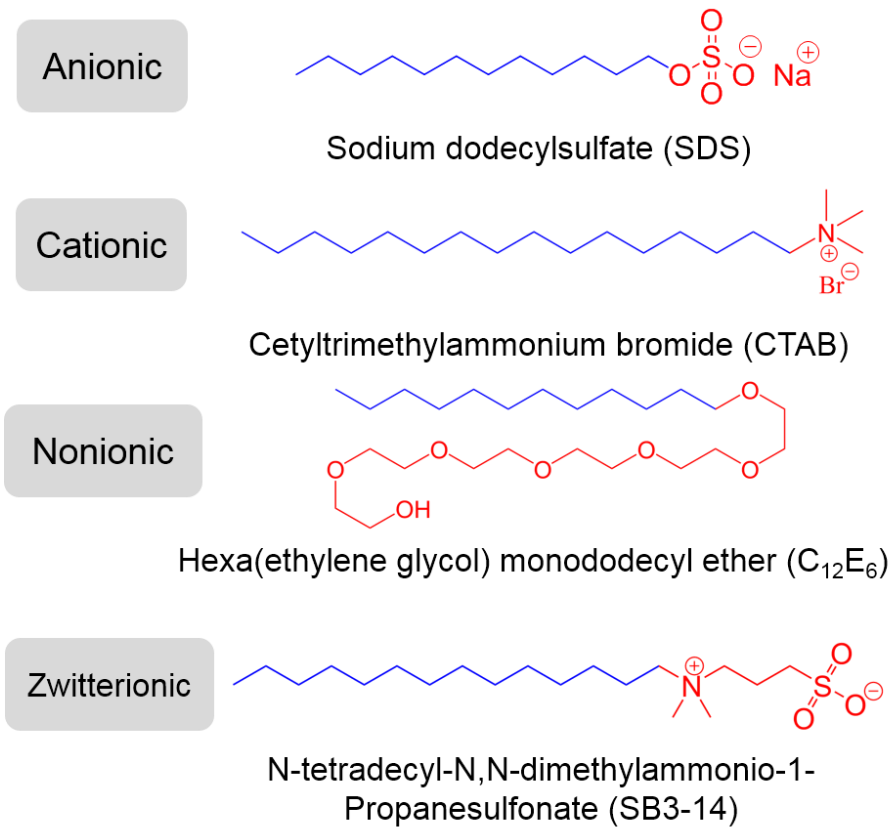

Figure 1-3 Typical categories of surfactants and representative molecules of each category.

Surfactants aggregates have a plethora of structures that depends on surfactant, concentration, solvent and temperature (Figure 1-4).[79] Generally in a surfactant/water mixtures, with increasing surfactant concentration the surfactants aggregates will transit from spherical to rod-like micelles, then to hexagonal stacking and a lamellar mesophase. If surfactants are mixed with water and oil, the mixtures may form thermodynamically stable microemulsions or unstable emulsions. Emulsions will gradually separate into

multiple phases. The properties of micelle, emulsions and microemulsions will be discussed in following sections.

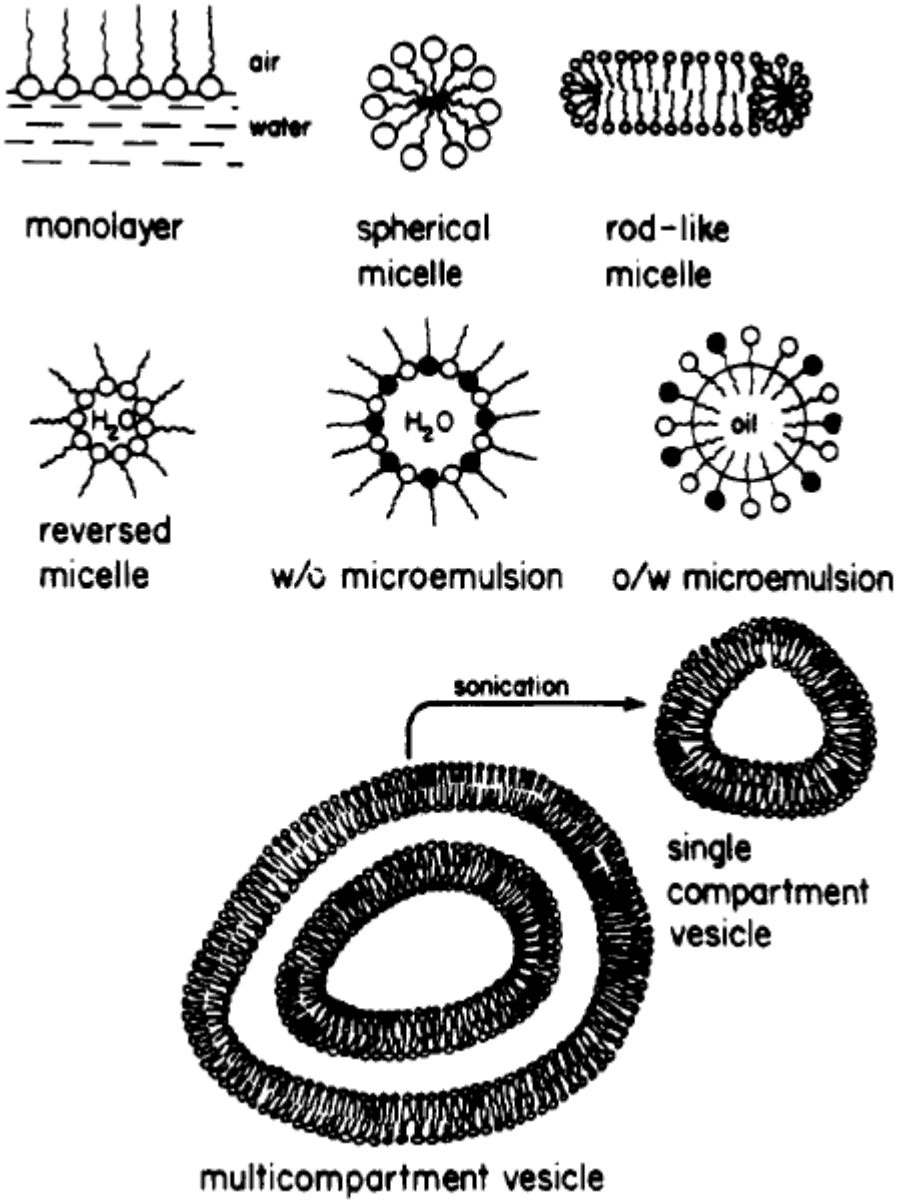

Figure 1-4 Various possible structures of surfactant aggregates [80]

1.2.2 Micelles

In aqueous solutions surfactants spontaneously self-assemble into micelles. At very low surfactant concentration, surfactants exist as isolated monomers. When the concentration of a particular surfactant reaches its characteristic critical concentration, which is called the critical micelle concentration (cmc), the monomers spontaneously assemble into micelles, with the tails forming a liquid-like hydrocarbon core and the hydrated headgroups and counterions surrounding the surface. This process is called micellization and it only happens spontaneously above the critical concentration. In the process of micellization the free energy of the system is lowered, which mainly derives from the increase in entropy of the system, rather than the decrement of enthalpy, due to the release of the hydration shell around the surfactant tail into the bulk water, which is greater than the entropy decrease derived from the surfactants self-assembling.[81] The enthalpy change during micellization process is small because there are no chemical bonds formed or broken, only non-covalent interactions e.g. electrostatic interaction, hydrophobic interaction and van der Waals forces are involved in the process, which barely change the enthalpy of the whole system.

The cmc, aggregation number and ionization degree are three very important properties and the next three sections will be about them.

CMC

As noted previously, surfactants spontaneously aggregate above the cmc. The cmc is not a point on concentration profile but in a narrow concentration range. During this transition various physical properties of the surfactants solutions change significantly.

Values of the cmc can be obtained by measuring the change of these physical properties when surfactants concentration is close to the cmc, such as conductivity, surface tension, nonpolar substance solubility, and diffusivities. Figure 1-5 illustrates the changes in a variety of physical properties with increasing surfactants concentration in general cases.[82]

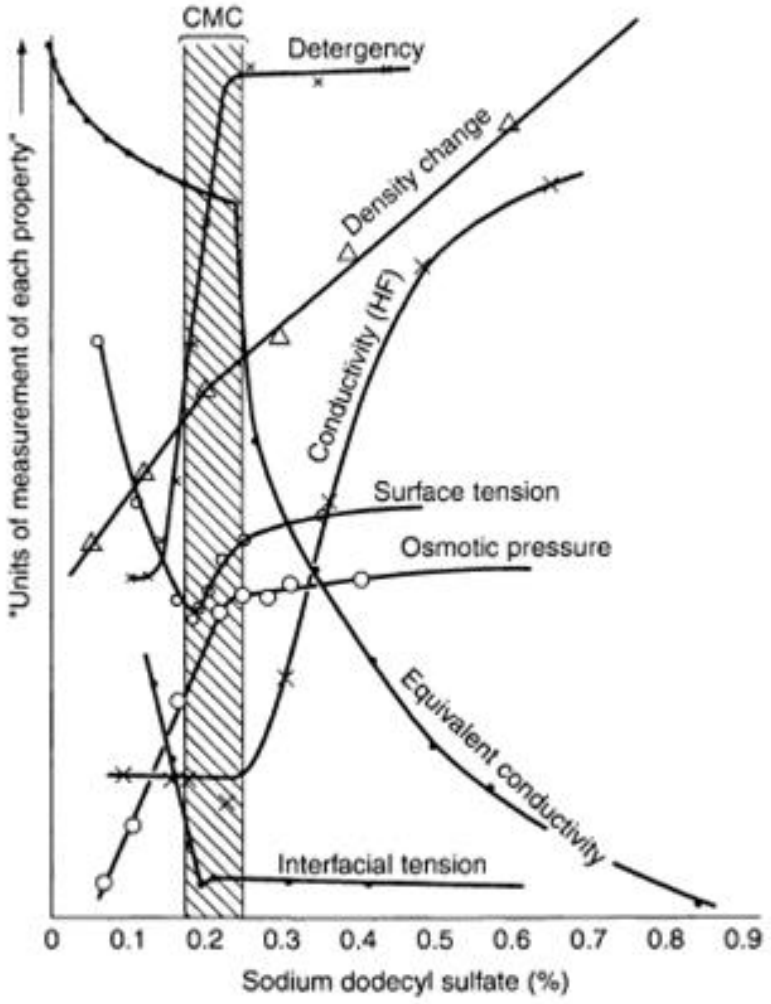

Figure 1-5 Dramatic change of surfactants solution physical properties when surfactants concentrations are around the cmc measured at ca. 1948. [83]

The cmc depends on temperature, headgroup type, tail type, tail length, counterion type of ionic and type of solvents.[84] Added components such as salts and organic small molecules can influence the value of cmc, indicating a change on the interactions between water and surfactants.

Aggregation number

The aggregation number is the average number of surfactant monomers per micelle. The real aggregation number of one micelle is not a constant value. On the contrary, at all times surfactant molecules leave and enter the micelles, changing the number of monomers per micelle. Statistically, the numbers of monomers in micelles should follow Gaussian distribution but the value of aggregation number that common experimental instruments measure is the average aggregation number. As long as the whole system reaches equilibrium, the aggregation number will become dynamically stable.

The aggregation number is influenced by temperature[85], counterion type[86] and the shape of micelles (spherical, rod-like, lamellar, etc.). As the surfactant concentration is raised, micelles shape transform from spheres to rods or other shapes, the aggregation number will increase significantly.

One common method used to measure aggregation number is Fluorescence Quenching.[87] Fluorescent probes and quencher molecules are hydrophobic and strongly associate with micelles. When increasing the concentration of surfactants, the number of micelles increases so that the volume of micellar media increases and the fluorophore and the quencher concentrations within micelles are diluted, which slows down the quenching rate of fluorophore. By fitting the fluorescence decay rate with theoretical model, the

molarity of micelles as a whole can be obtained and the aggregation number can be calculated.[88]

However, when considering chemical reactivity in micelles, the aggregation number may not be important at all. In the following sections the pseudophase model will be introduced, in which micellar solutions are treated as 2 phases systems: the micellar pseudophase and the aqueous bulky phase. The totality of all surfactants aggregates is treated as a single phase in which reactants reach distribution equilibrium between it and the bulk aqueous phase.[89] No matter how large the aggregation number, as long as the total concentration of surfactant stays the same the volume of the micellar pseudophase remains unchanged, so the distribution of reactants between the two phases won't change and its reactivity in the two phases will stay the same. So when dealing with chemical reactivity in micellar solutions, the aggregation number is not a critical factor to determine the results.

Ionization degree

The ionization degree, generally denoted as α, characterizes the fraction of counterions dissociated from micelles into the bulk phase. Above the cmc, surfactant monomers self-assemble into micelles with the charged headgroups organized around the micellar core. The newly formed charged monolayer strongly attracts counterions and create a layer of counterions around the micellar core. A large fraction of the counterions associate in the interfacial region and move with the micelles, but the other fraction of counterions diffuse freely in bulk phase. Nevertheless the counterions are in dynamic equilibrium in and out of the micelles. When the interaction between counterion and headgroup is stronger, α is

smaller. If the interaction becomes weaker, α becomes bigger. So α can be used as an indicator of the strength of interaction between headgroups and counterions.

There are two ways to calculate the ionization degree α. The most common way is that α is equal to the ratio of slopes of the conductivity-concentration plots above and below the cmc, respectively: [90]

$$\alpha_Z = S_2 \,/\, S_1$$

Equation 1-1

where S_1 is slope of the conductivity-concentration plot below the cmc, S_2 is slope of the conductivity-concentration plot above the cmc.

However it was generally accepted that the α_Z overestimates the ionization degree because this equation presumes that a micelle with *n* net charges has the same contribution to the conductivity of the micellar solution as *n* free ions in aqueous phase, which oversimplify the conductivity contribution of micelles.[91] Evans proposed a new method backed up by Zana which corrected the calculation of the contribution of micelles to the solution conductivity.[92, 81]

The conductivity of the surfactant solution when the concentration is below cmc is giving by equation 1-2:

$$\kappa = \lambda_S C_S + \lambda_C C_C$$

Equation 1-2

where λ_S and λ_C are the molar conductivities of the surfactant monomer ions and counterions for unit concentration in water and C_S and C_C are the concentrations of surfactant and counterions.

Above the cmc, the conductivity is assumed to be the sum of three components: free surfactants, free counterions and micelles:

$$\kappa = \lambda_S C_S + \lambda_C C_C + \lambda_M C_M$$

Equation 1-3

where λ_M and C_M are the conductivities and concentration of micelles.

In Kwetkat's paper, the conductivity of micelles is equal to $N_{agg}\alpha * \lambda_S$, which means that in micelles there is a fraction of monomers that no counterions associate to them, and the micelles conductivity is equal to the conductivity as though this fraction of monomers were in bulk phase.[75]

$$\lambda_M = N_{agg}\alpha * \lambda_S$$

Equation 1-4

To make the estimation more precise, Evans took into account the screening effect of counterions on micelle surface and corrected Equation 1-4 into Equation 1-5: [81]

$$\lambda_M = {N_{agg}}^{5/3} * \alpha^2 * \lambda_S$$

Equation 1-5

So S_2 can be redefined into Equation 1-6 by combining Equation 1-3 and Equation 1-5 followed by some transformations: [3]

$$S_2 = \alpha_E{}^2 N_{agg}^{2/3}(S_1 - \lambda_C) + \alpha_E \lambda_C$$

Equation 1-6

where λ_C is the conductivities of the free surfactant counterions, and α_E is the Evans ionization degree. α_E is obtained by solving Equation 1-6 with help from measured S_1, S_2, N_{agg} and λ_C. When the cmc is low, the λ_C at infinite dilution can be used in the equation. The N_{agg} value is obtained from fluorescence quenching experiment at 2x cmc and 3x cmc. It is widely accepted that the Evans ionization degree is closer to the real value than the original one.

Reactivity in micelles – pseudophase model

Studies have demonstrated that the polarity of micelle core is close to that of alcohols[52], so many organic molecules tend to strongly dissolve into the micelles. The dissolving can significantly influence the chemical reactions between the solutes[80] because reactants are concentrated within the micelle interfacial region, so the chance they meet and react becomes larger. Surfactants headgroup have electrostatic interactions with the reactants which also helps stabilize reaction intermediates and lower the activation energy.[93, 94]

Several models were developed to describe the chemical reactions in micellar solution over the past several decades. The most successful one is the pseudophase model.[95, 96]

The pseudophase model treats the sum of all micelles in solution as a separated pseudophase, and the distribution of molecules between the bulk water and the micellar pseudophase are described by association constant K_s, as show in Equation 1-7:

$$S_W + D_n \overset{K_S}{\Leftrightarrow} S_M$$

Equation 1-7

where S_W and S_M indicate the substrates in water phase and micellar phase, and D_n stands for micellized surfactants. The K_S is the distribution equilibrium constant of the substrates between the two regions, described by Equation 1-8:

$$K_S = \frac{[S_M]}{[S_W][D_n]}$$

Equation 1-8

where $[D_n] = [D_T] - cmc$. $[D_T]$ is the stoichiometric concentration of surfactant molecules in solution. At concentrations above cmc the free surfactant monomer concentration is set to be equal to cmc. However, for most of cases $[D_T]$ >> cmc so cmc is usually negligible, i.e., $[D_n] \approx [D_T]$.

The mass balance equation for the substrates defines the stoichiometric concentration of substrate S_T, as illustrated in Equation 1-9:

$$[S_T] = [S_W] + [S_M]$$

Equation 1-9

The observed reaction rate of substances is the sum of the rates in two phases, the aqueous phase and micellar pseudophase:

$$Rate = k_{obs}[S_T] = k_w[S_W] + k_M[S_M]$$

Equation 1-10

where k_{obs}, k_w, k_M are the observed aqueous and micellar rate constants. This equation is based on the assumption that reactants distributions are in dynamic equilibrium and the speed that the distribution reaches equilibrium is orders of magnitude faster than the reactions rates.[97] However, this assumption might not work for fast enzyme-catalyzed reactions in micelles or photochemical reactions that are near the diffusion controlled limit.[98]

Chemical Trapping Experiments

As mentioned before, there are many methods that detect ions at liquid/liquid interface, but most of them are physical methods such as photon spectroscopy or electron spectroscopy.[64] We have developed a special chemical method, named the chemical trapping method, that provide an estimate of the interfacial concentrations of ions and water molecules and it has been applied to different systems such as micellar solutions, emulsions and microemulsions.[99] The essential part of this method is a surfactant-like long chain arenediazonium ion, or "probe" as we call it, and the logic is that the probe associates into the interfacial region because it is polar and ionic and its tail resides in the micellar core. The headgroup reacts with interfacial ions and water molecules and to give respective products. The products yields are measured and the amount of ions and water molecules at the interface can be estimated based on the yields, because interfacial ions and waters are competing with each other to react with the probe, so their molar ratio determines the ratio of their respective products. With help from a standard curve that provides the selectivity

of the arenediazonium ion toward ions and water molecules, the interfacial concentration of ions and water molecules is calculated.[100]

The probe is a 4-hexadecyl-2,6-dimethylarenediazonium ion, abbreviated as 16-ArN_2^+, prepared and stored as its stable BF_4^- salt. The heterolytic reactivity of arenediazonium ion has been well studied by Zollinger.[101] The reactions between the probe and nucleophiles are illustrated in Figure 1-6. The products are separated and quantified by HPLC to get the yields of dediazoniation reaction products.

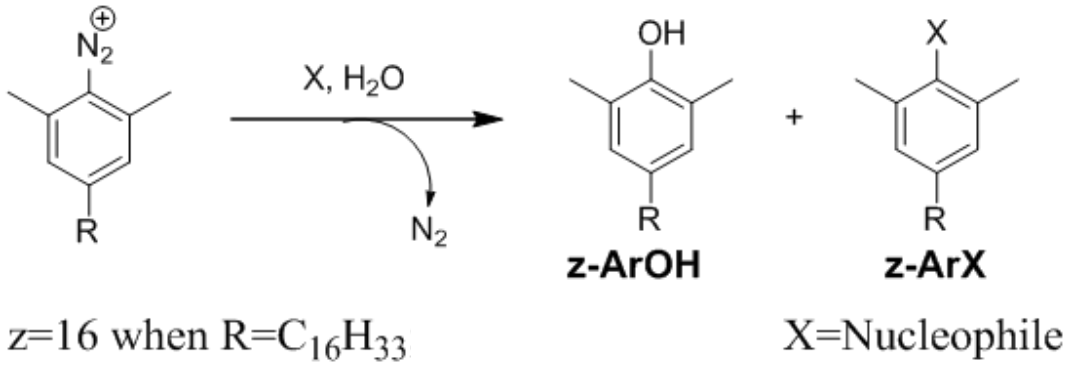

Figure 1-6 The dediazoniation reaction of the chemical trapping experiment probe. Main products include phenol and aryl product, where X is a nucleophile like water, e.g. Cl^-

In addition to ion and phenolic products, the dediazoniation reaction also produces other side products generally in low yield such as 4-hexadecyl-2,6-dimethylbenzene, 16-ArH, 5-hexadecyl-7-methyl-1H-indazole, 16-ArInd, 4-hexadecyl-2,6-dimethylphenyl-acetamide, 16-ArNHAc and 2-fluoro-5-hexadecyl-1,3-dimethylbenzene, 16-ArF. 16-ArH is produced by the reaction between 16-ArOH and the unreacted 16-ArN_2^+, so when calculating the interfacial concentration of water molecules, %16-ArOH and %16-ArH

needs to be combined to represent the yield of phenol product formed from water. 16-ArInd is formed when 16-ArN_2^+ is reduced by hydroxide ion or general base in water, so usually its production is suppressed by acidifying the solution pH. 16-ArNHAc is the product between MeCN and 16-ArN_2^+. 16-ArF is from the decomposition of 16-ArN_2^+ BF_4^-. So 16-ArInd, 16-ArNHAc and 16-ArF are not related to the competition between ions and water molecules to react with the probe. As a result, in the process of calculating water and ions interfacial concentrations, these compounds are not involved. They are needed when calculating the total yield of all dediazoniation products.

To calculate the interfacial ion and water concentrations from the ratio of reaction products, the selectivity of probe toward ions and water molecule is an important parameter. The selectivity $S_W{}^X$ is defined as the ratio between $\%\mathrm{ArX}/_{[\mathrm{X}^-]}$ (the ions product yield for ions unit concentration) and $\%\mathrm{ArOH}/_{[\mathrm{H_2O}]}$ (the water product yield for water unit concentration), as shown in Equation 1-11. The %ArOH contains the yields of all products produced from water, so %ArOH = %16-ArOH + %16-ArH.

$$S_W{}^X \equiv \frac{\%\mathrm{ArX}/_{[\mathrm{X}^-]}}{\%\mathrm{ArOH}/_{[\mathrm{H_2O}]}}$$

Equation 1-11

If the selectivity is known to us, the interfacial concentration of ions and water will be easy to calculate based on the yields of phenol and substitution dediazoniation products. However, selectivity value cannot be directly obtained from yields at an aggregate interface, so an analog system is created to obtain the selectivity. The analog system is required to

simulate the environment of long chain arenediazonium ion at the interfacial region of micellar solution so that the same selectivity can be measured in the analog system. It was finally determined that an aqueous solution of M^+X^- salt with added water soluble 4-methyl-2,6-dimethylarenediazonium ion, 1-ArN_2^+, is a satisfactory analog system, where M^+ can be Na^+ or Me_4N^+ or other cations, depending on the micellar solution, as illustrated in Figure 1-7. The dediazoniation reaction products of analog systems also contains phenol product 1-ArOH, substitution product 1-ArX and side products 1-ArNHAc. Due to the pH control in the analog system, the amounts of side products 1-ArInd, 1-ArH and 1-ArF are usually very low.

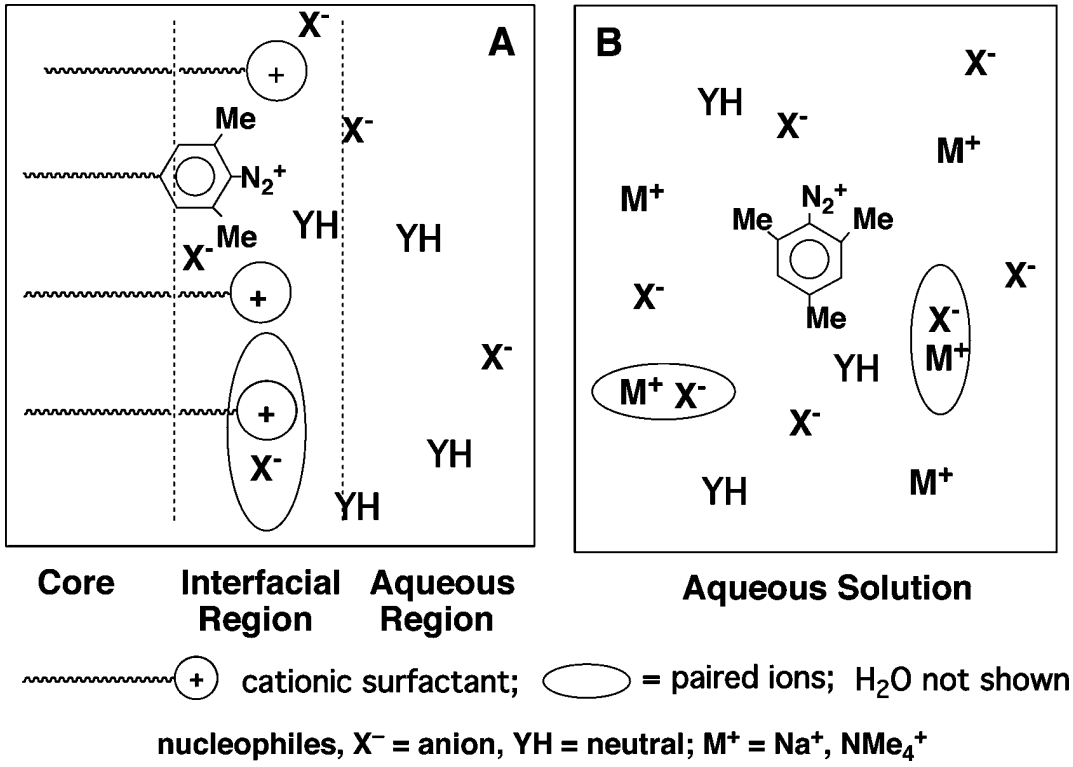

Figure 1-7 (Left) Interfacial region of a micellar solution with cationic surfactant, 16-ArN_2^+, and ion-pairing. (Right) Aqueous solution containing salt, MX, 1-ArN_2^+.[99]

There are two assumptions required when using this analog system:

1). 1-ArN_2^+ selectivity toward ions and water molecule in aqueous solution is considered to be the same as 16-ArN_2^+ at interfacial region, as shown in Equation 1-12 (in the equation the values on the left are for micellar solutions while the values on the right are for the analog systems.). This is reasonable because the length of hydrocarbon chain has little influence on the arenediazonium functional group's reactivity. Additionally, previous studies show that first order rate constants of dediazoniation reactions of arenediazonium ion change very little in solvents of greatly differing dielectric constants, because the reactivity of arenediazonium functional group is very insensitive to solvent polarity and nucleophile concentration.[102] The chemical environments of micelle interface and salt solution are very similar, so it is reasonable to assume that the selectivity of 1-ArN_2^+ in aqueous solution and the selectivity of 16-ArN_2^+ at micellar interface toward ions and water molecules are the same.

In real experiments, the measured $S_W{}^X$ is not unchanged all the time. Our previous studies show that the $S_W{}^X$ of 1-ArN_2^+ gradually decreases with increasing [X^-] because of the ion-pairs formation at high salt concentration which reduces the concentration of free X^-. As a result, to correctly apply the $S_W{}^X$ obtained in analog system to the micellar solution, we assume that as long as local [X^-] is the same in micellar interfacial region and in aqueous solution, the $S_W{}^X$ of 16-ArN_2^+ and 1-ArN_2^+ are the equal.

$$S_W{}^X \equiv \frac{\%16-\mathrm{ArX}/_{[\mathrm{X}^-]_{interf}}}{\%16-\mathrm{ArOH}/_{[\mathrm{H_2O}]_{interf}}} = \frac{\%1-\mathrm{ArX}/_{[\mathrm{X}^-]}}{\%1-\mathrm{ArOH}/_{[\mathrm{H_2O}]}}$$

Equation 1-12

2). Based on assumption in point 1, another crucial assumption can be deduced: when the %16-ArX in micellar solution is the same as %1-ArX in analog system, i.e., when %16-ArX = %1-ArX, the interfacial concentration of X^- in micellar solution is the same as concentration of X^- in analog solution, i.e. X_m = [X]. For water molecules a somewhat relationship is used. Because the selectivity of arenediazonium ion in two environments are the same, %16-ArX = %1-ArX is certain to give that the local [X^-] are the same in both environments.

With these assumptions, standard procedures for estimating interfacial counterions concentrations can be established: 1) Determine the products yields of reaction between 1-ArN_2^+ and X^- in analog salt solutions and create the standard curves of %1-ArX against [MX] in analog system. The salt concentrations are usually ranging from 0.5 M to 4.0 M. 2) Conduct chemical trapping experiments with 16-ArN_2^+ in micellar solutions at a certain surfactant concentration to obtain the dediazoniation products yields %16-ArX and %16-ArOH. 3) By referring to the %1-ArX vs. [MX] standard curve that was obtained from 1-ArN_2^+ experiment, the interfacial concentration of X^- can be calculated based on Equation 1-12. The interfacial H_2O concentration can be calculated by a similar procedure that includes the selectivity toward ions.

Let's take one of our group's previous project as an example.[100] In the paper, the chemical trapping method was used to measure the interfacial Br^- and H_2O concentrations

in CTABr(cetyltrimethylammonium bromide) micellar solution. Its analog system is the aqueous solution of TMABr(tetramethylammonium bromide). As illustrated in Figure 1-8, the standards curves of %1-ArBr vs. [TMABr] and %1-ArOH vs. [TMABr] were obtained from the analog system. The curves of %16-ArBr vs. [CTABr] and %16-ArOH vs. [CTABr] were measured in micellar solution. To obtain the Br^- interfacial molarity at 0.01M CTABr, the %16-ArBr at 0.01M CTABr is first located, then referred to the %1-ArBr vs. [TMABr] standard curve to find its corresponding TMABr concentration(dashed line), which is 2.25 M. Based on the analysis above, the interfacial Br^- concentration in CTABr micelles is 2.25 M, i.e. *when the yields are the same, the concentrations are the same*. After knowing $[Br^-]_{interf}$, with Equation 1-12 and the value of (%16-ArBr)/(%16-ArOH) obtained from HPLC results, it is very easy to calculate the value of $[H_2O]_{interf}$.

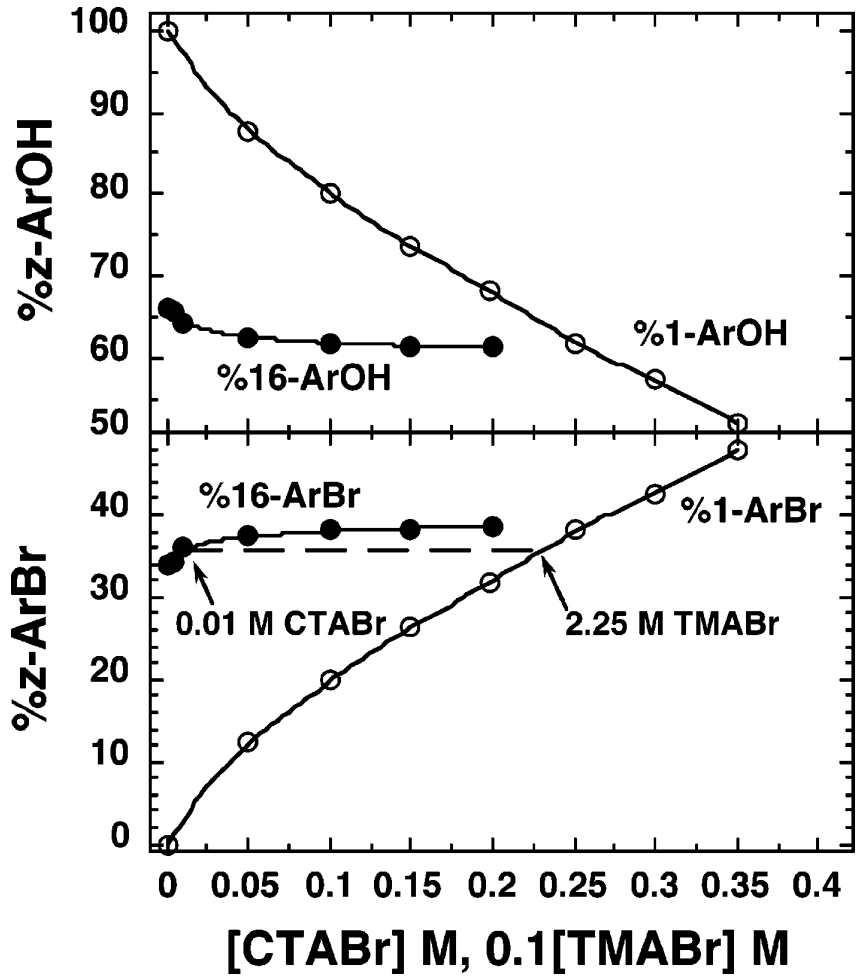

Figure 1-8 Dediazoniation product yields from reaction with H_2O (top) and Br^- (bottom) at 40 ℃ from reaction of 16-ArN_2^+ in CTABr micelles (solid dot) and 1-ArN_2^+ in TMABr salt solutions (empty dot). To put the CTABr and TMABr data on the same scale, each stoichiometric TMABr concentration is multiplied by 0.1 [100]

Compared to other interface characterization method, the chemical trapping method does not need expensive instruments and relies on the long chain arenediazonium ion probe, which is not hard to synthesize.[100] It provides the unique interfacial ions and water concentrations of micelles that depict the scenario at the interface in a straightforward way. It can be a powerful tool to study specific ion effects at various kinds of interfaces.

1.2.3 Emulsions

Emulsions are oil and water mixtures in which one liquid phase is dispersed in the other immiscible liquid phase. If water and oil are mixed without any other additives, the mixture is very unstable and will phase separate in a short time. Surfactants are typically used to make emulsions more stable because they interact simultaneously with both water and oil phases at the same time. Emulsions have application in many areas such as foods and food processing,[103] pharmaceutics and clinical industry,[104] cosmetics,[105] and petroleum industry.[106]

Emulsions are categorized into several types. Depending on which phase is the dispersing phase, emulsions can be classified into oil-in-water (o/w) type and water-in-oil (w/o) type. Depending on the droplet size, emulsions can be classified into normal emulsions and nanoemulsion (size < 1 μm). Microemulsion is a confusing name, but it is totally different from emulsion, because it is a thermodynamic stable system while emulsion is not. Metastable emulsions can be prepared by mechanically mixing the oil and water phases and their stabilities depend on various parameters such as the types of oil and surfactant, the method and strength of mixing, etc.

Stability is a very important factor to evaluate the performance of emulsions. It means resistance to phase separation. Emulsion stability is maintained by repulsion between droplets, which comes from electrostatic and steric repulsions. Ionic surfactants are commonly utilized to prepare emulsions because its charged headgroup can slow droplet merging. Polymers, especially polysaccharides are usually added to emulsion to increase the stability because they can form a steric barrier on the surface of emulsion droplets to

increase stability.[107] Emulsions stabilities can be modified by changing the type of oil, surfactants and other additives.

Reactivity in emulsions

Because emulsions have many applications in different industries, research on chemical reactivities in emulsions is of great importance. The pseudophase model is being used to interpret compounds' reactivity in emulsions, in which the interfacial region is treated as a separate pseudophase that exists between water and oil phases, as in Figure 1-9.[108]

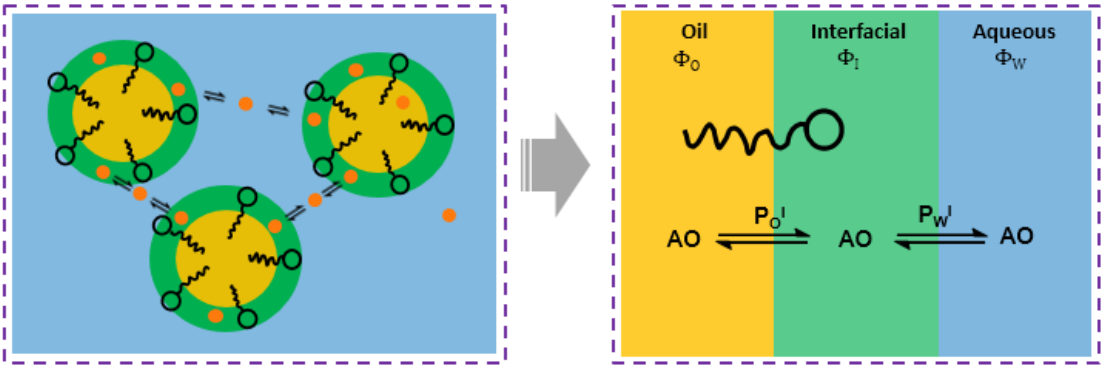

Figure 1-9 Illustration of pseudophase model of an emulsion. The interfacial region is the pseudophase and molecules reach equilibrium between it and the other two phases.

In this model, reactants are in dynamic equilibrium between the aqueous, oil and interfacial regions of emulsions. Since the diffusivities of small molecules are orders of magnitude faster than the reactions in emulsions, the reactants will reach equilibrium state before chemical reactions start. To quantify the process, the emulsion's total volume can be expressed as the sum of all three regions,

$$V_{Total} = V_{oil} + V_{interface} + V_{water}$$

where $V_{interface} = V_{surfactants}$ because interfacial region is mainly composed by surfactants. Accordingly, the total reaction rate is equal to the sum of the rates in 3 regions:

$$Rate = k_{obs}[S_T] = k_w[S_W] + k_I[S_I] + k_O[S_O]$$

Chapter 2 described how an arenediazonium ion probe is used to determine effect of added salts on the reaction rate between an antioxidant and an arenediazonium ion in the interfacial region of an emulsion. By monitoring the change of the reaction rate, the direction of the change in interfacial pH is discussed.

Chapter 2 Specific Ion Effect on Interfacial pH of Zwitterionic Emulsions

The research is about specific ion effects on interfacial pH of a zwitterionic emulsion. Different kinds of salts have been added into emulsion prepared by glyceryl trioctanoate (GTO), water and zwitterionic surfactant *N*-tetradecyl-*N*,*N*-dimethylammonio-1-propanesulfonate (SB3-14). The reaction rates of a pH sensitive reaction between the antioxidant (*t*-butylhydroquinone, TBHQ) and the arenediazonium ion probe (4-hexadecylbenzenediazonium ion, 16-ArN_2^+) has been measured at different salt concentration. Due to the nature of TBHQ and 16-ArN_2^+, the reaction only occurs at the interfacial region of the emulsion, so the reaction rate changes with the variation of interfacial pH. Added NaX salts with different anions decrease the observed first order rate constant, k_{obs}, for the reaction in the order: $X^- = ClO_4^- > Br^- \approx CCl_3CO_2^- > Cl^- > MeSO_3^-$. Added MCl_n salts of increasing cation valence at constant total Cl^- concentration increase k_{obs} in the order: $M^{n+} = Cs^+ < Ca^{2+} < Al^{3+}$ in the same emulsions. The ions influence the interfacial pH through the specific interactions between the ions and surfactant headgroup.

2.1 INTRODUCTION

In the absence of added salt, association colloids such as micelles, microemulsions and vesicles composed of zwitterionic surfactants are formally neutral, as are their analogs composed of nonionic surfactants. However, the ion binding properties of zwitterionic interfaces in micellar solutions are more like those of cationic surfactants. Both cationic and zwitterionic micellar interfaces selectively bind anions and the ion binding order

typically follows the Hofmeister series.[79, 109, 110, 111] However, added ClO_4^- precipitates cationic micelles, but zwitterionic micelles remain in solution. Results with zwitterionic micelles have been recently reviewed in detail.[110] Specific ion effects on the properties of zwitterionic micelles have been dubbed the "chameleon effect" for the dependence of micellar charge on the change in ionic environment, common with zwitterionic surfactants, but not observed with cationic or anionic surfactants. Addition of salts to zwitterionic micellar solutions make the interface more negative and the interfacial charge depends strongly on anion type for sulfobetaines, like the surfactant studied here, *N*-tetradecyl-*N*,*N*-dimethylammonio-1-propanesulfonate, SB3-14, Figure 2-1. The anionic interface attracts cations and creates an electrical double layer.[112] The interfacial anion and cation concentrations can be significantly greater than in the surrounding aqueous region.[112, 113] The cartoon in Figure 2-1 illustrates selective anion binding and the increase in local cation concentration in the

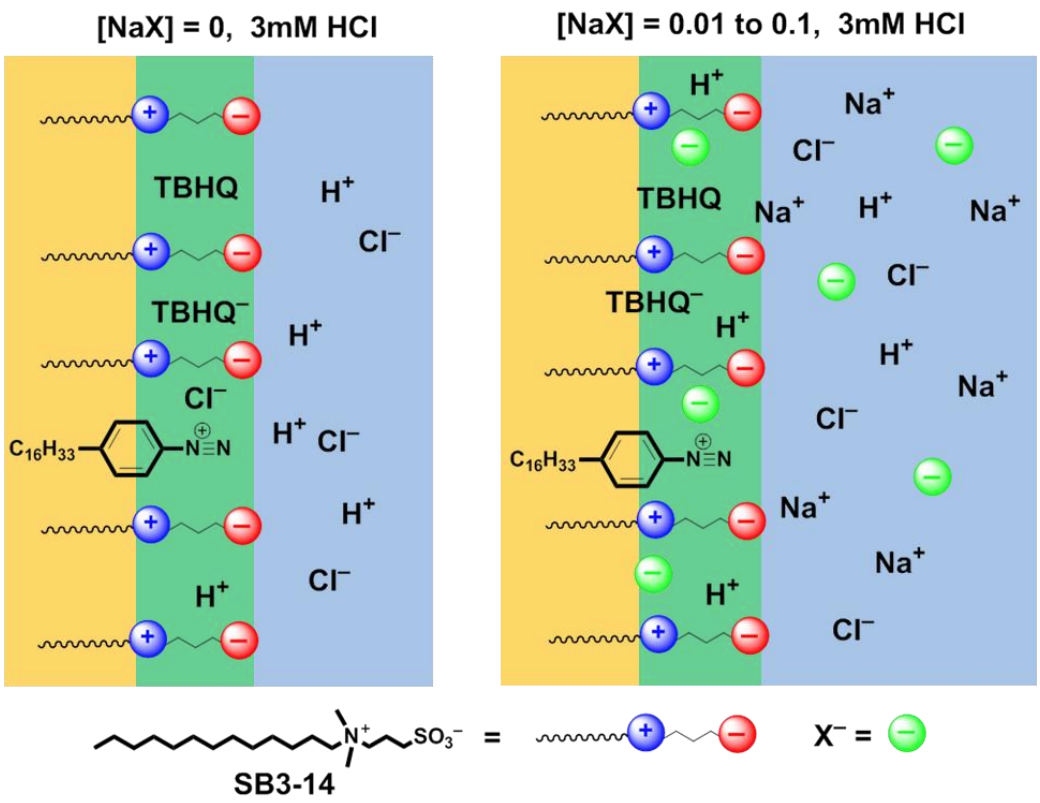

Figure 2-1. Cartoon illustrating the effect of added NaX on the properties of zwitterionic interfaces, quaternary ammonium ions blue, sulfonate ions red.

interfacial region of micelles of the zwitterionic surfactant, and, as we show here, zwitterionic emulsions. The locations of headgroups, anions, and cations in Figure 2-1 are hypothetical because the radial distributions of anions and cations and water in the vicinity of and within the interfacial region are unknown. The chameleon effect is a unique property of zwitterionic interfaces, i.e., selective anion binding/induced cation binding.[110] It provides a coherent explanation for specific anion effects on acid catalyzed reactions and shifts in acid-base equilibria in micellar solutions based on pseudophase models.[109, 110] The binding orders of anions to zwitterionic interfaces are qualitatively consistent with the Pearson hard-soft concept,[114] i.e., larger, more polarizable, less strongly hydrated anions

associate with zwitterionic interfaces more strongly than smaller, more strongly hydrated, less polarizable anions. For the halide ions, the size of the effect follows the Hofmeister series: $I^- > Br^- > Cl^- > F^-$.[115] Cations associate more weakly and less specificity but association increases with cation valence.[112]

Pseudophase kinetic models, originally developed to treat chemical reactivity in aqueous micellar solutions two score years ago, over time have been shown to work in microemulsions,[116] vesicles,[117, 118] nonionic emulsions,[119] and very recently, cationic and anionic emulsions.[120] Understanding emulsion effects on chemical reactivity is important because many important commercial applications and scientific research areas are emulsion based including: polymerization,[121] lipid digestion,[122] food preservation,[123] water purification,[124] phase transfer catalysis,[125] and synthesis.[126]

Oil-in-water emulsions have the same basic properties as association colloids in terms of interpreting reactions within them, but one, droplet size. In micelles the "oil core" is composed of surfactant tails and in emulsions the droplets are "fat" with added oil (literally when the oil is a triglyceride). Typical scale ranges are: spherical micelles (~2-5 nm); microemulsions (~10-200 nm); and macroemulsions (~200-50,000 nm).[127] As with association colloids, we assume that molecular diffusion in micelles and in stirred emulsions is near the diffusion-controlled limit and that rates of ordinary thermal reactions are not affected by molecular diffusion in stirred, kinetically stable, emulsions. In pseudophase models, the totality of the surfactant aggregates in association colloids and oil-in-water (o/w) emulsion droplets are divided into the same three regions in which chemical reactions may occur, oil, interfacial and water.[119] Thus, the primary differences between modeling reactions in micelles, emulsions and other surfactant aggregates are the

volume fractions of oil, surfactant and water. As a result, Figure 2-1 is applicable to all types of aggregated systems composition of SB3-14 or some other zwitterionic surfactant.

The aim of these experiments was to determine if adding salts containing different interfacial anions to emulsions prepared with zwitterionic surfactants also demonstrated chameleon-like properties. A SciFinder search for studies of chemical reactivity in zwitterionic emulsions came up empty, probably because: (a) emulsions are opaque and most methods for monitoring chemical reactions are typically carried out with spectrometers that require optically transparent solutions, or significantly higher reactant concentrations if NMR is used; and (b) emulsions are biphasic and only relatively recently were experimental methods developed for monitoring reactions within them.[119]

The results reported here show that the observed rate constant, k_{obs}, for the reaction of the antioxidant (*t*-butylhydroquinone, TBHQ) with the arenediazonium ion probe (4-hexadecylbenzenediazonium ion, 16-ArN_2^+) in zwitterionic micelles of SB3-14 is strongly affected by the type and concentration of anion added to the emulsion, to a lesser extent by the valence of added cations, and that the results are fully consistent with the chameleon effect.[110]

2.2 EXPERIMENTAL SECTION

2.2.1 Materials

Inorganic salts, including $AlCl_3(H_2O)_6$, glyceryl trioctanoate (GTO, ≥ 99%), *tert*-butylhydroquinone (TBHQ, 97%) were purchased from Sigma-Aldrich. 3-(*N*,*N*-Dimethylmyristylammonio)propanesulfonate (SB3-14,> 98%) was purchased from Fluka.

N-(1-Naphthyl)ethylenediamine dihydrochloride (NED, 96%) was purchased from Alfa Aesar. SB3-14 and TBHQ were recrystallized three times from ethanol and dried. The cmc was determined by surface tension (Du Noüy tensiometer) and was without a minimum and was 0.288 mM. All other reagents were used without further purification. 4-Hexadecylbenzenediazonium tetrafluoroborate (16-ArN_2BF_4) was synthesized from 4-hexadecylaniline (Aldrich, 97%) by a method developed previously.[100] All water used to prepare stock solutions and emulsions was doubly distilled and deionized.

2.2.2 Preparation of emulsions and determination of k_{obs}

A 1:1 oil:water emulsion was prepared in an Erlenmeyer flask by stirring together: 7.5 mL of glyceryl trioctanoate (GTO) with 7.5 mL of an aqueous solution containing the following concentrations of stock components: (a) a 3.0 mM HCl solution (prepared from a 0.5 M standardized HCl); (b) 4 wt% SB3-14; (c) weighted amounts of inorganic sodium salts, NaX. The final concentrations of the components in the total emulsion volume: 2 wt% SB3-15 (0.055 M), 0.005 to 0.1 M NaX, and 1.5 mM HCl. Note that in 1:1 oil:aqueous emulsions that because the solubility of HCl in oil is negligible, [HCl] ≈ 3.0 mM in the aqueous region. Each mixture was stirred at constant speed using a bench top magnetic stirrer for about 30 minutes and the resulting emulsion was uniformly opaque and white. None of the emulsions showed visible signs of phase separation on standing without agitation until after about 1 day. The pH values of the emulsions were measured by using an Accumet AR50 pH-meter, standardized with pH 1.68 and 4.00 buffers. The pH values varied between 2.52 ~ 2.60 for all emulsions, Table 2-2. The emulsions containing sodium salts were transferred into a continuously stirred, water-jacketed cell, equilibrated at 27 ℃. An aliquot (75 μL) of a 0.66 M TBHQ stock solution in MeOH (final concentration in the

total emulsion volume = 3.2×10^{-3} M) was added followed by an aliquot (43 μL) of 0.12 M 16-ArN_2BF_4 stock solution in acetonitrile (final concentration in the total emulsion volume = 3.24×10^{-4} M) to initiate the reaction. The structure of the 16-ArN_2^+ is shown in Figure 2-2. As the reaction proceeded, aliquots (200 μL) of the reaction mixture were withdrawn from the cell at specific time intervals and placed in a series of test tubes containing 2 mL of 0.1 M NED in ethanol that reacts with 16-ArN_2^+ to produce a purple dye with a strong UV absorbance. The half-life of the slowest reaction in 0.1 M $NaClO_4$, Table 2-2, was ca. 16 min and the reaction was complete ($10 \times t_{1/2}$) in 2.7 hours. Thus, the slowest reaction was significantly faster than the rate of phase separation without stirring and simple stirring keeps the phases mixed.

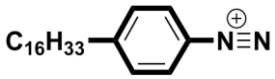

Figure 2-2 Structure of the diazonium ion probe utilized in emulsion

2.2.3 Determining k_{obs} by Azo Dye-Derivatization Method

All absorbance measurements were taken on a Perkin-Elmer LAMBDA 45 UV/vis dual-beam spectrophotometer under room temperature. Each absorbance measurement was made in matched 1-cm cuvettes.

The azo dye-derivatization method has been described earlier.[128] The rate constant of reaction between 16-ArN_2^+ and TBHQ in the emulsions was measured by trapping unreacted 16-ArN_2^+ with the reagent NED as a function of time. The half-life of the

reaction, $t_{1/2}$, between 16-ArN_2^+ and NED, Figure 2-3, is less than 5 s, much shorter than the rate

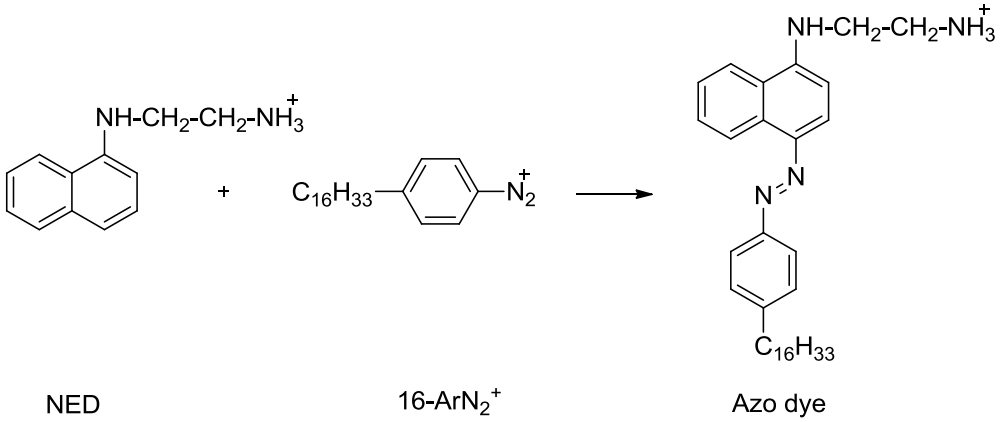

Figure 2-3 Reaction of the arenediazonium ion with *N*-(1-naphthyl)ethylenediamine (NED) in ethanol to give an azo dye.[128]

of reaction of TBHQ with 16-ArN_2^+, ca. 70-2000 s, and NED rapidly consumes unreacted 16-ArN_2^+. The UV-Vis absorbance of dye is linearly proportional to the concentration of unreacted 16-ArN_2^+.

2.2.4 Typical kinetic data processing

All kinetic data are processed in the same way to obtain the k_{obs}. All reactions run in excess TBHQ, [TBHQ] >> [16-ArN_2^+], and were first order in [16-ArN_2^+]. Values of k_{obs} were obtained from integrated first order expression for absorbance versus time,[129] equation s1, where A_t, A_o, and A_e are measured absorbance at any time t, at t = 0, and at t infinity, respectively, and the value of k_{obs} is obtained from the slope of the line.

$$\ln(A_t - A_e) = -k_{obs}t + \ln(A_o - A_e)$$

Figure 2-4 and Figure 2-5 show typical absorbance and ln Abs versus time plots used to obtain k_{obs}.

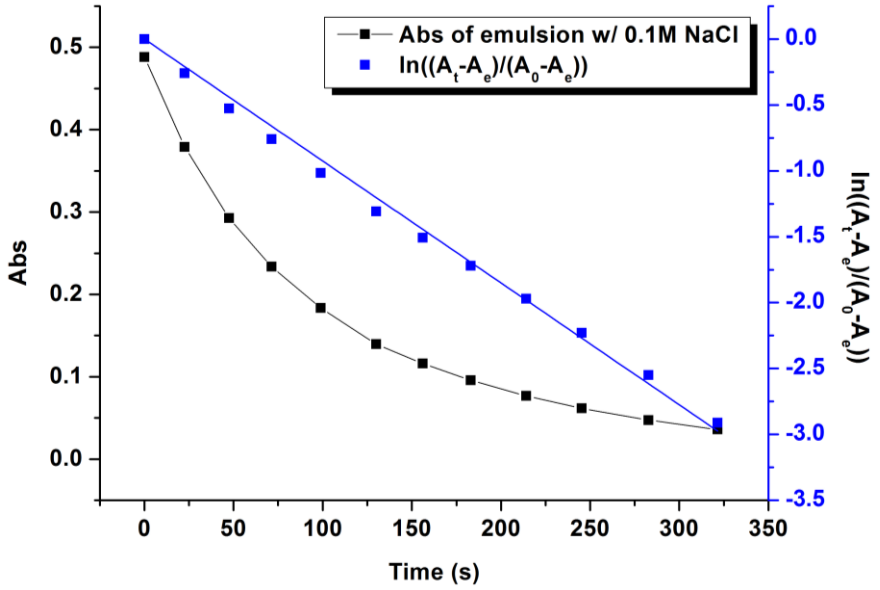

Figure 2-4 Absorbance and ln Abs versus time plots for emulsion with 0.1 M NaCl

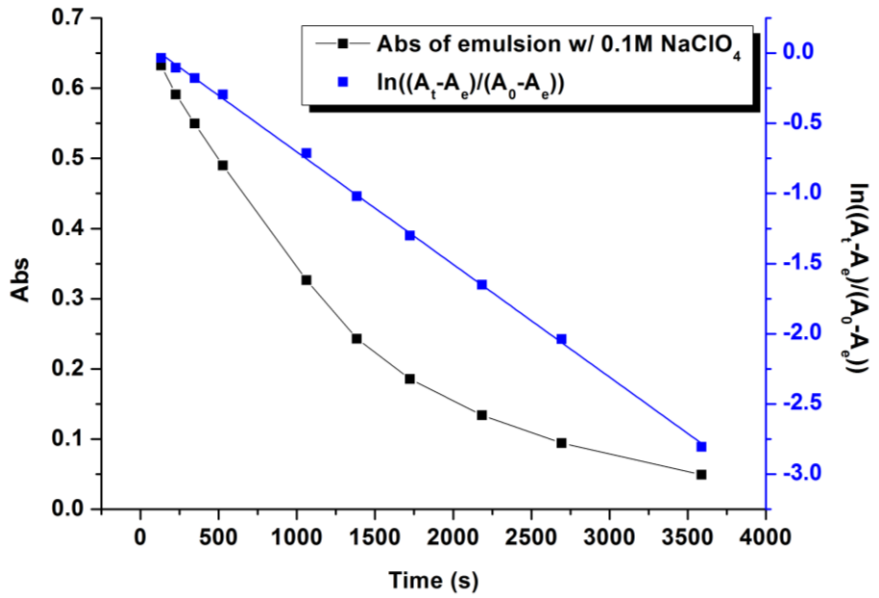

Figure 2-5 Absorbance and ln Abs versus time plots for emulsion with 0.1 M $NaClO_4$

2.3 RESULTS

The reduction of a benzenediazonium ion by hydroquinone, HQ, is an overall second order reaction that includes a single electron transfer reaction step between the benzenediazonium ion, PhN_2^+, and the anion of hydroquinone.[130] In aqueous solutions, log k_{obs} for HQ decreases with increasing solution acidity at pH values ≤ 9. At constant pH or $[H^+]$, the reaction is generally first order in PhN_2^+ and $[HQ^-]$.[130] Note, square brackets here and throughout the paper indicate concentration units of moles per liter of total emulsion volume. We assume that the basic mechanism for reaction of $TBHQ^-$ and 16-ArN_2^+ is the same, Figure 2-6, and that

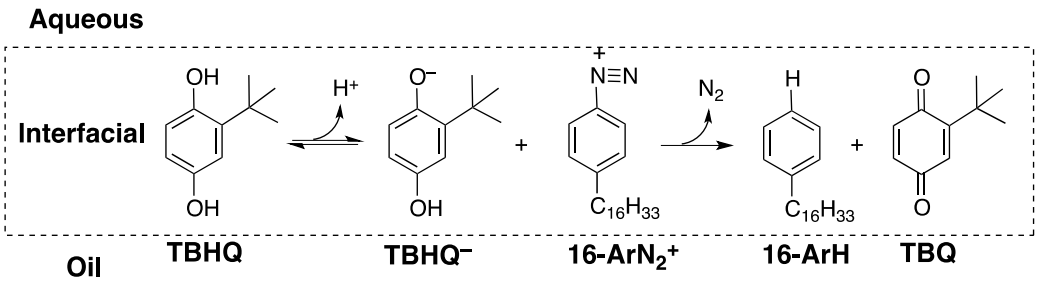

Figure 2-6 Overall reaction between 16-ArN_2^+ and TBHQ.

the observed rate is given by Equation 2-1,

$$\text{rate} = k_2[\text{16-Ar}N_2^+][\text{TBHQ}^-] = k_{obs}[\text{16-Ar}N_2^+]$$

Equation 2-1

where k_{obs} and k_2 are first and second order rate constants respectively, in units of s^{-1} and $M^{-1}s^{-1}$, K_a is the acidity constant of TBHQ, pK_a = 10.8.[131]

Figure 2-6 summarizes the reduction pathway of 16-ArN_2^+ by TBHQ showing deprotonation and reduction steps leading to the arene, 16-ArH, and *t*-butylquinone, TBQ products,[130] in the interfacial region of SB3-14 emulsions. At pH values in the vicinity of the pK_a of hydroquinone, 9.48,[132] the rate of reaction with PhN_2^+ is near the diffusion-controlled limit[130] and our results are consistent with this observation. To slow the reaction with TBHQ sufficiently to monitor it by the dye-derivatization method used here, the stoichiometric [H^+] was fixed at a single concentration for all runs at 1.5 mM in the whole emulsion. However, the measured pH varied somewhat with the salt added, Table 2-2. Under these conditions, [$TBHQ^-$] << [TBHQ] and [TBHQ] > 10 x [16-ArN_2^+] such that [TBHQ] is effectively constant.

Prior research on the reaction of 16-ArN_2^+ with TBHQ and other antioxidants in micelles, microemulsions and emulsions,[89, 119] is consistent with 16-ArN_2^+ being oriented in the interfacial region of surfactant aggregates with the surfactant headgroups, but the antioxidants are distributed between the oil, interfacial, and aqueous regions. Figure 2-7 shows the equilibria that influenced by the distribution of the

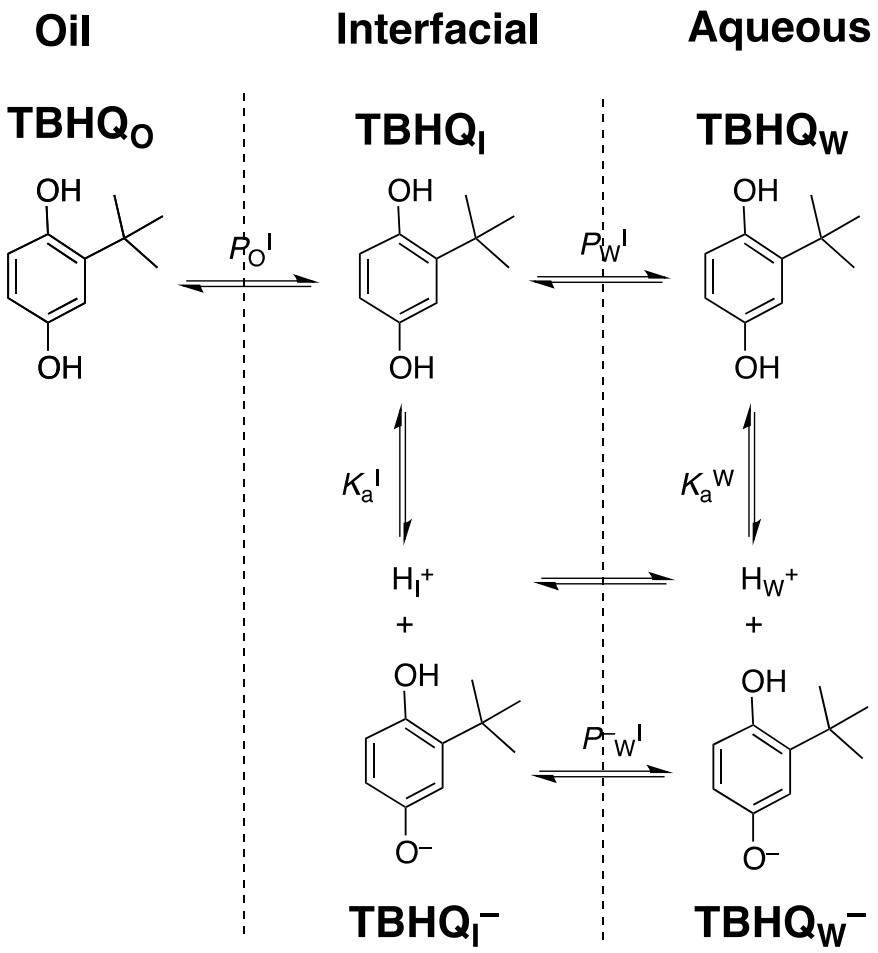

Figure 2-7 Distributions of TBHQ, $TBHQ^-$, and H^+ between the oil, interfacial and aqueous regions of an emulsion in aqueous acid.

proton, the acid-base equilibria of TBHQ, and the distributions of its acid and base forms between the oil, aqueous, and interfacial regions. The same conceptual models are used to fit acid-base equilibria in micelles[133, 134] and reactions in vesicles and microemulsions.[116, 117] Because 16-ArN_2^+ is located in the interfacial region, negligible reaction occurs in the oil and aqueous regions and the observed rate depends on [$TBHQ^-$] in the interfacial region, which in turn depends on the [H^+] in the interfacial region.

Figure 2-8 contains plots of k_{obs} versus [NaX] for 5 different sodium salts in emulsions of 1:1 vol:vol GTO:aqueous phase and the final concentrations in the whole emulsion are aqueous SB3-14 containing 2% by weight (0.055 M) SB3-14 and 1.5 mM HCl at 27 ℃. Stoichiometric anion concentrations range from 0 to 0.1 M. The results in Figure 2-8 clearly show that increasing [NaX] slows the TBHQ reduction of 16-ArN_2^+ and that anion effectiveness at decreasing k_{obs} follows the order: $ClO_4^- > Br^- \approx CCl_3CO_2^- > Cl^- > MeSO_3^-$. Other anions were not included for a variety of reasons, e.g., because they might react with the arenediazonium by some other mechanism, e.g., I^- or F^- (HF_2^- in acidic solution) or because they are not strong enough acids to be completely ionized in 3 mM HCl, e.g., acetic acid or bisulfate ions, whereas $MeSO_3^-$ is completely ionized and $CCl_3CO_2^-$ substantially ionized in aqueous 3 mM HCl, assuming the pK_as of the acids in the interfacial region and water are about the same. Finally, the five anions in the series are sufficient to demonstrate the trend and show that the effectiveness of the anions at slowing the reaction do not correlate with the pK_as of their conjugate acids.

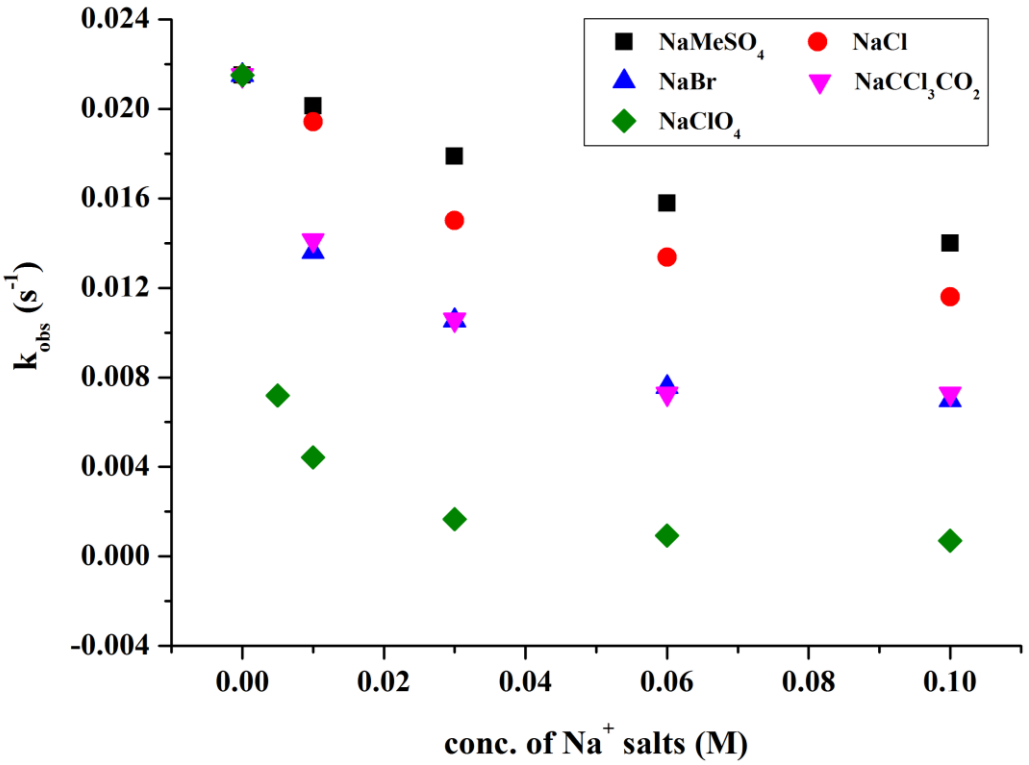

Figure 2-8 Effect of added NaX on k_{obs} for the reaction between 3.24×10^{-3} M TBHQ and 3.24×10^{-4} M 16-ArN_2^+ in an emulsion of 1:1 aqueous solution: GTO and the stoichiometric concentrations in emulsion are: 0.055 M (2% wt) SB3-14 and 1.5 mM HCl at 27 ℃.

Table 2-1 All values of the rate constants in Figure 2-8. Corresponding half lives are given in the parenthesis besides. For all sets of kinetic data, an average R^2 > 0.999 with a standard deviation of 0.001 for each reaction followed for 4-5 half lives were obtained. The high R^2 demonstrates the reliability of our kinetic data.

Conc. (M)	k_{obs} (s^{-1}) ($t_{1/2}$ s)				
	$NaMeSO_3$	NaCl	NaBr	$NaCl_3CO_2$	$NaClO_4$
0	0.0215 (32.1)				
0.005	--	--	--	--	0.00719 (96.0)
0.01	0.02012 (34.3)	0.01943 (35.5)	0.01360 (50.7)	0.01413 (48.8)	0.00442 (156.1)
0.03	0.01788 (38.6)	0.01501 (46.0)	0.01054 (65.5)	0.01058 (65.2)	0.00166 (415.7)
0.06	0.01579 (43.7)	0.01338 (51.6)	0.00756 (91.3)	0.00726 (95.0)	0.000929 (742.8)
0.1	0.01400 (49.3)	0.01161 (59.4)	0.00697 (99.0)	0.00727 (94.9)	0.000708 (974.6)

To illustrate the relative effectiveness of the different ions at inhibiting the reaction, Table 2-2 lists k_{obs} values at 0.1 M NaX, compared to k_{obs} at NaX = 0 M. Table 2-2 also shows the pK_a values of the five salts, the $k_{0MNaX}/k_{0.1MNaX}$ ratio, the factor by which k_{obs}

decreases from 0 to 0.1 M NaX, and the equivalent pH required to reduced k_{obs} by that factor in water.

Table 2-2 Comparisons of the effects of added 0.10 M NaX on k_{obs} for emulsions with the same compositions as in Figure 1. The table includes: k_{obs} values at 0.1 M NaX; ratios of k_{obs} values at 0.1 M NaX and 0 M NaX; approximate values for equivalent interfacial H^+ concentrations and the pH (see text); and literature pK_a values for the conjugate acids of each salt. a. Equivalent interfacial hydrogen ion molarity. b. pH (calculated interfacial pH) = log (0.003 M HCl*$k_{0.1MNaX}/k_{0MNaX}$) c. NSDL, http://nsdl.org/resource/2200/20061121124513540T, Aqueous pK_a Values, originally collected by W.P. Jencks and F.H. Westheimer and compiled by R. Williams.

Salt type	$NaMeSO_3$	NaCl	NaBr	$NaCCl_3CO_2$	$NaClO_4$
$10^2 k_{obs}$ (s^{-1})$_{0.0\ M\ NaX}$	2.15 (3 mM HCl, pH_{calc} = 2.52)				
$10^2 k_{obs}$ (s^{-1})$_{0.1\ M\ NaX}$	1.40	1.16	0.697	0.727	0.0708
$k_{0M\ NaX}/k_{0.1M\ NaX}$	1.54	1.85	3.09	2.96	30.4
$[H^+_I]$ mM[a]	4.62	5.55	9.27	8.88	91.2
pH[b]	2.34	2.26	2.04	2.05	1.04
pK_a (HX)[c]	–0.6	–9.3[180]	–9.00	0.65	–10 (70%)

Table 2-3 The concentrations of the different chloride salts when the concentration of Cl^- are fixed at 0.1 M and the bulk H^+ concentration in emulsions.

MCl_n (n = 1-3)	CsCl	$CaCl_2$	$AlCl_3$
Conc. (M)	0.10	0.050	0.033
$10^2 k_{obs}$ (s^{-1})	1.20	1.44	1.89
k_{obs}/k_{CsCl}	1.00	1.20	1.58
Emulsion bulk pH	2.58	2.59	2.45

Table 2-3 shows the effect of increasing cation valence on k_{obs} at Cl^- = 0.1 M. The corresponding [Cs^+], [Ca^{2+}] and [Al^{3+}] are 0.1 M, 0.05 M and 0.033 M, respectively. The stoichiometric concentration of HCl is 1.5 mM. The measured pH is approximately constant for CsCl and $CaCl_2$, and a bit smaller for $AlCl_3$. This decrease for Al^{3+} is probably not caused by hydrolysis because in this pH range, the amount of hydrolysis should be negligible.[135] In principle, increasing interfacial H^+ concentration should slow the reaction between 16-ArN_2^+ and TBHQ, however k_{obs} is increased by the addition of Ca^{2+} and Al^{3+} compared to Cs^+ and Na^+ at 0.1 M Cl^-. The increase in k_{obs} with metal ion valence suggests that added cations displace interfacial H^+ and the acid-base equilibrium for TBHQ shifts in favor of $TBHQ^-$ which speeds the reaction and therefore increases k_{obs}.

2.4 DISCUSSION

The kinetic results in stirred, opaque, SB3-14/GTO/aqueous acid emulsions are interpreted using the same basic pseudophase assumptions that we use to interpret the effect of nonionic emulsions on the reaction of TBHQ with the 16-ArN_2^+:[119] (a) the emulsion is

divided into three separate reaction regions, oil, interfacial, and aqueous; (b) neutral TBHQ partitions between all three regions;16-ArN_2^+, because of its cationic surfactant properties, is located only in the interfacial region which is also the site of reaction; (c) the distributions of TBHQ depend on the totality of the volumes of the oil, interfacial, and aqueous regions which are the same in all experiments and therefore TBHQ distribution is independent of droplet size; (d) the diffusivities of the reactants are near the diffusion-controlled, their distributions are in dynamic equilibrium and many orders of magnitude faster than the observed rate of reaction of TBHQ and 16-ArN_2^+. To a first approximation, the volume fraction of the interfacial region of 0.055 M SB3-14 is about 2% of the emulsion volume and the TBHQ volume is about 3% of the SB3-14 volume and the 16-ArN_2^+ volume is about 10 times smaller than that of TBHQ. Thus the interfacial regions of the emulsion droplets function as a uniform reaction medium just like the oil and water regions. The application of the pseudophase model to emulsions is strongly supported by the good first order kinetics obtained in all experiments reported here and in other emulsions,[119] For ionic and zwitterionic surfactants, the concept of specific ion binding by the interfacial region is also included.

The trends reported in Table 2-2 and Table 2-3, i.e., (a) the decrease in k_{obs} with increasing [NaX] and with increasing anion size; and (b) the increase in k_{obs} with increasing cation valence from +1 to +3, are consistent with prior specific ion effects produced by increasing anion concentration and size and with cation charge effects on reactions in zwitterionic micelles.[110, 112, 119] The distributions of components of wide ranging concentrations that populate the interfacial region, SB3-14 (headgroups and nearby methylenes in the tail), TBHQ, $TBHQ^-$, 16-ArN_2^+, H^+, Na^+, and anions, X^-, water and GTO,

are in dynamic equilibrium because their diffusivities are near the diffusion controlled limit and bulk stirring prevents phase separation. The reactive headgroup of 16-ArN_2^+ is located in the interfacial region with negligible amounts dissolved in the GTO and aqueous regions. The fraction of TBHQ associated with zwitterionic emulsion interfaces at 0.055 M SB3-14 is on the order of 90+%, assuming that it is similar to the binding of TBHQ to cationic and nonionic emulsions.[119, 120] Changes in k_{obs} are caused by changes in the concentration of the reactive anion, $TBHQ^-$, induced by added anion or cation effects on the interfacial H^+ concentration. Thus, the basic assumptions used in the pseudophase model for the treatment of indicator equilibria and rate constants for zwitterionic emulsions are the same as those used for zwitterionic micelles[110] and in pseudophase models of cationic and anionic micelles and emulsions.[119, 120] The only difference between micelles and emulsions at the molecular level of the chemical reaction is that emulsion droplets are much fatter.

Addition of NaX salts to zwitterionic micelles leads to selective binding of anions more than cations as noted above. Selective binding of anions produces a net negative charge on the micellar interface, Figure 2-1, as shown zeta potential measurements in the presence of added salt in which the micelles migrate toward the positive electrode.[110] The higher the concentration of added salt and the stronger the specific anion interaction with the SB3-14 micellar interfaces, the greater the negative charge on the micellar surface. The zeta potentials appear to approach a plateau at about 0.04 M, the highest concentration of NaX added, with the larger ions having greater zeta potentials, and the curves fit a Langmuir isotherm.[109, 110] However, chemical trapping experiments show that the plateau

is only apparent because the interfacial molarities of Cl^- and Br^- increase gradually, but continuously up to about 1 M added NaCl and NaBr.[113]

Micelles of zwitterionic surfactants with negatively charged surfaces attract cations, both H^+ and Na^+ of NaX salts, although the local concentrations of these ions and the strengths of their interactions with the sulfonate group are not sufficient to neutralize the net negative charge of the interfacial region as shown by the zeta potential experiments.[112] Increasing the interfacial H^+ concentration leads to protonation of $TBHQ^-$ to give TBHQ, Figure 2-7, which decreases [$TBHQ^-$] and k_{obs}, equation 1. The more strongly an anion associates with the interfacial region of SB3-14 emulsions the greater the increase in negative surface charge, the greater the increase in interfacial H^+ (and Na^+), thus increasing the degree of protonation of $TBHQ^-$, and reducing k_{obs}. This explanation accounts for the Hofmeister order observed in Figure 2-8 and shown in Table 2-2 at 0.1 M NaX. Finally, the zeta potential becomes more negative with added ClO_4^- than Cl^- in micellar solutions of zwitterionic hexadecyl phosphorylcholine [136] showing that specific anion binding is more important than the location of the charges on the headgroup because the negatively charged phosphate is adjacent to the core instead of the quaternary ammonium group as in SB3-14.

Addition of the constant 0.1 M Cl^- molarity of the salts of the three cation salts of increasing valence, Table 2-3, increase k_{obs} in the order $Cs^+ < Ca^{2+}$ (20% increase) < Al^{3+} (60% increase). Note that in the pH range of these experiments, Cl^- does not form strong complexes with Al^{3+} and complexes of the lower valence ions will be weaker.[137, 138] These cations may complex the sulfonate group of SB3-14 to an increasing extent and give the interfacial region a net positive charge.[112] Increasing the non reactive cation concentration

in the interfacial region reduces the interfacial H^+ concentration and shift the acid-base equilibrium of TBHQ in favor of $TBHQ^-$, Figure 2-7, and increase k_{obs} as observed.

2.5 CONCLUSIONS

The anion and cation specific salt effects (up to 0.1 M added salt) on k_{obs} for reaction of *t*-butylhydroquinone with an amphiphilic arenediazonium ion in GTO and SB3-14 emulsions follow the Hofmeister series for the anions ($ClO_4^- > Br^- \approx CCl_3CO_2^- > Cl^- > MeSO_3^-$) and ion valence for cations ($Cs^+ < Ca^{2+} < Al^{3+}$). These results are fully consistent with the pseudophase kinetic models used in micelles and demonstrate that these models are applicable not only to homogeneous surfactant solutions, but also stirred, two-phase emulsions prepared with sulfobetaine zwitterionic surfactants. The results also suggest that "tuning" the rates of acid-sensitive reactions in zwitterionic emulsions can be accomplished by selecting the right salt concentration and anion type, may be useful in phase transfer catalysis[125] or for promoting reactions between water insoluble organic substrates that are catalyzed by acid or base or react with nucleophiles.[126]

Chapter 3 Specific Ion Effects on the Micellization of Gemini Surfactants with Different Counterions

The research is about specific counterions effects on the properties of gemini surfactant 10-2-10 2X (X represents carboxylates groups from formate (C1) to octanoate (C8). It is conducted from 2 approaches. One is measuring physical properties of the micellar solution such as critical micelle concentration (cmc), aggregation number (N_{agg}), ionization degree (α) and free energy of micellization ($\Delta G°_M$). The second approach is to measure interfacial molarity of the counterions with chemical trapping method that was developed in our group. The results show that as the hydrophobicity of the counterions increases, the physical properties and interfacial counterion concentrations change synchronously, and the variations of macroscopic and microscopic properties are well correlated, especially for ionization degrees and the interfacial counterion concentrations.

3.1 INTRODUCTION

Since Franz Hofmeister first reported specific ion effects on protein precipitation, scientists have carried out thousands of studies on specific ion effects on surfactant aggregates which can be used as a prototype of protein surface.[3, 139, 140, 141, 142, 143, 144] The effectiveness orders of anions and cations are called the Hofmeister Series. The micellar interfaces are good model systems for biological interfaces because many surfactants have carboxylate and ammonium functional groups, which are common polar functional groups at protein interfaces. The micelle interface is a hydrophobic/water interface, which is

similar to the interface of proteins and biomolecules. So the studies on the specific ion effects in micellar solutions can provide meaningful guidance to the understanding of salt effects in biological areas.[145, 146]

Specific ion effects on surfactants properties such as solubility, critical micelle concentration, aggregation number and ionization degree generally follow the Hofmeister series.[3, 5, 6, 50, 147, 148, 149, 150] Classical theories that treat ions as point charges can not explain the Hofmeister Series as noted in Chapter 1. Many attempts have been made to correlate the Hofmeister series with various ion properties, for example the free energy and entropy of hydration, free energy of transfer from an aqueous to organic phase, partial molar volume, hydrated ionic radius and polarizability.[41, 151, 152, 153] However there is still a lack of satisfactory explanation to the Hofmeister Series at molecular level. The ultimate goal of this research is to find a general model that explains the Hofmeister series and also predicts the behavior of uninvestigated ions in new systems. For micellar systems, the key to understanding the change of their various physical properties is knowing about the subtle balance of interactions between water molecules, headgroups, counterions and hydrophobic tails at the interface. Ions affect the balances of these forces at the interface, and the subtle balances finally determine the physical and chemical properties of the micellar systems.[16]

Our collaborator Dr. Reiko Oda's group has investigated ion specific effects on various properties of cationic surfactants, such as micellization, solubilization and melting behaviors.[3, 54] The aliphatic carboxylate ions show clear trends in their effects on the cmc, aggregation number, ionization degree and micellization free energy. They are good models to show the effect of counterion hydrophobicity on micelles properties. However,

although the specific ion effects of ions on bulk properties of micelles have been intensively studied, their effects on microscopic interface properties were rarely explored. In this chapter, I used chemical trapping method to determine the local concentrations of carboxylate counterions at gemini surfactant micelles interface. The physical properties such as cmc, aggregation number and ionization degree were measured and correlated to the interfacial counterion concentrations.

As introduced in Chapter 1, chemical trapping method was developed to estimate the interfacial molarities of counterions and water on the micellar interface.[99, 154, 155] Reference experiments were carried out in aqueous carboxylate solutions with 1-ArN_2^+, the standard curves for reactions between carboxylates and arenediazonium ion were obtained. Applying the standard curve onto the results of 16-ArN_2^+ reactions in carboxylate gemini surfactant micellar solutions will finally give the interfacial concentrations of carboxylate counterions and water molecules at the micelles interface. Previous results from our group[53] confirmed that in the solutions containing mM scale concentration of surfactants the interfacial molarities of counterions can reach 1.0 – 3.0 M, which means there is a dramatic concentrating effect on counterions as they transfer from bulk phase to micelle interfaces. Ion types and stoichiometric concentrations also have significant effects on counterions association onto the interface through influencing the delicate balances of various interactions on micelles surface.[3, 144, 155]

This study is a part of a larger study on the specific counterions effect on cationic gemini surfactant 10-2-10 2X micelles with chemical trapping experiments and MD simulations. In this study the interfacial molarities of counterions and H_2O in 10-2-10 2X gemini surfactant micelles with X = acetate (C2), propionate (C3) and butyrate (C4) were

estimated. The results were compared with the measured cmc, aggregation number and ionization degree to correlate the microscopic and macroscopic properties obtained in Bordeaux by our collaborators.

3.2 EXPERIMENTAL SECTION

3.2.1 Synthesis of gemini surfactants

Quaternary ammonium 10-2-10 2X gemini surfactant with different counterions were synthesized according to the procedure reported for 14-2-14 2X salts by Manet et al.[3] with modification.

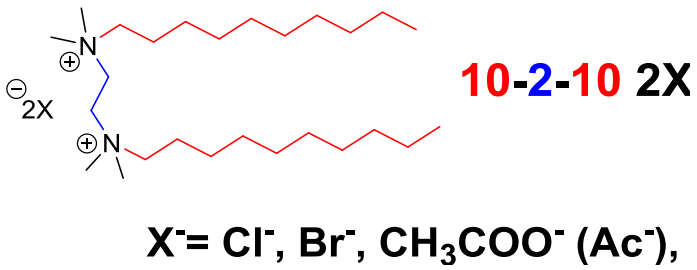

Figure 3-1 Molecular structure of 10-2-10 2X gemini surfactant

10-2-10 2Br was synthesized by a dialkylation reaction of *N*,*N*,*N'*,*N'*-tetra-methylethylenediamine (TMEDA) with decylbromide. It is used as a starting material to synthesize other gemini surfactants. The following synthetic routes were selected based on the pK_a of the conjugate acid of counterions: if the pK_a of the conjugate acid of counterions is higher than 3, then the gemini surfactants can be synthesized by the following reaction:

$$\mathrm{HX} + \mathrm{Ag_2CO_3} + 10-2-10\ 2\mathrm{Br} \rightarrow 10-2-10\ 2\mathrm{X} + \mathrm{AgBr}$$

where X can be various carboxylates. If the pK_a of the conjugate acid of counterions is lower than 3, then the gemini surfactants can be synthesized with the help of 10-2-10 2Ac:

$$2\mathrm{AgAc} + 10-2-10\ 2\mathrm{Br} \rightarrow 10-2-10\ 2\mathrm{Ac} + 2\mathrm{AgBr}$$

$$2\mathrm{HX} + 10-2-10\ 2\mathrm{Ac} \rightarrow 10-2-10\ 2\mathrm{X} + 2\mathrm{HAc}$$

where X can be various halides, SCN^-, etc. Specific synthesis steps are described below.

Synthesis of 10-2-10 Br

1-bromodecane (62.2 mL, 65.94 g, 298 mmol) was added to an MeCN solution (120 mL) of *N*,*N*,*N*'*N*'-tetramethylenediamine (15 mL, 11.55 g, 99.4 mmol) at molar ratio 1:3 and the reaction mixture was stirred at 80 ℃ for 48 h. The mixture was cooled to 4 ℃ and the precipitate was filtered and washed with acetone (3x500 mL), dried under vacuum and lyophilized. 10-2-10 2Br was obtained as a white solid in 85% yield (47.2 g, 84.5 mmol). ^{1}H NMR (300 MHz, methanol-D_4, 25˚C, δ in ppm): δ = 4.06 (s, 4H, $(CH_3)_2N^+$-($\underline{CH_2}$)$_2$-$N^+(CH_3)_2$), 3.51 (m, 4H, CH_3-$(CH_2)_7$-CH_2-$\underline{CH_2}$-N^+-), 3.28 (s, 12H, ($\underline{CH_3}$)$_2N^+$-$(CH_2)_2$-N^+($\underline{CH_3}$)$_2$), 1.85 (m, 4H, CH_3-$(CH_2)_7$-$\underline{CH_2}$-CH_2-N^+), 1.42-1.31 (m, 28H, CH_3-($\underline{CH_2}$)$_7$-CH_2-CH_2-N^+), 0.90 (t, 6H, $\underline{CH_3}$-$(CH_2)_9$-N^+). ^{13}C NMR (300 MHz, MeOD, 25˚C, δ in ppm): 65.6 ($^+NCH_2$), 55.8 ($^+NCH_2$), 50.5 ($^+NCH_3$), 31.7 (CH_2), 29.3 (CH_2), 29.2 (CH_2), 29.1 (CH_2), 28.9 (CH_2), 25.9 (CH_2), 22.4 (CH_2), 22.3 (CH_2), 13.1 (CH_3).

Synthesis of 10-2-10 2Ac

Silver acetate (22.41 g, 134.3 mmol) was added to a MeOH solution (200 mL) of 10-2-10 2Br (30 g, 53.7 mmol) at a molar ratio of 2.5:1. The flask was wrapped in aluminum foil to block the light, and the solution was stirred at 40 ˚C until the completion of the

acetate-bromide ion exchange. Product was analyzed by ^{1}H NMR to check the appearance of a signal at 1.90 ppm, which belongs to the methyl group of acetate anion. Small amount of unreacted gemini bromide cannot be detected by ^{1}H NMR, so an additional method was applied. An aliquot of the reaction mixture was taken and an excess of silver acetate was added to this aliquot, followed by heating the mixture at 60 ℃ for 10 min to accelerate the anion exchange between acetate and Br^-. Then the mixture was exposed to light. If the ions exchange was not complete, this mixture would become black due to the AgBr reduce to black silver metal and molecular Br_2. If the exchange reaction was complete, the test will be negative, and no black silver metal will be produced. After the reaction is completed, the mixture was filtered through celite. After vacuum evaporation of the solvent, the residue was redissolved in MeOH at 60 ℃ and then recrystallized with 700 mL of acetone. 10-2-10 2Ac was obtained as white crystals in 70% yield (19.4 g, 37.6 mmol). ^{1}H NMR (300 MHz, MeOD, 25 ˚C, δ in ppm): δ = 3.94 (s, 4H, $(CH_3)_2N^+$-($\underline{CH_2}$)$_2$-N^+-$(CH_3)_2$), 3.42 (m, 4H, CH_3-$(CH_2)_7$-CH_2-$\underline{CH_2}$-N^+-), 3.20 (s, 12H, ($\underline{CH_3}$)$_2$-N^+-$(CH_2)_2$-N^+-($\underline{CH_3}$)$_2$), 1.90 (s, 6H, $\underline{CH_3}$-COO^-), 1.82 (m, 4H, CH_3-$(CH_2)_7$-$\underline{CH_2}$-CH_2-N^+-), 1.41-1.30 (m, 28H, CH_3-($\underline{CH_2}$)$_7$-CH_2-CH_2-N^+-), 0.90 (t, 6H, $\underline{CH_3}$-$(CH_2)_9$-N^+-). ^{13}C NMR (300 MHz, MeOD, 25˚C, δ in ppm): 178.7 (C=O), 65.6 ($^+NCH_2$), 55.7 ($^+NCH_2$), 50.3 ($^+NCH_3$), 31.7 (CH_2), 29.3 (CH_2), 29.2 (CH_2), 29.0 (CH_2), 28.9 (CH_2), 25.9 (CH_2), 23.2 (CH_3CO_2), 22.4 (CH_2), 22.3 (CH_2), 13.1 (CH_3).

Synthesis of 10-2-10 2X surfactants with carboxylate counterions, C3, C4, C6, C8

Since the conjugate acid of the carboxylate counterions have pK_a > 3, the gemini surfactant was prepared by mixing Ag_2CO_3 (0.75 eq.) and HX (1 eq., X = C3, C4, C6, C8) in MeOH (75 mL) under continuous stirring at 40 ℃ for 30 min. Then 10-2-10 Br (0.4 eq.)

dissolved in 75 mL MeOH was added into the mixture, and stirred at the 40 ℃ for 2 days. To prevent photolysis of silver salt, aluminum foil was used to protect the reaction mixture from light.

When the reaction was finished, the solvent was concentrated under vacuum and the silver salts were removed by filtration through celite for several times. Then the excess methanol was evaporated off. Impure C3-C4 gemini surfactants crystals were recrystallized from 10 mL CH_3CN at 60 ^oC. Impure C6-C8 gemini surfactants were recrystallized from the methanol/acetone solvent pair at 60 ^oC. Recrystallization needed to be repeated for several times until the crystals became white powder. Final products were dried under vacuum. The yields were between 70-80% for all gemini surfactants. 10-2-10 2C3 ^1H NMR (300 MHz, MeOD, 25˚C, δ in ppm): δ = 3.94 (s, 4H, $(CH_3)_2N^+$-($\underline{CH_2}$)$_2$-N^+-$(CH_3)_2$), 3.42 (m, 4H, CH_3-$(CH_2)_7$-CH_2-$\underline{CH_2}$-N^+-), 3.21 (s, 12H, ($\underline{CH_3}$)$_2$-N^+-$(CH_2)_2$-N^+-($\underline{CH_3}$)$_2$), 2.22 (m, 4H, CH_3-$\underline{CH_2}$-COO^-), 1.83 (m, 4H, CH_3-$(CH_2)_7$-$\underline{CH_2}$-CH_2-N^+-), 1.41-1.30 (m, 28H, CH_3-($\underline{CH_2}$)$_7$-CH_2-CH_2-N^+-), 1.10 (t, 6H, $\underline{CH_3}$-CH_2-COO^-), 0.90 (t, 6H, $\underline{CH_3}$-$(CH_2)_9$-N^+-).

10-2-10 2C4 ^1H NMR (300 MHz, MeOD, 25˚C, δ in ppm): δ = 3.94 (s, 4H, $(CH_3)_2N^+$-($\underline{CH_2}$)$_2$-N^+-$(CH_3)_2$), 3.42 (m, 4H, CH_3-$(CH_2)_7$-CH_2-$\underline{CH_2}$-N^+-), 3.21 (s, 12H, ($\underline{CH_3}$)$_2$-N^+-$(CH_2)_2$-N^+-($\underline{CH_3}$)$_2$), 2.13 (m, 4H, CH_3-CH_2-$\underline{CH_2}$-COO^-), 1.65-1.52 (m, 4H, CH_3-$\underline{CH_2}$-CH_2-COO^-), 1.41-1.30 (m, 28H, CH_3-($\underline{CH_2}$)$_7$-CH_2-CH_2-N^+-), 0.94-0.87 (m, 12H, $\underline{CH_3}$-$(CH_2)_9$-N^+- + $\underline{CH_3}$-CH_2-CH_2-COO^-).

10-2-10 2C6 ^1H NMR (300 MHz, MeOD, 25˚C, δ in ppm): δ = 3.94 (s, 4H, $(CH_3)_2N^+$-($\underline{CH_2}$)$_2$-N^+-$(CH_3)_2$), 3.42 (m, 4H, CH_3-$(CH_2)_7$-CH_2-$\underline{CH_2}$-N^+-), 3.21 (s, 12H, ($\underline{CH_3}$)$_2$-N^+-$(CH_2)_2$-N^+-($\underline{CH_3}$)$_2$), 2.13 (m, 4H, CH_3-CH_2-CH_2-CH_2-$\underline{CH_2}$-COO^-), 1.65-1.52 (m, 4H, CH_3-

CH_2-CH_2-$\underline{CH_2}$-CH_2-COO^-), 1.38-1.29 (m, 36H, CH_3-$(\underline{CH_2})_7$-CH_2-CH_2-N^+- + CH_3-$\underline{CH_2}$-$\underline{CH_2}$-CH_2-CH_2-COO^-), 0.94-0.87 (m, 12H, $\underline{CH_3}$-$(CH_2)_9$-N^+- + $\underline{CH_3}$-CH_2-CH_2-CH_2-CH_2-COO^-).

10-2-10 2C8 ^{1}H NMR (300 MHz, MeOD, 25˚C, δ in ppm): δ = 3.94 (s, 4H, $(CH_3)_2N^+$-$(\underline{CH_2})_2$-N^+-$(CH_3)_2$), 3.42 (m, 4H, CH_3-$(CH_2)_7$-CH_2-$\underline{CH_2}$-N^+-), 3.21 (s, 12H, $(\underline{CH_3})_2$-N^+-$(CH_2)_2$-N^+-$(\underline{CH_3})_2$), 2.13 (m, 4H, CH_3-CH_2-CH_2-CH_2-CH_2-CH_2-$\underline{CH_2}$-COO^-), 1.65-1.52 (m, 4H, CH_3-CH_2-CH_2-CH_2-CH_2-$\underline{CH_2}$-CH_2-COO^-), 1.41-1.31 (m, 44H, CH_3-$(\underline{CH_2})_7$-CH_2-CH_2-N^+- + CH_3-$\underline{CH_2}$-$\underline{CH_2}$-$\underline{CH_2}$-$\underline{CH_2}$-CH_2-CH_2-COO^-), 0.94-0.87 (m, 12H, $\underline{CH_3}$-$(CH_2)_9$-N^+- + $\underline{CH_3}$-CH_2-CH_2-CH_2-CH_2-CH_2-COO^-).

3.2.2 Chemical Trapping Experiments

Chemical trapping reactions were conducted in gemini surfactants micellar solutions following the routine procedure. Percent yields of products %16-ArOH and %16-ArX (X = C2, C3 and C4) were measured by HPLC. A parallel set of trapping experiments were conducted with 1-ArN_2^+ in aqueous MX solutions to determine the selectivity of arenediazonium ion toward X^- and H_2O at each [MX]. The selectivity values in MX solutions were not constant, but gradually decreased with increasing MX concentration as observed in these and prior experiments. Following the rule mentioned before, *when the yields are the same, the concentrations are the same*, so when the yield of %16-ArX in the micellar interface are the same as the yield of %1-ArX in MX solution, the interfacial molarity of X^- of the micelles are the same as the bulk molarity of X^- in the MX solution.[100]

Longer counterions such as C6 was not considered in the experiment because phase separation occurs when HC6 was added into the micellar solution to adjust pH and there was no effective mixing methods that made the situation better. The aqueous solution of the analog salt of the surfactant headgroup 1-2-1 2C2 was chosen to be the reference system. The standard curve obtained from 1-2-1 2C2 solution was applied to the experimental data of 10-2-10 2C2, 10-2-10 2C3 and 10-2-10 2C4 chemical trapping experiments, meaning that the selectivity of arenediazonium ions towards all three carboxylates and water was the same, because the carboxylates share the same functional group. The measurement of 1-2-1 2C2 standard curve and the identification of related products were carried out by Dr. Changyao Liu and they are summarized in the supplementary information section. The details of 10-2-10 2X and 1-2-1 2X experiments are described below.

General Methods

HPLC measurements were performed on a Perkin-Elmer Series 200 equipped with a UV/Vis detector, a Varian Microsorb MV C_{18} column (length, 25 cm; particle size, 5 μm), and a computer-controlled Perkin-Elmer 600 Series Interface. All pH values were obtained by a Fisher AR50 dual channel pH/Ion/Conductivity Meter. ^{1}H NMR spectra were recorded on Varian VNMRS 400 and 500 MHz spectrometers.

Standard curve obtained in aqueous 1-2-1 2C2 reference solutions with 1-ArN_2^+

Before experiment the 1-2-1 2C2 was vacuum dried for several days until it reached constant weight. During experiment the calculated salt was weighed in a 10 mL flask and water was added to the mark. The weight of added water was measured as well. The weights of water and salt were used to calculate the molarities of C2 and H_2O. The 1-2-1

2C2 solutions are basic ($CH_3CO_2^-$ + H_2O -> CH_3CO_2H + OH^-) and were acidified by adding glacial acetic acid (HCl was not used here because Cl^- would compete 1-ArN_2^+ with C2). The solutions were titrated to ca. pH 6. The titration was monitored by using a pH meter. To initiate the dediazoniation reactions, 10-20 μL of freshly prepared stock solution of 1-ArN_2BF_4 in ice-cold MeCN was added to give a final probe concentration of 4-4.5 x 10^{-3} M. 50-100 μL of cyclohexane were layered on top of the solutions to prevent the evaporation of volatile 1-ArX and 1-ArOH products (the long chain products, 16-ArX and 16-ArOH, are not volatile). The volumetric flasks were sealed with Parafilm and equilibrated at 25 ^oC for 24 hours. Prior to HPLC analysis, the product mixture was diluted 5-fold with MeOH to dissolve the cyclohexane and the aqueous salt solution. HPLC conditions for products separation were the following: an 80% MeOH/20% H_2O (v/v) mobile phase; flow rate = 0.6 mL/min; detector wavelength λ = 230 nm; the injection volume was 50 μL. Percent yields were obtained from average values of peak areas from triplicate injections. The standard curve of acetate was measured by Dr. Changyao Liu as shown in Figure 3-2, even though the S_W^{Ac} scatters at higher 1-2-1 2Ac concentration, the fluctuation is within ±10%. The standards curve of other carboxylates were assumed to be the same as acetate because they share the same functional group. The selectivities of carboxylates used during calculation are listed in Table 3-3 - Table 3-5 in section 3.6, Supporting Information.

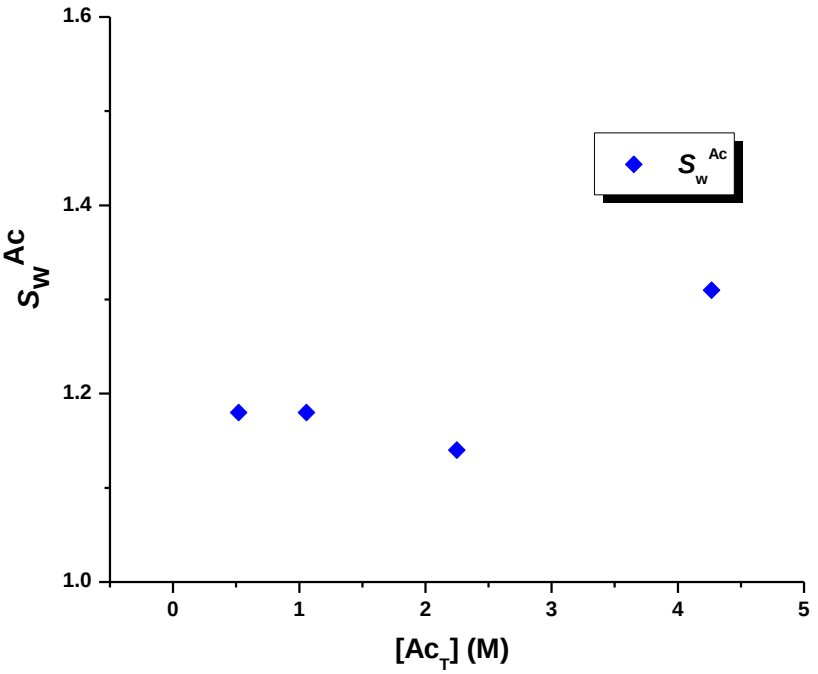

Figure 3-2 S_W^{Ac} as a function of [Ac^-] measured in analog 1-2-1 2Ac solutions at 25 °C and pH6. Detail information can be found in Table 3-9, Supporting Information

Chemical trapping experiments with 16-ArN_2^+ in aqueous 10-2-10 2C2, 2C3, 2C4 micellar solutions

2 mL 10-2-10 2X aqueous surfactant solutions were prepared at different concentrations (surfactants concentrations can be found on the x axis of Figure 3-5). Prior to the addition of 16-ArN_2BF_4, the solutions were titrated dropwise to ca. pH 5 (different from 1-2-1 2C2 experiments, 10-2-10 2X experiments need a lower pH to suppress the side products) with corresponding conjugate acids of counterions (HX, X = C2, C3, C4). Then

20 μL freshly prepared stock solutions of 16-ArN_2BF_4 dissolved in ice-cold MeCN was added to the 2 mL 10-2-10 2X micellar solutions. The final probe concentration was around 10^{-4} M. The volumetric flasks were sealed and thermostated at 25 ^{o}C for 24 hours. HPLC conditions for products separation were: a 65% MeOH/35% i-PrOH (v/v) mobile phase; flow rate = 0.4 ml/min; detector λ = 220 nm; and the injection volume was 100 μL. Percent yields were obtained from average peak areas of triplicate experiments. Figure 3-3 shows a typical chromatogram of the reaction products of 16-ArN_2^+ in 10-2-10 2X solutions. The amount of HX used in experiments and the final products yields are listed in Table 3-10, Table 3-11, and Table 3-12 in the supplementary information session.

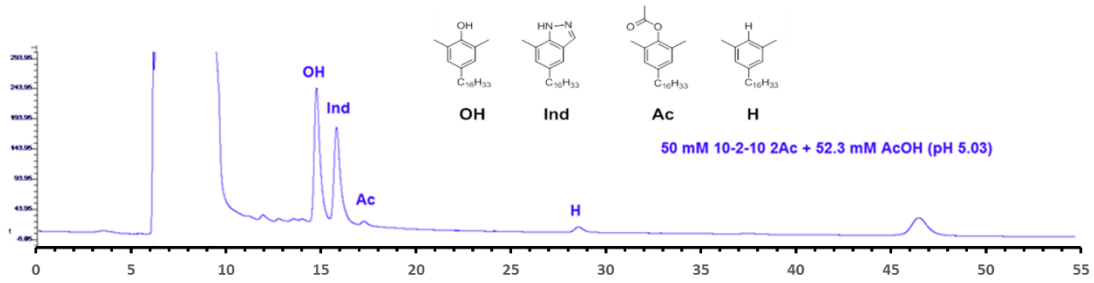

Figure 3-3 Typical chromatogram of 16-ArN_2^+ reaction in 10-2-10 2C2 solution. Reactions in other 10-2-10 2X (X = C3, C4) will generate similar chromatograms. The peak at ~47 minutes is an unknown peak and details are in the Discussion section.

3.2.3 Electrical conductivity measurements

Critical micelle concentration (cmc) values (Table 3-7) were measured by using a Benchtop CONSORT C860 meter with platinum electrode SK10T (Belgium). The temperature was maintained at 30 ± 0.1 ˚C using a Huber Ministat cc thermostat.

All solutions were prepared with milliQ water (18.2 MΩ·cm). The surfactant concentration was increased by adding aliquots of a concentrated stock solution (0.1 M).

At each concentration the solution was stirred for 5-10 min to ensure equilibrium was reached prior to collecting data. The cmc was determined by using the Williams and Phillips method,[156] which linearly fits the both linear parts of the conductivity plot below and above the cmc. The intersection point is the cmc.[81]

3.2.4 Ionization degree, α

The degree of ionization was obtained by using both the original equation defining α_Z and Evans' method, as introduced in Chapter 1. The original method is straightforward: the ionization α_Z is a ratio of the slopes of the conductivity plot above and below the cmc:[81]

$$\alpha_Z = S_2 \,/\, S_1$$

Equation 3-1

where S_1 is slope of the specific conductivity as a function of concentration below the cmc, S_2 is slope of the specific conductivity as a function of concentration above the cmc.

Evans Equation 3-2 also provides an estimate of α with the 2 slopes above and below the cmc:[157]

$$S_2 = \alpha_E{}^2 N_{agg}^{2/3}(S_1 - \lambda_X) + \alpha\lambda_X$$

Equation 3-2

where λ_X represents the equivalent molar conductivity of the surfactant counterion, and α_E is the Evans ionization degree. However, because gemini surfactants have two headgroups and two chains per amphiphile monomer, Equation 3-2 must be corrected by multiplying λ_X with 2,[3] giving Equation 3-3:

$$S_2 = {\alpha_E}^2 N_{agg}^{2/3}(S_1 - 2\lambda_X) + \alpha_E 2\lambda_X$$

Equation 3-3

Note that Nagg was measured at 2x cmc and 3x cmc in our study. Nagg cannot be determined at the cmc concentration because only a very small fraction of the surfactant monomer aggregate to micelles.

3.2.5 Free energy of micellization

The Gibbs energy of micellization $\Delta G°_M$ of single chain ionic surfactants is usually given by the equation:[158]

$$\Delta G_M^o = RT(1+\beta)\ln cmc$$

Equation 3-4

where β is the counterion degree of binding by definition ($\beta = 1 - \alpha$), and calculated by using the ionization degree estimated from Evans' model. R. Zana [158] described $\Delta G°_M$ equations for the different types of ionic surfactants by taking into account various factors such as the numbers of hydrophobic and hydrophilic substructures per molecule, per charge, and per numbers of counterions, headgroups and added salt, etc.. For gemini surfactants with two monovalent headgroups linked to two tails and two monovalent counterions, the free energy of micellization per mole of surfactant is:[86]

$$\Delta G_M^o = RT(0.5+\beta)\ln cmc_{chain} - RT * \ln 2\ /2$$

Equation 3-5

Where cmc_{chain} is the molarity of each alkyl chain, so in Equation 3-5

$\mathrm{cmc}_{\mathrm{chain}} = 2 * \mathrm{cmc}_{\mathrm{gemini\ surfactant}}$.

3.2.6 Aggregation Numbers

The average aggregation numbers (Nagg) of the micelles for the different surfactants were determined by using time-resolved fluorescence quenching.[159, 160, 161] The fluorescence decay curves were recorded on a FL3-22 SPEX spectrofluorometer equipped with a pulsed nanosecond LED excitation source at ambient temperature. The excitation wavelength was 310 nm, and the emission was at 370 nm. 1-methylpyrene and cetylpyridinium chloride were used as the fluorescent probe (P) and quencher (Q), respectively. The measurements were carried out at surfactant concentrations of 2x cmc, and a probe concentration of 2 – 3 μM was chosen to minimize excimer formation. The decay of emission was recorded in absence of quencher, giving a lifetime of τ_0(P*) of around 110 ns (in the case of Br^- counterions, a shorter lifetime of ca. 70 ns was obtained, presumably due to the external heavy atom effect of Br^-). Fluorescence decays were recorded at different quencher concentrations [Q] and hence different quencher/micelle molar ratios. The average number of quencher molecules per micelle ranges between 0.2 and 1.3. The fluorescence decay curves were recorded on a FL3-22 SPEX spectrofluorometer at ambient temperature.

To obtain the aggregation number, the data was analyzed using Equation 3-6 based on the Infelta-Tachiya model:[162]

$$I(t) = A_1 \mathrm{exp}[-A_2 t - A_3\{1 - exp(-A_4 t)\}$$

Equation 3-6

where A1 is the fluorescence intensity at time equals zero $I(0)$; A2 the fluorescence decay constant in the absence of Q; A3 is the average occupation number of quenchers per micelle (<n>); and A4 is the quenching rate constant for the reaction between the quencher and the excited probe within the micelle (kQ). A3 is the parameter that we need. The fluorescence decay curves were fitted to Equation 3-6 using a non-linear least-squares fitting program provided with the instrument or with the program developed by Boens et al.[163] The aggregation number for each sample (Nagg) was calculated using Equation 3-7:

$$N_{agg} = < n > \frac{(C - cmc)}{[Q]}$$

Equation 3-7

where C is total surfactant concentration and [Q] the quencher concentration.[159, 160, 161]

3.3 RESULTS

3.3.1 Physical chemical properties of carboxylate gemini surfactants

The cmc, α_Z, α_E and $\Delta G°_M$ of 10-2-10 gemini surfactants with carboxylic counterions are listed in Table 3-1. The values of the cmc and α vs. counterion chain length are plotted against chain length in Figure 3-4. Except 10-2-10 2C1, other carboxylate surfactants' cmc and two α values decrease with increasing chain length of the counterions, and the relationship between cmc and chain length is quite linear, indicating that counterion hydrophilicity decreases as chain length increases while the polar functional group keeps the same. For a group of surfactants with same headgroup, *lg(cmc)* decreases linearly with

increasing monomer chain length: $lg(cmc) = A - B*n$, where n is the chain length of monomer.[164]

Counterion	Temperature, °C	CMC, mM	α_Z	α_E	$-\Delta G°_M$, kJ·mol^{-1}
C1	30	21.7	0.49	0.23	10.88
C2	30	22.7	0.52	0.26	10.25
C3	30	20.0	0.38	0.22	11.30
C4	30	14.3	0.33	0.21	12.09
C5	30	9.4	0.28		
C6	30	5.7	0.22		
C8	30	1.0	0.10		

Table 3-1 Physical properties (cmc, α_Z, α_E and $\Delta G°_M$) of 10-2-10 2X (X=C1~C8) gemini surfactant micelles measured at 30°C.

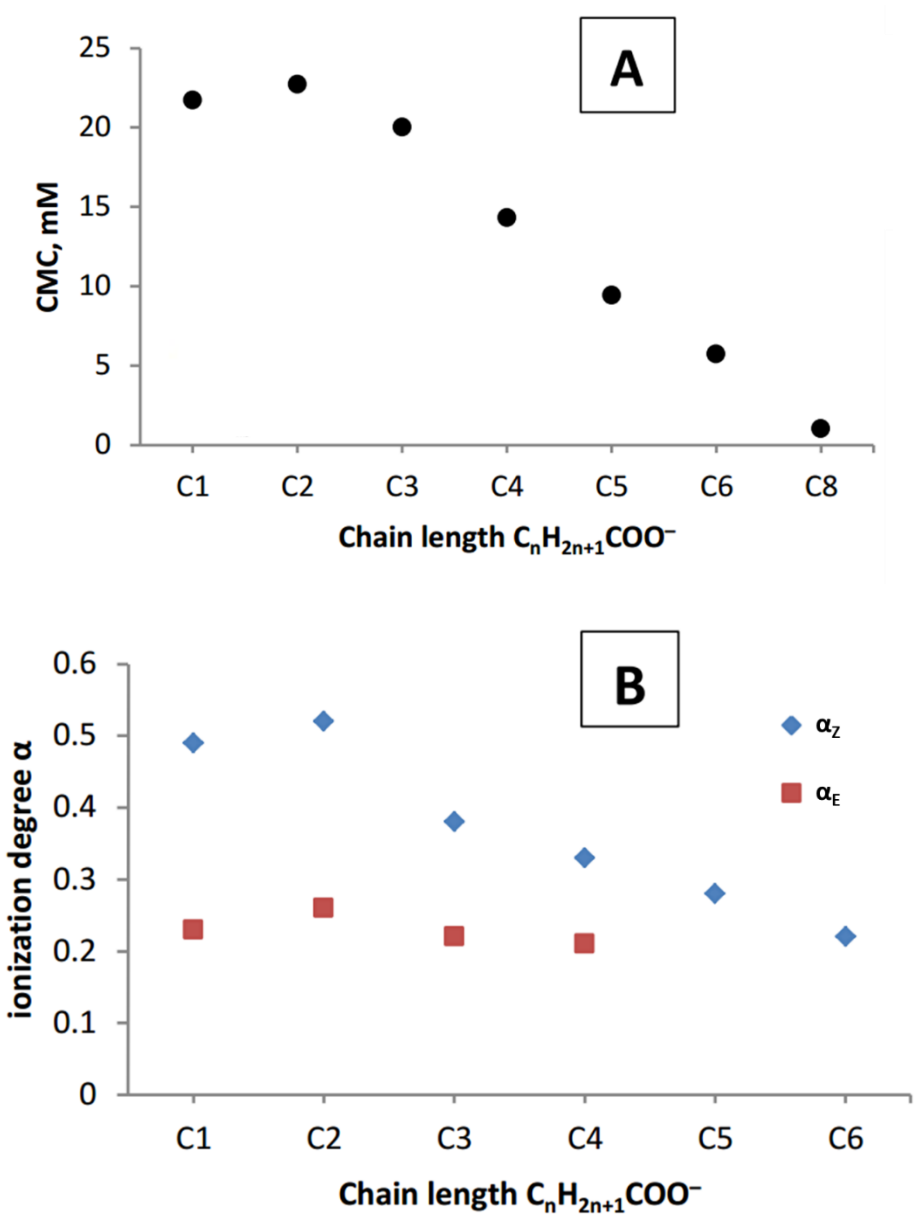

Figure 3-4 Plots of cmc (A) and ionization degrees (B) against counterion chain length of 10-2-10 2X at 30 ºC. Data were measured by both Dr. Alla Malinenko and me. Our data were very close to each other.

Comparing the two ionization degrees, α_Z is much bigger than α_E as illustrated previously from the literature, and the difference diminishes when carboxylate chain length becomes longer. It was shown in literature that α_Z overestimates α_E because the original

equation presumes that a micelle with *n* net charges has the same contribution to the conductivity of the micellar solution as *n* free ions in aqueous phase, which oversimplify the conductivity contribution of micelles.[81] Except C1, other carboxylates' ionization degrees vary linearly with surfactant chain length. The trend is similar to the linear change of cmc in Figure 3-4, which also confirms our expectation that when counterions becomes more hydrophobic, a large percentage of them associate with the micelles and therefore less counterions are in the bulk solution.

The $-\Delta G°_M$ increases as hydrocarbon chain elongates, indicating that micellization becomes more energy favorable when the counterions become more hydrophobic. Generally the variation of gemini surfactants counterions chain length has a predictable effect on the micelles bulk properties.[3]

C1 is an outlier in the plots of cmc, ionization degree and $-\Delta G°_M$, like in the previous case of 14-2-14 2X gemini surfactants[3] and other similar systems.[165, 166, 167] Anacker and Underwood studied the micellization of DTAB with sodium carboxylates NaC_m added in the solution, and they also observed that C1 deviated from the cmc – chain length plot.[168] Even though C1 is more hydrophilic from perspectives of hydration free energy and p*Ka*, it is possible that the absence of alkyl group attaching to the carbonyl group has a strong effect to the electron distribution of the carboxylate group. This is partly illustrated by the big difference between formic acid p*K*a (3.75) and other alkyl carboxylates acids p*K*a (around 5.0). This structural difference is likely the source of its deviant behavior compared to other carboxylate counterions.

Aggregation numbers of gemini surfactants with different carboxylate counterions were obtained by Dr. Alla Malinenko in Dr. Reiko's group with TRFQ method at 2x cmc

and 3x cmc concentration, respectively, as shown in Table 3-2. I measured the aggregation number for C1, C3, C4, C6 and the N_{agg} results are the same as Alla's, but standard deviation results are smaller than hers. To align with French collaborators analysis, Alla's data was shown here. The table lists the averaged aggregation number, N_{agg}, and the standard deviation $\boldsymbol{\sigma}$. The average N_{agg} and $\boldsymbol{\sigma}$ were calculated from 3 repeating measurements.

Counterion	**cmc(mM)**	**N_{agg}**	**σ**	**N_{agg}**	**σ**
		2x cmc		**3x cmc**	
C1	21.7	28	19	37	42
C2	22.7	23	7	25	49
C3	20	24	6	26	25
C4	14.3	23	21	27	37
C5	9.4	25	7	30	21
C6	5.7	26	10	28	21

Table 3-2 Values of cmc and Nagg of 10-2-10 X micellar solution at 2x cmc and 3x cmc obtained from TRFQ experiments at ambient temperature.

The table shows that the aggregation numbers of all carboxylate gemini surfactants are quite similar, but the $\boldsymbol{\sigma}$ are broad compared to the N_{agg}. This may indicate that there is a

distribution of micellar sizes. N_{agg} at 3x cmc is larger than at 2x cmc, showing that the micelles grow modestly with increasing concentration, although the difference is relatively small. This trend was also observed in previous studies of gemini surfactants.[3]

3.3.2 Interfacial counterion molarity

Interfacial molarities (X_m) of carboxylate counterions and interfacial water molarities (H_2O_m) for 10-2-10 2C2, C3, C4 are shown in Figure 3-5. The data for 10-2-10 2C2 were obtained by Dr. Changyao Liu. In the figure the interfacial counterion molarities of all three counterions increase linearly along with increasing 10-2-10 2X surfactant concentrations, possibly because at low concentration, a large fraction (50% at 2x cmc, 33% at 3x cmc, etc.) of surfactants are in bulk solution so that the associations of counterions onto the interface are not saturated. As the concentration of surfactant increases, more counterions tend to bind to the interface. Note that $C2_m$ is significantly lower than $C3_m$ and $C4_m$, and $C3_m$ and $C4_m$ are numerically similar as shown in Table 3-4 and Table 3-5, indicating their concentration at the interface are similar. The results indicate that the effect of counterion hydrophobicity on the interfacial counterion molarity starts to plateau while chain length grow to 3 or 4. The results of longer counterions (chain length > 4) are not shown here because the chemical trapping experiments need an acidic environment to prevent side reactions, but for 10-2-10 2C6 and 10-2-10 2C8, adding acid into their micellar solution produces phase separation and micelle structures change. This also partly explains the scattering data of $C3_m$ and $C4_m$ plots because when the chain length of couterions approaches to six carbons, the whole system is not favorable to form spherical micelles, or even stable micellar solutions, so the polydispersity of the system might be high which means a big variation on the micelles shape and aggregation number, which can also induce

a variation on carboxylate interfacial concentrations. When the probe is added into the system, the measurements will be an average of interfacial concentrations of ions and water molecules in aggregates of different sizes.

The H_2O_m data of 10-2-10 2C2, C3 and C4 are included in Table 3-3, Table 3-4 and Table 3-5. As the counterions concentration in the interfacial region increase, the value of H_2O_m decrease. From C2 to C4 at the same surfactant concentration, H_2O_m gradually decreases because when a more hydrophobic counterion binds to the interface, more space is occupied by the counterions and therefore concentrations of water molecules in the interfacial region are lower. For 10-2-10 2C2 and 10-2-10 2C3, the H_2O_m changes from ~50 M to ~47 M when concentration change from 2x cmc to 7x cmc, while in the same surfactant concentration range the H_2O_m of 10-2-10 2C4 micellar solutions changes from ~49 M to ~46 M. The H_2O_m of 10-2-10 2C4 is lower than that of 10-2-10 2C2 and 10-2-10 2C3 possibly because C4 has a bigger size and repels more water when it binds stronger to the interface.

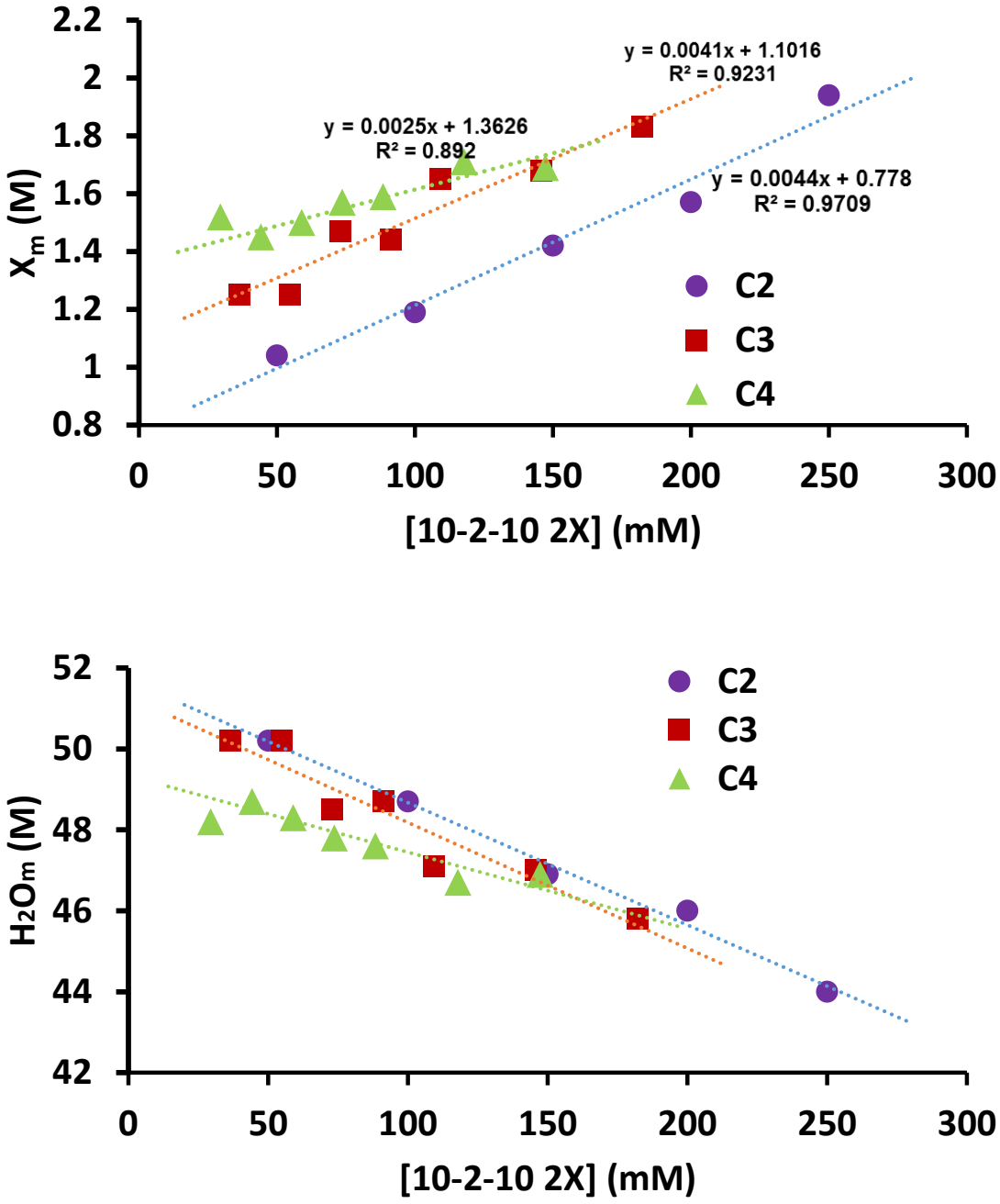

Figure 3-5 Counterion and water interfacial molarities in 10-2-10 2X micellar solutions from 25 mM to 250 mM at 25 ^{O}C measured by chemical trapping experiments. pH is adjusted by corresponding conjugate acids.

[10-2-10 2C2] mM	$C2_m$ M	S_w^{C2}	H_2O_m M	H_2O_m/ $C2_m$
50	1.04	1.24	50.2	48.3
100	1.19	1.22	48.7	40.9
150	1.42	1.20	46.9	33.1
200	1.57	1.19	46.0	29.4
250	1.94	1.17	44.0	22.7

Table 3-3 Estimated values of $C2_m$, H_2O_m, S_w^{C2} in 10-2-10 2C2 micellar solutions from 50 mM to 250 mM, at 25°C at pH5. pH is adjusted by adding HC2.

[10-2-10 2C3] mM	$C3_m$ M	S_w^{C3}	H_2O_m M	H_2O_m/ $C3_m$
36.46	1.25	1.18	50.2	40.2
54.69	1.25	1.18	50.2	40.2
72.92	1.47	1.18	48.5	33.0
91.15	1.44	1.18	48.7	33.7
109.38	1.65	1.18	47.1	28.5
145.84	1.68	1.18	47.0	28.0
182.30	1.83	1.18	45.8	25.0

Table 3-4 Estimated values of $C3_m$, H_2O_m, S_w^{C3} in 10-2-10 2C3 micellar solutions from 36.46 mM to 182.30 mM, at 25°C at pH 5. pH is adjusted by adding HC3.

[10-2-10 2C4] mM	$C4_m$ M	S_w^{C4}	H_2O_m M	H_2O_m/ $C4_m$
29.46	1.52	1.18	48.2	31.8
44.19	1.45	1.18	48.7	33.6
58.92	1.50	1.18	48.3	32.3
73.65	1.57	1.18	47.8	30.5
88.38	1.59	1.18	47.6	29.9
117.84	1.71	1.18	46.7	27.3
147.30	1.69	1.18	46.9	27.7

Table 3-5 Estimated values of $C4_m$, H_2O_m, S_w^I in 10-2-10 2C4 micellar solutions from 29.46 mM to 147.3 mM, at 25°C at pH 5. pH is adjusted by adding HC4.

Overall, the chemical trapping results follow the same trend as the other physical chemical properties of carboxylate gemini surfactants. X_m increases when counterion becomes more hydrophobic, demonstrating that more hydrophobic counterions tend to associate more tightly to the micelle interface.

3.4 DISCUSSION

The changes in 10-2-10 2C2, C3, C4 physical properties (shown in Table 3-1) follow the same trend as those of 14-2-14 2X (X = C1 ~ C8) (partly shown in Table 3-6), but the cmc values of 10-2-10 2X are larger.[3] The cmc of 14-2-14 2X changes from ~0.6 mM to

~0.35 mM, while the cmc values for the 10-2-10 analogues are from ~24.0 mM to ~1.0 mM.

The larger cmc of 10-2-10 2X means that the surfactant monomers are more water soluble and have less tendency to associate together, in part because the hydrophobic hydrocarbon chain is shorter.

Gemini	**cmc(mM)**	α_Z	α_E
14C1	0.58	0.43	0.33
14C2	0.61	0.48	0.33
14C3	0.42	0.54	0.36
14C4	0.35	0.52	0.38
14C6	0.23	0.37	0.29

Table 3-6 Values of cmc, α_Z and α_E for quaternary 14-2-14 gemini surfactants with carboxylate counterions measured at 30 ºC. α_E is calculated at N_{agg} = 25.[3]

Although cmc value of 10-2-10 2X are larger than those of 14-2-14 2X, 10-2-10 2X ionization degrees are close to those of 14-2-14 2X. For 14-2-14 2X (X = C1 ~ C6), the α_Z is around 0.54 ~ 0.35 and C3 α_Z is the highest, while for 10-2-10 2X, the α_Z is around 0.5 ~ 0.25 in Table 3-1, with C2 α_Z being the highest one. 14-2-14 2X α_E are between 0.35~0.25, while 10-2-10 2X α_E are between 0.26 ~ 0.21 in Table 3-1. The difference of α_Z and α_E between these two systems are small, implying that the balance between counterion-headgroup and counterion-water interactions does not change significantly even though the hydrophobicity of the whole surfactant (headgroup + counterion) varies a lot as illustrated by the change in cmc.

Counterion	Temperature, °C	CMC[a], mM	α_Z	α_E	$-\Delta G°_M$, kJ·mol^{-1}
Br	30	6.5	0.21	0.15	15.69
Cl	30	12.8	0.43	0.21	12.88
F	30	34.9	0.68	0.29	9.28
NO_3	30	6.4	0.24	0.15	15.69
$MeSO_3$	30	15.3	0.44	0.23	12.04
PH	30	26.4	0.49	0.25	10.18
C2	30	23.3	0.52	0.26	10.53
TFA	30	6.4	0.17		
I	50	3.0	0.12		

Table 3-7 CMC, α_Z, α_E and $-\Delta G°_M$ for 10-2-10 2X gemini surfactant with inorganic counterions measured at 30 ºC.

Table 3-7 summarizes the physical properties of 10-2-10 2X with inorganic counterions obtained by our collaborators in Dr. Reiko Oda's group. The comparison between 10-2-10 2Cn physical properties (Table 3-1 and Table 3-2) and other 10-2-10 2M (M = inorganic counterions) suggests that 10-2-10 2C2 physical properties is close to the properties of 10-2-10 2PH (dihydrogen phosphate), and 10-2-10 2C4 are close to 10-2-10 2Cl. 10-2-10 2C8 has the most hydrophobic carboxylate counterion, and its physical properties are similar to 10-2-10 2I, the surfactant with the most hydrophobic inorganic counterions.

The data points of interfacial molarity of carboxylate counterions in Figure 3-5 scatter more strongly when the chain length changes from 2 to 4. Adding small amounts of acid to micellar solutions containing C6 or C8 carboxylates leads to phase separation suggests that the micelles structures are at transitional status when counterions chain length is 6 at greatest.

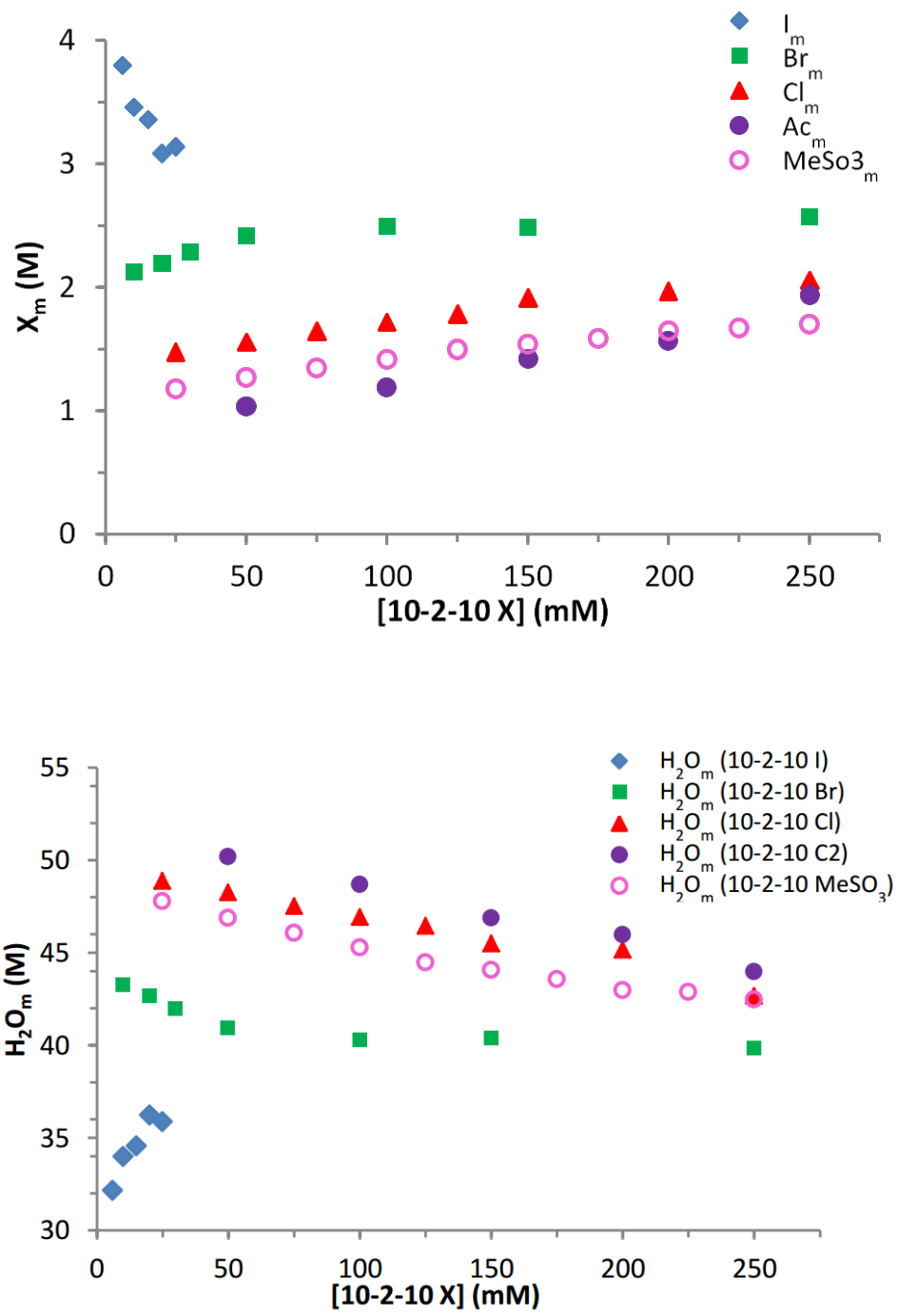

Figure 3-6 Interfacial counterion (X_m) and water (H_2O_m) molarities in 10-2-10 2X micellar solutions from 25 to 250 mM at 25 ºC (I^- data was measured at 50 ℃). Data were measured by Changyao Liu.

Figure 3-6 shows the interfacial concentrations of counterions in inorganic 10-2-10 2X (X = Cl, Br, I, $MeSO_3$, Acetate). In Figure 3-6 the interfacial molarity of C2 in 10-2-10 2C2 micelles is ~1.0 M at 2 x cmc (50 mM), and increases to ~1.4 M at 7 x cmc (150 mM) . This concentration range is close to 10-2-10 2$MeSO_3$, but as analyzed before, the 10-2-10 2C2 cmc and aggregation number is close to those of 10-2-10 2PH and a bit higher than 10-2-10 2$MeSO_3$, so C2 hydrophobicity is somewhere between PH and $MeSO_3$. The interfacial molarity of C4 from Figure 3-5 in micelles is ~1.3 M at 2x cmc, and increases to ~1.6 M at 7 x cmc (150 mM). The range is close to that of 10-2-10 2Cl, and the 10-2-10 2C4 cmc and aggregation number are also close to that of 10-2-10 2Cl, so C4 hydrophobicity is comparable to Cl^- hydrophobicity. The hydrophobicity of C3 is between C2 and C4, which fits our expectation. The close values of interfacial molarities of inorganic and organic counterions indicate the similarity of their hydrophobicity.

From the analysis above a correlation between the interfacial counterion molarity and the micellar solution's physical property can be observed. In principal, interfacial counterion concentrations are related to the ionization degrees, because for a certain gemini surfactant solution at a fixed concentration, if the ionization degree becomes higher, there will be less counterions associated to the interface provided that the interfacial volume stays the same. The following analysis shows a good correlation between the ionization degrees and interfacial counterions molarities of the C2, C3, C4 gemini surfactants. The ionization degree data and interfacial counterions molarities data were picked at 3x cmc because at this concentration large amount (66%) of surfactants are in the micelles. Higher concentrations may lead to a shape transition of micelles.

To accurately obtain the interfacial counterions concentration for 10-2-10 2C2, 2C3, 2C4 at 3x cmc, the data in Figure 3-5 (top) are fitted linearly. The fitting equations are in the same figures. Note that for 10-2-10 2C4 data, the first data point was excluded because it deviates significantly from the trend of the other points.

Interpolation of the fittings in Figure 3-5 (top) estimates the interfacial counterion concentrations of C2, C3 and C4 at 3x cmc, which have been correlated with ionization degrees at the same concentrations in Table 3-8 and Figure 3-7.

10-2-10 2X Counterion	Cmc (mM)	3x cmc (mM)	Molarity (M)	α_Z	α_E
C2	22.7	68.1	1.1	0.52	0.26
C3	20.0	60.0	1.3	0.38	0.22
C4	14.3	42.9	1.5	0.33	0.21

Table 3-8 Interpolated 10-2-10 2X (X=C2, C3, C4) interfacial counterions concentrations and their corresponding ionization degrees at 3x cmc. The X_m values are from Figure 3-5.

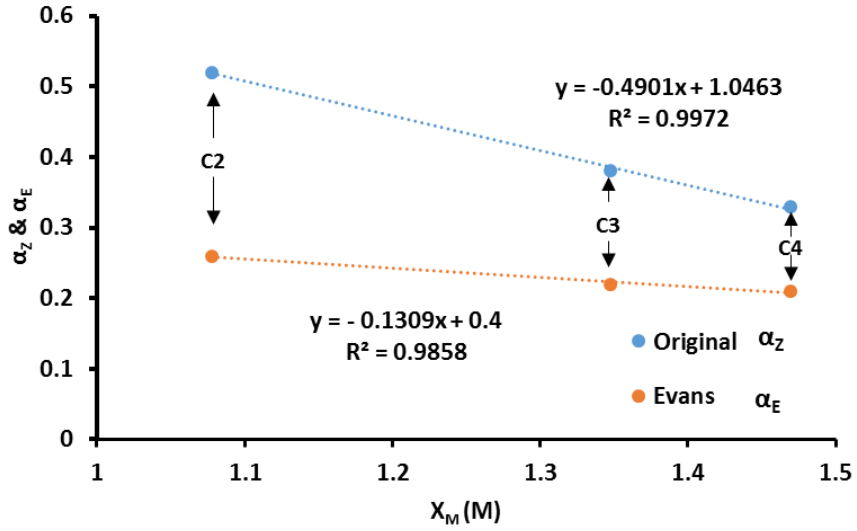

Figure 3-7 Correlation between 10-2-10 2X (X = C2, C3, C4) X_m and their α_Z & α_E at 3x cmc. Ionization degrees were measured at 30 °C and X_m were measured at 25 °C.

Both the α_Z and α_E show good correlations with interfacial counterions concentration. The correlation makes sense because the ionization degree is a measure of the fraction of dissociated counterions and the interfacial molarity is a measure of interfacial counterions

density which also depend on the numbers of counterions within unit volume of interfacial region. As long as the interfacial volume does not change significantly (which is rare unless micelle shape transition happens), the correlation between α and interfacial concentration persists. This correlation strengthens the significance of combining the two methods, which is connecting both the microscopic interfacial molarity and the macroscopic ionization degree of micellar solutions.

Complications

Like all other methods, the chemical trapping method has limitations.[169] A new limitation appeared during the chemical trapping experiments on gemini surfactants with carboxylate counterions that did not show up when we were treating gemini surfactants with inorganic counterions. An unidentified and unidentifiable peak appeared in the HPLC chromatograms of products at a high retention time, Figure 3-8. The "weird" peak is probably formed within the micellar interface due to the high concentrations of reactants. No dependence of the retention time on the chain length of the carboxylate couterions was observed. Attempts to isolate and analyze the unknown compound by NMR and HPLC were unsuccessful. The NMR spectrum showed a complicated structure while HPLC chromatogram indicated decompositions of it into several species, as shown in Figure 3-9 and Figure 3-10 (in Figure 3-9, the flow rate has been set as 0.6 mL/min, so the retention time of "weird" peak became 17 min. The decomposed product is much more hydrophobic and appeared at 32min). The size of the "weird" peak decreases with increasing pH, indicating its break down process is acid catalyzed. The existence as well as the

decomposition of the products have been confirmed by our Spanish collaborator Dr. Carlos Bravo-D ́az and his colleagues.[170]

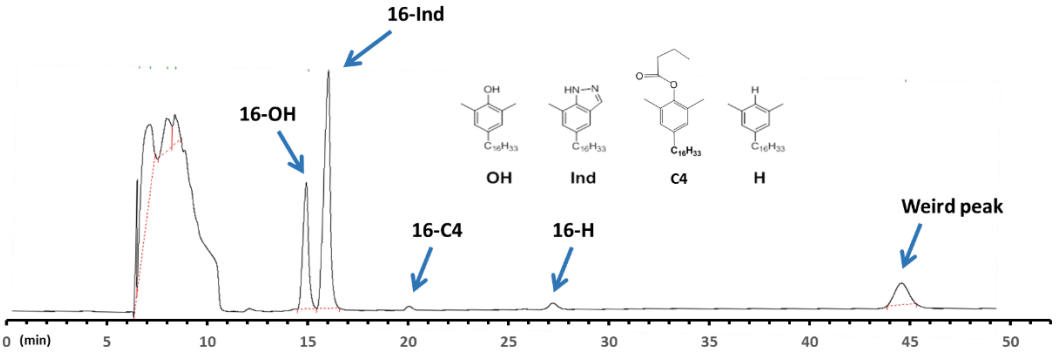

Figure 3-8 HPLC of dediazoniation reaction products in 10-2-10 2C4 micellar solution at 25ºC. Conditions: 100 µL sample injections. Flow rate: 0.4 ml/min; Detector wavelength: 220 nm. Eluting solvents: 80%MeOH/20%i-PrOH.

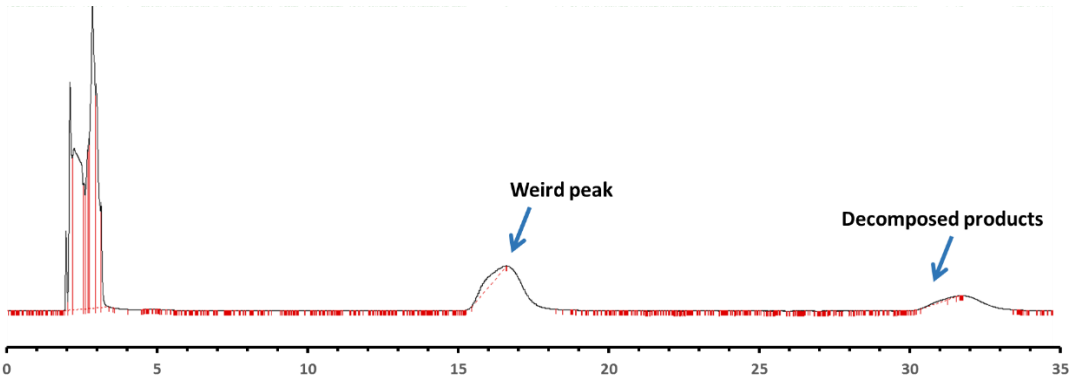

Figure 3-9 HPLC chromatogram of the weird peak after the peak was collected from HPLC in a typical HPLC run of chemical trapping experiments and re-injected into HPLC at 25ºC. Conditions: 100 µL sample injections. Flow rate: 0.6 ml/min; Detector wavelength: 220 nm. Eluting solvents: 80%MeOH/20%i-PrOH.

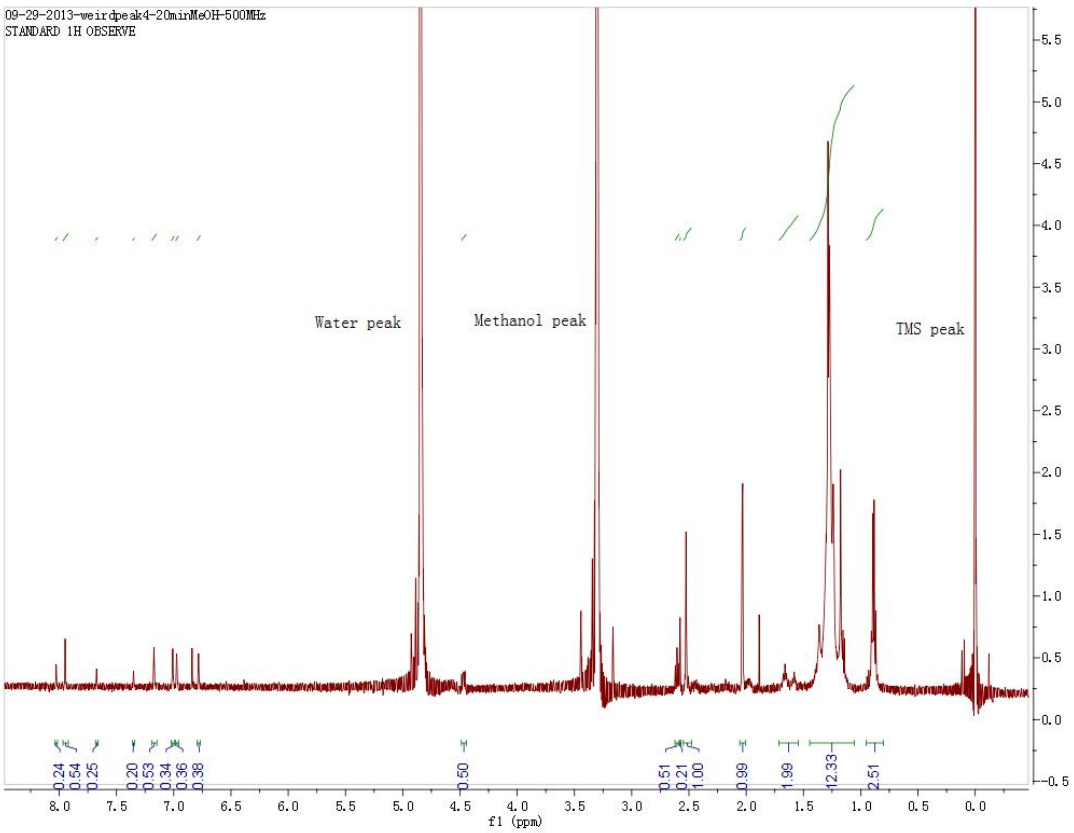

Figure 3-10 500MHz NMR spectrum of the weird peak in *d*-methanol. One scan was 30 seconds, and the total measuring time was 20 min.

After long characterization process and numerous attempts to identify the weird peak, we concluded that it is probably a diazoether formed in a reaction between 16-ArN_2^+ and the phenolic product, which is general base catalyzed by interfacial carboxylate groups because of the high concentrations of carboxylate ions at the interfacial region: 16-ArOH is deprotonated and reacts with 16-N_2^+ to produce an uncharged very hydrophobic diazoether, in Figure 3-11. Attempts to isolate the product in pure form were unsuccessful because it is quite temperature sensitive and will decompose during isolation as shown by the ^{1}H NMR in Figure 3-10.

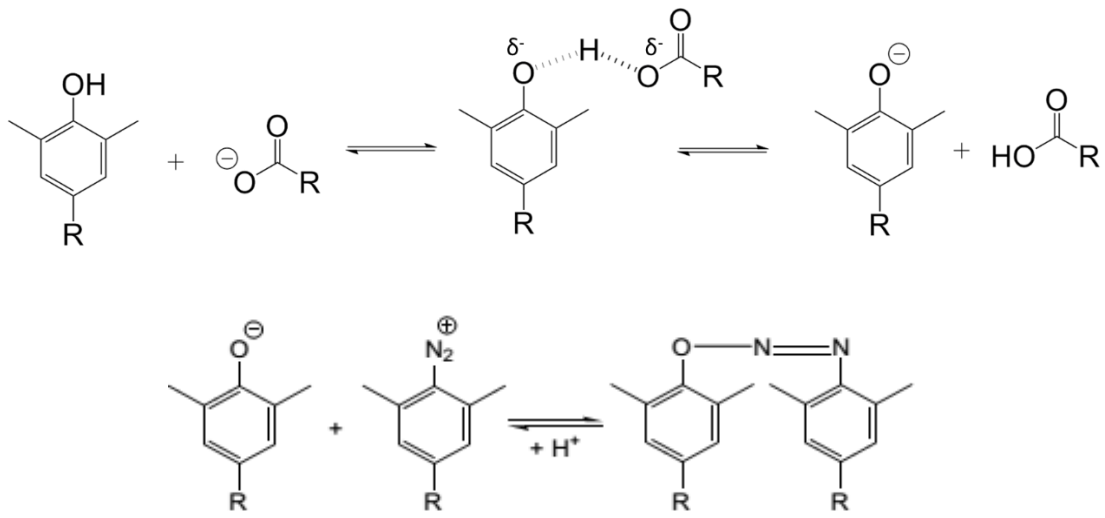

Figure 3-11 Proposed formation of diazoether product from the reaction between phenol and arenediazonium ion catalyzed by carboxylates.

3.5 CONCLUSION

For the first time, the chemical trapping method was applied to micellar solution of 10-2-10 gemini surfactants with carboxylate counterions to study ion specific effects through quantification of interfacial counterion and water molarities. The results show that X_m strongly depends on ion nature and follows the trend C4 > C3 > C2 for carboxylate counterions. In general, those poorly hydrated counterions tend to strongly associate to the interface and show a high X_m value. Conversely, highly hydrated counterions shows lower degrees of association to the interface and give smaller interfacial molarities. The chemical trapping results correlate well with the physical chemistry measurements, and follow a Hofmeister-like series. Quantitative relations between the hydrophobicity/hydrophilicity of counterions and the corresponding interfacial properties were demonstrated in this study.

3.6 SUPPLEMENTARY INFORMATION

Table 3-9 HPLC peak areas, observed and normalized product yields for dediazoniation of 1-ArN_2^+ in aqueous 1-2-1 2Ac solutions at 25°C and pH 6, and values for salts, acetic acid, water concentration, selectivities, S_w^{Ac} and H_2O/Ac molar ratios.[a] Results were obtained by Dr. Changyao Liu.

$[Ac_t]$[b] M	[1-2-1 2Ac] M	$[CH_3COOH]$[c] M	pH	$[H_2O]$ M	Peak Areas (10^6μv•s)[d]			Observed Yields (%)			Normalized Yields (%)[e]		S_w^{Ac}[f]	$[H_2O]/[Ac_t]$
					1-ArOH	1-ArAc		1-ArOH	1-ArAc	Total	1-$ArOH_N$	1-$ArAc_N$		
0.520	0.250	0.020	6.00	52.3	12.659	0.045		97.4	1.14	98.5	98.8	1.16	1.18	100
1.057	0.500	0.057	5.98	49.0	11.344	0.088		97.0	2.47	99.4	97.5	2.48	1.18	46.4
2.249	1.000	0.249	5.92	42.2	10.809	0.201		92.4	5.62	98.0	94.3	5.74	1.14	18.7
4.266	1.500	1.266	5.92	32.7	9.919	0.517		79.8	13.6	93.4	85.4	14.6	1.31	7.65

a. Reaction time ca. 24 hours. The concentrations of 1-ArN_2BF_4 were around 4 x 10^{-3} M, but vary in each experiment. 100 μl of cyclohexane was layered on top of 1-2-1 2Ac solutions in 2 ml volumetric flasks to prevent the evaporation of 1-ArAc. Prior to HPLC analysis, the product mixture was diluted 5 fold with methanol to dissolve both the cyclohexane and the aqueous salt solution.

b. $[Ac_t]$ represents the total acetate (CH_3COOH and CH_3COO^-) concentration in solution. ($[Ac_t] = 2[1\text{-}2\text{-}1\ 2Ac] + [CH_3COOH]$

c. Glacial acetic acid was added to control the pH. [CH_3COOH] is not the actual finally concentration in the solution, but the amount of CH_3COOH which was added to the 1-2-1 2Ac solution.

d. 50 μL sample injections. Peak areas are average of triplicate injections. Eluting solvents: 80%MeOH/20%i-PrOH; Flow rate: 0.6 ml/min; Detector wavelength: 230 nm.

e. % 1-$ArAc_N$ = 100 (%1-ArAc)/(%1-ArOH + %1-ArAc); % 1-$ArOH_N$ = 100 (%1-ArOH)/(%1-ArOH + %1-ArAc).

f. S_w^{Ac} = [H_2O](%1-ArAc)/[Ac_T](%1-ArOH).

Table 3-10 HPLC Average peak areas, observed yields and normalized yields for reaction of 16-ArN_2^+ in 10-2-10 2Ac micelles from 50 mM to 250 mM at 25°C. [a] Results were obtained by Dr. Changyao Liu.

[10-2-10 2Ac] mM	[CH_3COOH][b] mM	pH	Average Peak Areas (10^6μv•s)[c]					Observed Yields (%)						Normalized Yields (%)[e]	
			16-ArOH	16-ArH	16-ArAc	16-ArInd	weird peak	16-ArOH	16-ArH	16-ArAc	16-ArInd	?	Total[d]	16-$ArOH_N$	16-$ArAc_N$
50	52.3	5.03	4.550	0.322	0.123	3.557	1.882	40.9	2.8	1.2	21.0	~16.8	85.9	97.5	2.5
100	156.9	4.96	3.344	0.430	0.119	5.381	2.223	27.4	3.4	1.0	29.7	~18.1	83.4	97.1	2.9
150	217.9	4.99	3.853	0.341	0.152	6.354	2.557	31.6	2.7	1.3	35.4	~20.8	94.8	96.5	3.5
200	261.5	5.02	3.612	0.274	0.156	6.855	2.246	29.6	2.1	1.4	38.3	~18.3	92.1	96.1	3.9
250	313.8	5.00	3.517	0.331	0.204	6.791	1.871	29.6	2.7	1.8	38.8	~15.6	91.4	95.0	5.0
50	558	4.00	2.834	0.691	0.176	3.520	8.975	25.3	6.1	1.7	20.6	7.9	67.9	95.7	4.3

a. Reaction time ca. 24 h to ensure the complete dediazoniation reaction. The concentrations of 16-ArN_2BF_4 were around 10^{-4} M but vary in each experiments.

b. Glacial acetic acid was added to control the pH. [CH_3COOH] is not the actual finally concentration in the solution, but the amount of CH_3COOH which was added to the 1-2-1 2Ac solution.

c. 100 μL sample injections. Peak areas are average of triplicate injections. Eluting solvents: 65%MeOH/35%*i*-PrOH; Flow rate: 0.4 ml/min; Detector wavelength: 220 nm.

d. % Total = %16-ArOH + %16-ArAc + 2 %16-ArH + %16-ArInd + estimated unknown product yield (from the calibration curve of 16-ArOH in Section 4.6.4)

e. % 16-$ArAc_N$ = 100 (%16-ArAc)/(%16-ArOH + %16-ArH + %16-ArAc);

% 16-$ArOH_N$ = 100 (%16-ArOH + %16-ArH)/(%16-ArOH + %16-ArH + %16-ArAc).

Table 3-11 HPLC Average peak areas, observed yields and normalized yields for reaction of 16-ArN_2^+ in 10-2-10 2C3 micelles from 36 mM to 182 mM at 25 °C. [a]

#	[10-2-10 2C3]	[HC3][b]	pH	Average Peak Areas (10^6μv•s)[c]						Observed Yields (%)						Normalized Yields (%)[e]	
	mM	mM		16-ArOH	16-Ind	16-ArC3	16-ArH	weird peak		16-ArOH	16-ArInd	16-ArC3	16-ArH	?	Total[d]		16-$ArOH_N$	16-$ArAc_N$
1	36.46	same as 10-2-10 C3	4.8	3.730	4.850	0.107	0.307	1.900		33.9	31.4	1.1	2.8	11.2	83.3		97.2	2.9
2	54.69		4.8	3.890	5.470	0.113	0.359	1.680		35.3	35.4	1.1	3.3	9.9	88.5		97.2	2.9
3	72.92		4.9	2.900	4.560	0.099	0.170	0.862		26.4	29.5	1.0	1.6	5.1	65.1		96.6	3.5
4	91.15		5.0	4.850	7.800	0.168	0.460	1.700		44.1	50.5	1.7	4.2	10.0	114.8		96.6	3.4
5	109.38		5.1	3.850	6.970	0.152	0.228	1.240		17.5	22.6	0.8	1.1	3.7	93.2		96.0	4.0
6	145.84		5.1	3.700	7.610	0.150	0.246	0.994		16.8	24.7	0.8	1.1	2.9	94.8		96.0	4.0
7	182.30		5.4	3.530	8.200	0.161	0.239	0.870		32.1	53.1	1.6	2.2	5.1	96.3		95.5	4.5

a. Reaction time ca. 24 h to ensure the complete dediazoniation reaction. The concentrations of 16-ArN_2BF_4 were around 10^{-4} M but vary in each experiments.

b. Propionic acid was added to control the pH. [C_3H_7COOH] is not the actual finally concentration in the solution, but the amount of CH_3COOH which was added to the 10-2-10 2C3 solution. Here sample #8 was achieved by using syringes, while others were done by eppendorf pipets.

c. 100 μL sample injections. Peak areas are average of triplicate injections. Eluting solvents: 65%MeOH/35%*i*-PrOH; Flow rate: 0.4 ml/min; Detector wavelength: 220 nm.

d. % Total = %16-ArOH + %16-ArC3 + 2x %16-ArH + %16-ArInd + estimated unknown product yield (from the calibration curve of 16-ArOH in Section 4.6.4). "2x %16-ArH" means that to produce 1 Molar 16-ArH, 2 Molar 16-N_2^+ needs to be consumed.

e. % 16-$ArC3_N$ = 100 (%16-ArC3)/(%16-ArOH + %16-ArH + %16-ArC3);

% 16-$ArOH_N$ = 100 (%16-ArOH + %16-ArH)/(%16-ArOH + %16-ArH + %16-ArC3).

f. The concentration of 10-2-10 2C3 are respectively around 2, 3, 4, 5, 6, 8, 10 times of cmc.

Table 3-12 HPLC Average peak areas, observed yields and normalized yields for reaction of 16-ArN_2^+ in 10-2-10 2C4 micelles from 50 mM to 250 mM at 25 °C. [a]

#	[10-2-10 2C4]	[HC4][b]	pH	Average Peak Areas (10^6μv•s)[c]						Observed Yields (%)							Normalized Yields (%)[e]	
	mM	mM		16-ArOH	16-Ind	16-ArC4	16-ArH	weird peak		16-ArOH	16-ArInd	16-ArC4	16-ArH	?	Total[d]		$16\text{-}ArOH_N$	$16\text{-}ArAc_N$
1	29.46	same as [10-2-10C4]	4.86	3.788	7.572	0.138	0.325	2.576		33.4	47.6	1.4	2.9	14.7	103.0		96.4	3.6
2	44.19		4.89	3.721	7.690	0.127	0.268	2.066		34.0	50.0	1.3	2.5	12.2	99.5		96.6	3.4
3	58.92		4.95	3.772	8.275	0.132	0.224	1.777		33.7	52.7	1.3	2.0	10.3	101.7		96.5	3.5
4	73.65		5.00	3.710	8.716	0.140	0.281	1.719		32.4	54.1	1.4	2.5	9.7	104.3		96.3	3.7
5	88.38		5.15	3.904	8.938	0.147	0.227	1.439		33.7	54.9	1.4	2.0	8.1	105.4		96.2	3.8
6	117.84		5.19	3.715	9.206	0.155	0.244	1.349		32.1	56.7	1.5	2.1	7.6	105.1		95.9	4.1
7	147.30		5.48	3.642	9.797	0.151	0.299	1.369		30.4	58.3	1.4	2.5	7.4	108.9		95.9	4.1

a. Reaction time ca. 24 h to ensure the complete dediazoniation reaction. The concentrations of 16-ArN_2BF_4 were around 10^{-4} M but vary in each experiments.

b. Butyric acid was added to control the pH. [C_4H_7COOH] is not the actual finally concentration in the solution, but the amount of CH_3COOH which was added to the 10-2-10 2C4 solution. Here sample #8 was achieved by using syringes, while others were done by eppendorf pipets.

c. 100 μL sample injections. Peak areas are average of triplicate injections. Eluting solvents: 65%MeOH/35%*i*-PrOH; Flow rate: 0.4 ml/min; Detector wavelength: 220 nm.

d. % Total = %16-ArOH + %16-ArC4 + 2x %16-ArH + %16-ArInd + estimated unknown product yield (by the calibration curve of 16-ArOH). "2x %16-ArH" means that to produce 1 Molar 16-ArH, 2 Molar 16-N_2^+ needs to be consumed.

e. % 16-$ArC4_N$ = 100 (%16-ArC4)/(%16-ArOH + %16-ArH + %16-ArC4); % 16-$ArOH_N$ = 100 (%16-ArOH + %16-ArH)/(%16-ArOH + %16-ArH + %16-ArC4).

f. The concentration of 10-2-10 2C4 are respectively around 2, 3, 4, 5, 6, 8, 10 times of cmc.

Chapter 4 Specific anions adsorption at neat water/oil interface

This chapter introduces a novel approach for measuring the Cl^-, Br^-, SCN^- and I^- concentrations at the neat water/tetradecane interface using the chemical trapping experiment. To date this is the only approach for making such measurements, Figure 4-1. The results show that all four ions associate with the interface in various degrees and the ions order roughly follows Hofmeister Series. Adsorption isotherms of ions are estimated, and adsorption isotherm of Cl^- and Br^- deviate significantly from Langmuir model, but those of SCN^- and I^- do not. The results are consistent with other related studies in the literature.

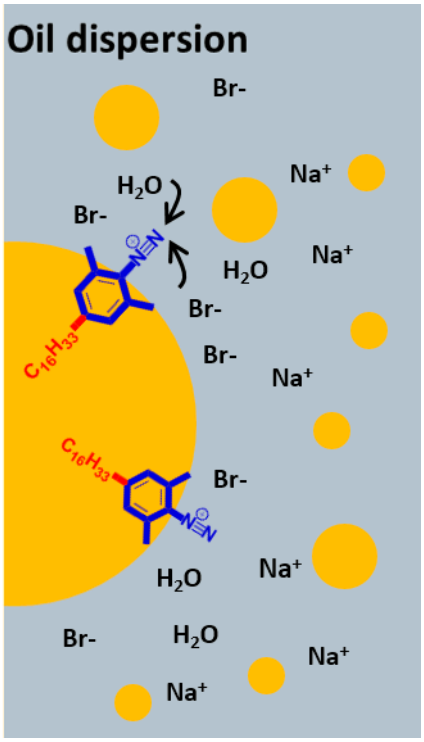

Figure 4-1 Cartoon to show the chemical probe at the oil/water interface in an oil/water mixture reacting with Br^- and water molecules.

4.1 INTRODUCTION

The water/oil interface, both charged and uncharged, plays an important role in many processes in biology, environment and material fields.[4, 5, 171, 172, 173] Anion adsorption onto the water/oil interface is fundamental to various chemical and biological phenomena including surfactant micellization, protein folding, solubility, and water molecule behavior at interfaces. The local molarities of anions affect the electrical properties, local acidity[174] and the hydration of functional groups.[53] In many cases the ions order follow the Hofmeister Series.

Many studies about the water/oil interface were carried out at water/air interface and the conclusions were extrapolated back to the water/oil interface. For example, a

combination of Sum Frequency Generation and Molecular Dynamics simulations showed that ions absorption onto polar groups of polymer residing at water/air interface follows Hofmeister Series.[64] An X-ray photoelectron spectroscopy experiments demonstrated that Br^- and I^- interfacial concentration enhancement are higher than those calculated by MD simulation.[72] The few studies directly on water/oil interface include the SFG experiments showing that NO_3^- has enhanced surface concentration at water/CCl_4 interface[175] and that long chain tetra-alkylated ammoniums (R_4N^+) absorb onto SDS stabilized water/tetradecane interface.[176] However, the Hofmeister Series ions affinity for neat water/alkane interface has been little researched. One study of nonpolarizable MD simulations with an electronic continuum correction which predicted the interfacial excess of Br^- and I^- at water/decane interface.[75]

Here we present a novel experimented setup that provides an estimate of the local concentrations of anions at the neat water/tetradecane interface. Adsorption of four different anions were studied from 0.1 M to 3.0 M and their orders of association followed the Hofmeister Series. The measurements were done with the same surfactant-like probe used in Chapter 3 that reacts with various anions and other weak nucleophiles, including water. To estimate interfacial molarities, we assume that the long chain arenediazonium ion has the same reaction selectivity at water/oil interface as the short chain arenediazonium ion in the aqueous phase toward the anions and water molecules. The anions' interfacial concentrations were estimated by referring to the experiment results of short chain arenediazonium ion in bulk salt solutions. The yields of the dediazoniation reaction products were converted to the local concentrations of the anions and water at the water/oil interface. The results show strong selective absorption of ions to the interface.

These are the first experimental estimates of interfacial molarities of these ions at neat a water/oil interface.

4.2 EXPERIMENTAL SECTION

4.2.1 Materials

Analytical grade NaCl, NaBr, NaI and NaSCN and tetradecane were purchased from Sigma-Aldrich. Tetradecane was distilled before use. All other reagents were used without further purification. All water used to prepare stock solutions was doubly distilled and deionized.

4.2.2 Synthesis of 16-ArN_2BF_4

4-Hexadecylbenzenediazonium tetrafluoroborate (16-ArN_2BF_4) was synthesized by Dr. Guy Lloyd-Jones group at University of Edinburgh using a new synthetic approach. The approach is using long chain alkyl zinc bromide to cross-couple 4-bromo-2,6-dimethylaniline to obtain 4-n-hexadecyl-2,6-dimethylaniline followed by diazoniation. The long chain aniline is treated with BF_3•Et_2O and *tert*-butyl nitrile to produce 4-n-hexadecyl-2,6-dimethylarenediazonium tetrafluoroborate, 16-ArN_2BF_4.

Step 1: Formation of the Organozinc

$$Zn(s) + I_2(s) \xrightarrow[DMA]{} ZnI_2$$

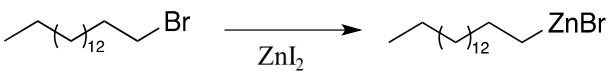

I_2 chips (1.52 g, 6 mmol) were added to a suspension of zinc powder (11.77 g, 180 mmol) in *N*,*N*-dimethyacetamide (DMA) under a nitrogen atmosphere and stirred at 25 ℃ for 10 min. 1-Bromohexadecane (36.7 mL, 120 mmol) was carefully added dropwise for 10 min and the mixture was stirred for 3 h at 80 ℃ to form a yellow solution. Titration of aliquots (1 mL) of the organozinc solution with iodine (0.127 g, 0.5 mmol) in THF (4 ml) showed a concentration of $C_{16}H_{33}ZnBr$ in DMA of (0.71 M, 88 %).

Step 2: Cross-coupling:

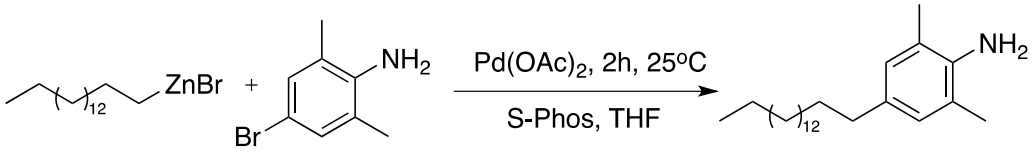

A dry N_2-flushed Schlenk tube was charged with $Pd(OAc)_2$ (135 mg, 6 mmol), S-Phos (2-dicyclohexylphosphino-2',6'-dimethoxybiphenyl, 493 mg, 12 mmol), 4-bromo-2,6-dimethylaniline (12.01 g, 60 mmol) and then THF (56 mL). The reaction mixture was stirred at 25 ℃ for 10 min. A THF solution of 1-hexadecylzinc bromide (120 mL, 85.2 mmol) was carefully added dropwise over 15 min and the reaction was stirred at 25 ℃ for 22 h (At this point TLC analysis showed complete consumption of the 4-bromo-2,6-dimethylaniline. If consumption of the aniline is not complete, further aliquots of the zinc reagent can be added with additional catalyst as needed). Consumption rate of the aniline can be detected by chromatograph.

The reaction mixture was quenched with 200 mL sat. aqueous NH_4Cl solution and filtered. The resulting brown solid was washed with ether (3 X 100 mL) and washings were combined with the filtrate before extracting into ether (3 X 350 mL). The combined organic phases were washed with an aqueous thiourea solution (150 mL), dried with $MgSO_4$ and

concentrated in vacuum, yielding 25.07 g of crude product as a beige solid. The crude product was dissolved in 500 mL of hot methanol and filtered while hot, removing black particulates, possibly palladium black. The filtrate was allowed to cool and afforded an off-white solid. The crystallized product was dissolved in dry ether (200 mL). HCl in ether (2 M, 60 mL) was added dropwise with vigorous stirring over 30 min. The precipitate was filtered and washed with 3 X 60 mL of ether. An aqueous solution of KOH (10.1 g, 200 mL) and 300 mL of ether was added and stirred vigorously until all solid dissolved. The product was extracted with ether (3x 150 mL), dried with anhydrous $MgSO_4$ and concentrated in vacuum affording 4-n-hexadecyl-2,6-dimethylaniline (12.59 g, 0.36 mol, 61 %). ^{1}H NMR (500 MHz, $CDCl_3$): δ ppm 6.77 (2H, s), 3.47 (2H, s), 2.45 (2H, t), 2.16 (6H, s), 1.55 (2H, m), 1.25 (26H, m), 0.87 (3H, t).

Step 3: Diazoniation

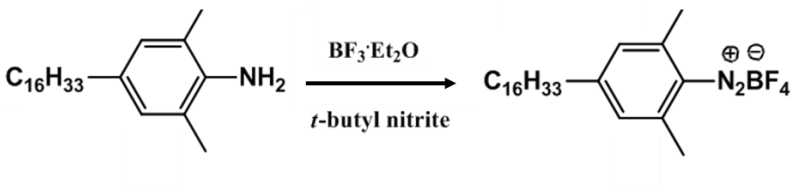

The method of Doyle and Bryker was used to synthesize the 4-hexadecylbenzenediazonium tetrafluoroborate. 30 mL of dry THF was injected into a three-necked 200 mL round bottom flask capped by septum and fitted with a magnetic stirring bar. The flask was cooled (10 min) to about -15℃ in an ice/MeOH bath and 3.4 mL (27.6 mmol) of fresh BF_3•Et_2O was added into the mixture by syringe. The mixture was stirred for 5 min, then 6 g (17.4 mmol) of 16-$ArNH_2$ dissolved in 30 mL of dry THF was added via syringe giving a clear solution followed by 2.6 mL (22 mmol) of *tert*-butyl nitrile in 30 mL THF over a 2 min period. After 15 min of stirring, the temperature was

increased to 0℃ by replacing the ice/methanol bath with an ice bath, and the solution was continuously stirred for 6 hours. A white precipitate gradually formed during the reaction. After reaction finished. The reaction mixture was transferred to a 1000 mL beaker and 200 mL cold pentane was added. The off-white crystal was collected on a Buchner funnel and then recrystallized three times with CH_3CN and cold anhydrous Et_2O. The product was dried under vacuum to give shiny white crystals then stored in refrigerator in the dark. The product yield was 60%. ^{1}H NMR (500 MHz, $CDCl_3$): δ ppm: 7.23 (2H, s), 2.72 (8H, s), 1.73 (2H, m), 1.24 (26H, m), 0.87 (3H, t).

The following experiments were used to confirm the purity of 16-ArN_2BF_4. The probe was used to perform chemical trapping experiment in CTACl micellar solution to compare with previous batches of probes. 1 mL 100 mM CTACl aqueous solutions were prepared followed by adjusting the pH to 3 by using 0.1M HCl. 20 μL of a freshly prepared stock solutions of 16-ArN_2BF_4 dissolved in ice-cold MeCN was added to the solution. The final probe concentration was around 10^{-4} M. The volumetric flasks were sealed and thermostated at 25 ^{o}C for 24 hours. HPLC conditions for products separation were: a 65% MeOH/35% i-PrOH (v/v) mobile phase; flow rate = 0.4 ml/min; detector λ = 220 nm; and the injection volume was 100 μL. Percent yields were obtained from average peak areas of triplicate experiments. The final yields of all products are above 95% and the calculated Cl^- and H_2O interfacial molarity matched with previous report.[100]

4.2.3 Synthesis of SCN^- dediazoniation reaction products

The reaction between arenediazonium ion and SCN^- has not been explored in our group before. Two dediazoniation products are possible, 2,4,6-trimethylphenyl-isothiocyanate and 2,4,6-trimethylphenylthiocyanate, 1-ArNCS , 1-ArSCN. They were synthesized and isolated and their ^1H NMR spectra, IR are present below. Because 1-ArN_2BF_4 is much easier to be synthesized in large amounts than 16-ArN_2^+, the short chain products 1-ArNCS and 1-ArSCN were analyzed in detail.

1-ArNCS, 1-ArSCN. 100 mg of 1-ArN_2BF_4 was dissolved in 0.5 mL acetonitrile and then mixed with 1.4 mL 5 M NaSCN aqueous solution in a 2 mL flask. The pH was adjusted to ~3 by adding appropriate amount of HCl. 100 μL cyclohexane was added to cover the surface to prevent volatile products from vaporizing. The vial was sealed and put into 40 ˚C water bath for 24 hours. After reaction, the top cyclohexane layer was removed with a micropipette and the rest of solvent was evaporated under vacuum to give a yellow solid. Small amount of isopropanol was added to facilitate the evaporation of water at a lower temperature (~65 ºC). The solid was purified by column chromatography, gradually eluted first by hexanes to collect 1-ArNCS (5.9 mg) and then 96%hexane/4%ethylacetate to collect 1-ArSCN (20.1 mg). The yields are: 1-ArNCS 7.8%, 1-ArSCN 26.6%.

1-ArNCS Mw (calcd.): 177.3 $g \cdot mol^{-1}$, ^1H NMR (500 MHz, $CDCl_3$): δ ppm 2.26 (3H, s), 2.33 (6H, s), 6.85 (2H, s). From literature the –NCS functional group has characteristic IR peak at 2050-2200 cm^{-1} as a doublet.[181] ChemDraw software has predicted 1-ArNCS ^1H NMR peaks at δ ppm 2.18 (3H, s), 2.34 (6H, s), 7.00 (2H, s). See ^1H NMR and FTIR spectra, Figure 4-2 and Figure 4-3.

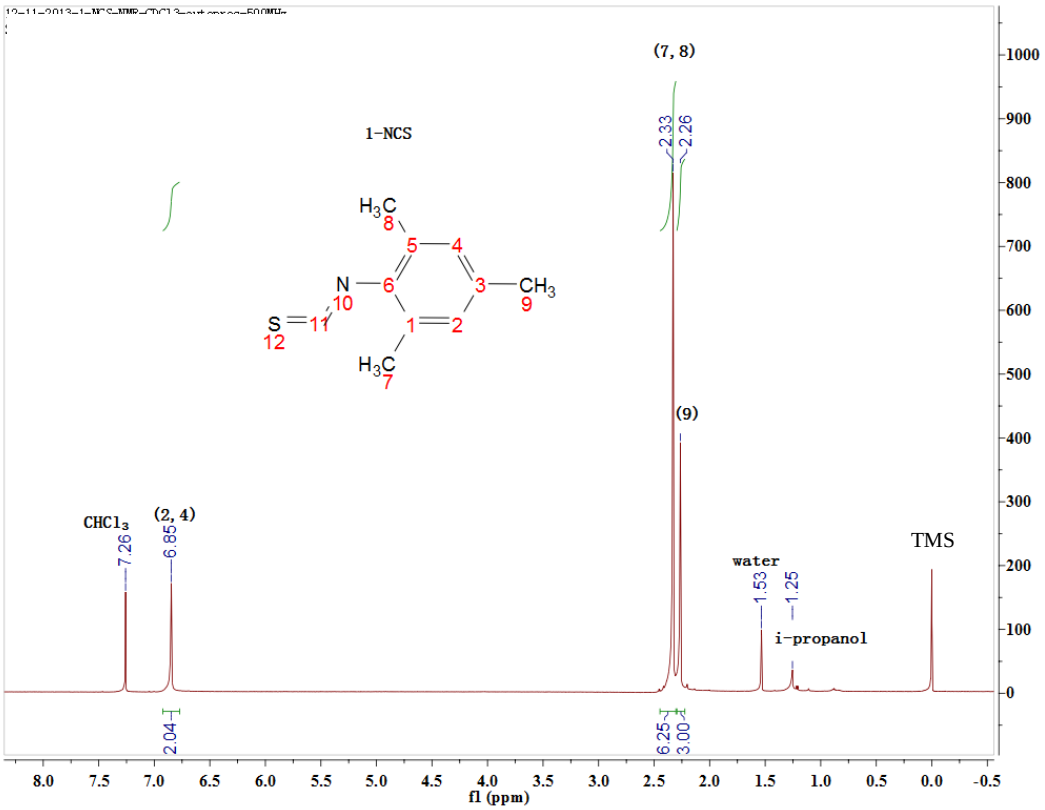

Figure 4-2 ^{1}H NMR of 1-ArNCS

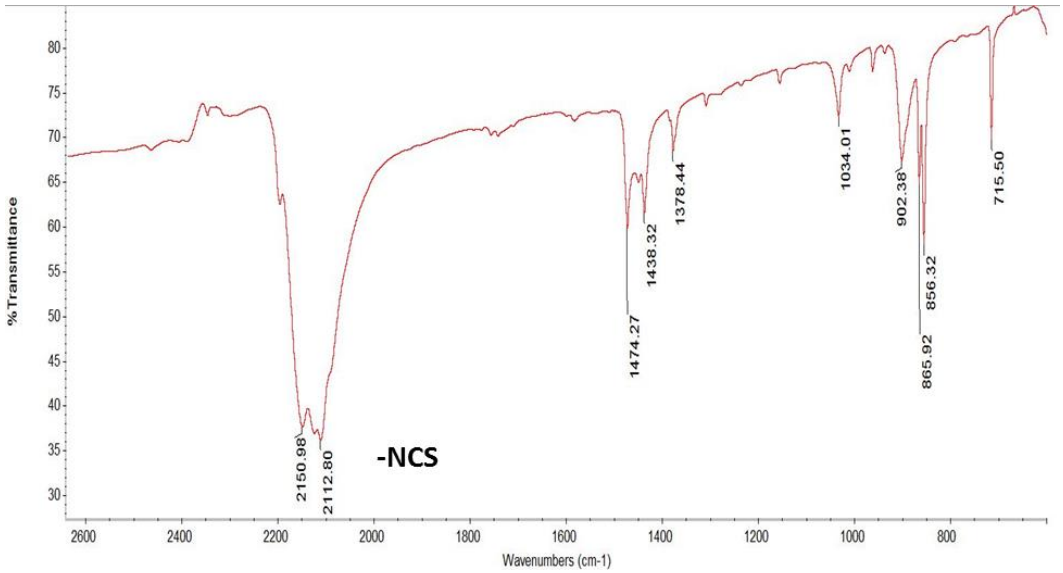

Figure 4-3 IR of 1-ArNCS

1-ArSCN Mw (calcd.): 177.3 g·mol^{-1}. ^{1}H NMR (300 MHz, $CDCl_3$): δ ppm 2.30 (3H, s), 2.55 (6H, s), 7.00 (2H, s). From literature the –SCN functional group has characteristic IR peak at 2130-2170 cm^{-1}.[181] ChemDraw software has predicted 1-ArSCN ^{1}H NMR peaks at δ ppm 2.18 (3H, s), 2.34 (6H, s), 6.81 (2H, s). See ^{1}H NMR & FTIR spectrum, Figure 4-4 and Figure 4-5:

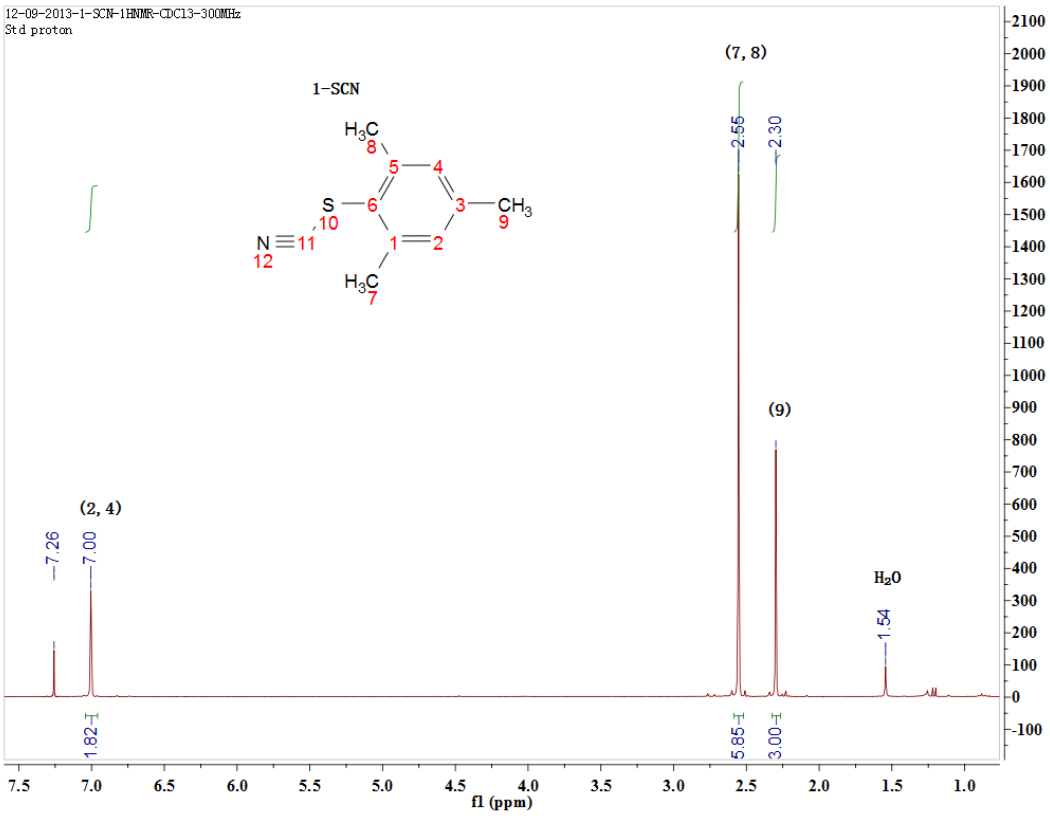

Figure 4-4 ^{1}H NMR of 1-ArSCN

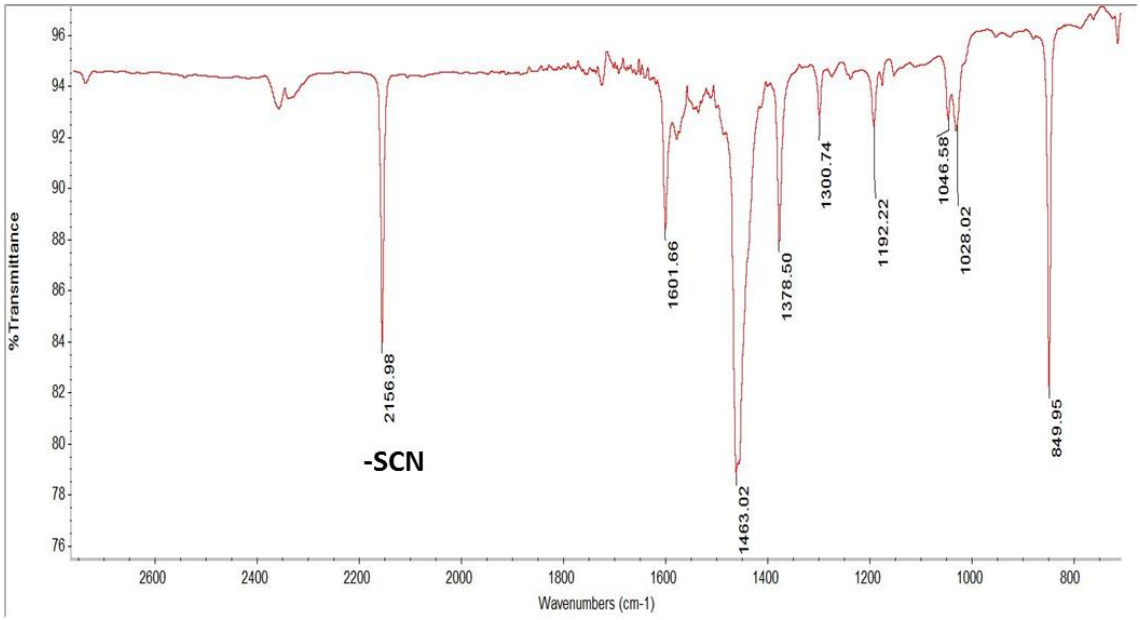

Figure 4-5 IR of 1-ArSCN

4-n-Hexadecyl-2,6-dimethylphenylthiocyanate, 16-ArSCN. 100 mg of 16-ArN_2BF_4 was dissolved in 0.5 mL acetonitrile and mixed with 1.5 mL 5 M NaSCN and 50 mM aqueous cetyltrimethylammonium bromide (CTAB) solution in a 2 mL flask. The pH was adjusted to 3 by adding aliquots of 0.1 M HBr with a micropipette. The flask was sealed with cork at room temperature for 24 hours. $NaClO_4$ was added to precipitate the CTAB and the products were extracted using diethyl ether. Rotary evaporation of the products mixture under vacuum to remove the ether and left orange solid. The solid was initially purified on a silica column chromatography using 98% hexane/2% ethyl acetate to eluent and then dried by rotaevaporation. The products were dissolved in methanol and 16-ArNCS and 16-ArSCN were separated by HPLC using 35%/65% v/v, *i*-PrOH/MeOH. Flow rate:

0.4 ml/min. Detector wavelength: 220 nm. Injection volume: 100 µL. The 16-ArSCN yield was 12.6%.

16-ArSCN: Mw (calcd.): 177.3 g·mol^{-1}. ^{1}H NMR (500 MHz, $CDCl_3$): δ ppm 0.88 (3H, s), 1.25 (26H, s), 1.58 (2H, m), 2.52 (2H, t), 2.56 (6H, s), 7.00 (2H, s). See ^{1}H NMR spectrum in Figure 4-6.

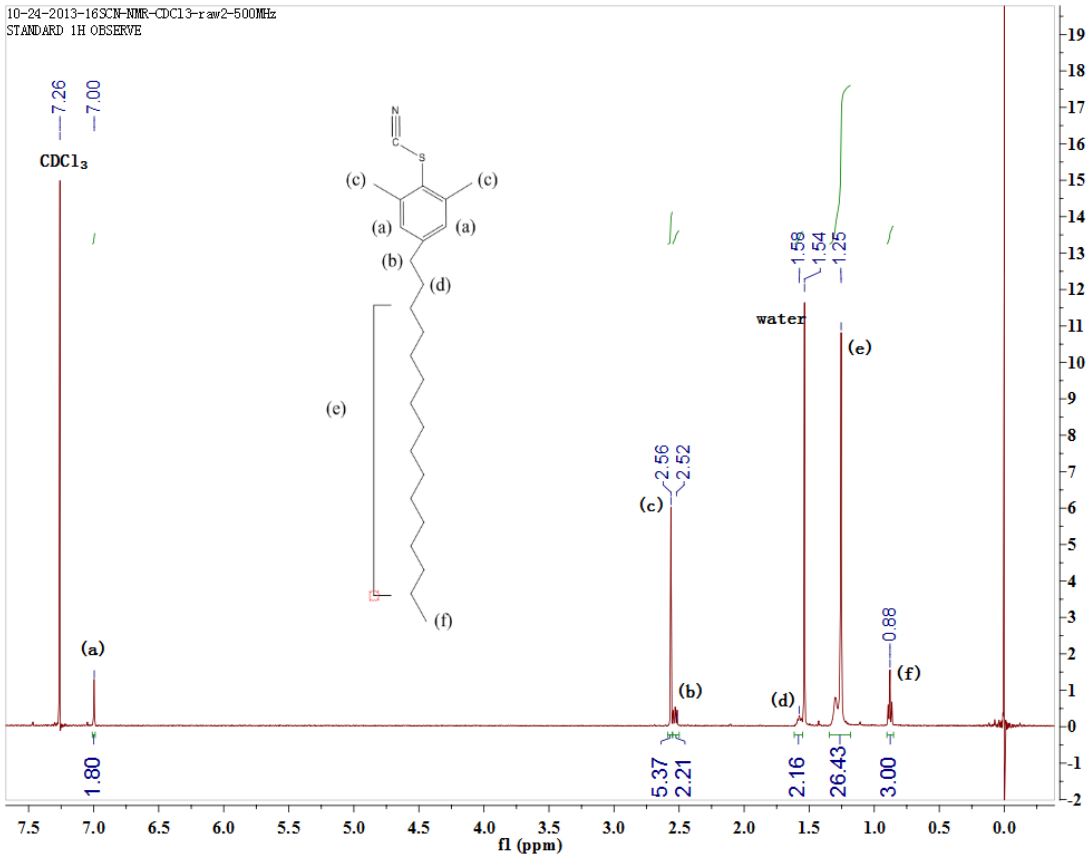

Figure 4-6 NMR of 16-ArSCN

Due to difficulty of isolating the n-NCS products (as a reference, yields of short chain products are 1-ArNCS 7.8% and 1-ArSCN 26.6%. n-NCS products are more hydrophobic than n-SCN products and hard to collect from column chromatography) and high consumption of 16-ArN_2BF_4 to obtain the products (0.1g 16-ArN_2BF_4 needed for enough 16-SCN amount to perform the NMR measurement), 16-ArNCS was not obtained from the

reaction. Its HPLC calibration curve was represented by that of 1-ArNCS under the same condition: a 65% MeOH/35% i-PrOH (v/v) mobile phase; flow rate = 0.4 ml/min; detector λ = 220 nm; and the injection volume was 100 μL. Since they have the same chromophore functional group, their calibration curves under same UV wavelength are regarded as the same.

4.2.4 Method

General Methods

HPLC measurements were performed on a Perkin-Elmer Series 200 equipped with a UV/Vis detector, a Varian Microsorb MV C_{18} column (length, 25 cm; particle size, 5 μm), and a computer-controlled Perkin-Elmer 600 Series Interface. Kinetic measurements were carried out on a Perkin-Elmer Lambda 45 UV/Vis spectrophotometer equipped with a Peltier Temperature Programmer 6 operated with UV WinLab 6.0.3 software. All pH values were obtained by a Fisher AR50 dual channel pH/Ion/Conductivity Meter. ^{1}H NMR spectra were recorded on Varian VNMRS 400 and 500 MHz spectrometers.

Chemical trapping experiments with 16-ArN_2^+ in mixture of NaX (X = Cl, Br, SCN, I) and tetradecane

Calculated volumes of 5.5 M NaX (X = Cl, Br, SCN, I) stock solution were mixed with 0.1 M HCl and water to make 1 mL solution with [NaX] ranging from 0.1 M – 5.0 M at pH 3 in 10 mL glass test tubes. The pH was checked using a pH meter. 100 μL tetradecane was added into each test tube containing a VWR 3 mL Triangular Stir Bar. Then the test tubes were placed onto a magnetic stirrer with stirring rate 1200 rpm. The stir

rate was measured by using a strobescope**.** 4-hexadecyl-2,6-trimethylarenediazonium fluoroborate stock solution (2 μL, conc. = 2.5x 10^{-3} M) was added into the mixture by syringe to give a final concentration 5 x 10^{-6} M, close to the detection limit of the HPLC UV detector. Because the concentrations of dediazoniation products are close to the detection limit of HPLC, the total yields of some experiments are within a bigger range of 100 ± 15% as shown in section 4.6.2. Then the test tubes were stoppered and kept in the dark by covering the whole setup with aluminum foil to prevent photolysis. The reaction run for 24 hours.

After 24 hours the water/oil mixtures were dissolved with aliquots of isopropanol and transferred to 5 mL volumetric flasks to the mark. (At high salt concentrations, isopropanol precipitates the added salt. To avoid this, part of the aqueous phase in the test tube was replaced with roughly equivalent volume of pure water by using micropipette before using isopropanol to increase the volume to 5 mL) Then the homogeneous solutions were analyzed by HPLC.

However, under conditions in which the probe molecule concentration needs to be less than 5 x 10^{-6} M (at this concentration the products concentration is under detection limit of HPLC), an alternative procedure is used. After 24 hours when the reactions were completed, the aqueous phase was carefully extracted with a micropipettes and isopropanol was used to replace the removed aqueous phase and dilute the organic phase into 1 mL solution. Because all the dediazoniation products are very hydrophobic, the removed aqueous phase contains negligible amount of them. In this way the dediazoniation products concentration was increased by 5 times compared with previous procedure where the solution were diluted to 5 mL. The homogeneous solution was injected into HPLC to obtain the products

concentration. Conditions for product separation on the HPLC were: a 65% MeOH/35% i-PrOH (v/v) mobile phase; flow rate = 0.4 ml/min; detector λ = 220 nm; and the injection volume was 100 μL. Typical chromatograms are shown in Figure 4-15 ~ Figure 4-18. Percent yields of each products were calculated from averaged peak areas with corresponding products' calibration curves shown in section 4.6.4. Interfacial concentrations of different ions were calculated by using to corresponding standard curves in section 4.6.5. Normalized yields of 1-ArOH and 1-ArX and the selectivities were used to calculate the interfacial concentration of each ion at the water/tetradecane interface from the 16-ArOH and 16-ArX yields. As noted in section 1.2.2, the reaction between 16-ArN_2^+ and SCN^- also produce side products such as 16-ArH and 16-ArInd. 16-ArH is taken into account when calculating the interfacial water molecules concentration because it is produced from the reaction between 16-ArOH and 16-ArN_2^+. 16-ArInd is not related to the reaction between 16-ArN_2^+ and SCN^- so in data processing its yield is not included in the normalization, but only when calculating the total yields of all products.

Data processing for SCN^-

Within the four types of ions, SCN^- is a new and unique ion in chemical trapping method. Reaction between 16-ArN_2^+ and SCN^- gives 2 SCN^- substituted products, 16-SCN and 16-NCS. 16-SCN is more hydrophilic than 16-NCS based on their retention time on chromatogram in Figure 4-18. Reaction between 1-ArN_2^+ and SCN^- also produces 1-SCN and 1-NCS. When plotting the standard curves after doing 1-ArN_2^+ dediazoniation reactions in the analog salt solutions, the yields of 1-SCN and 1-NCS obtained from HPLC chromatograms were combined together and noted as %1~SCN (i.e. %1~SCN = %1-SCN

+ %1-NCS), then the standard curve of SCN^- was plotted by the relationship between %1~SCN and the stoichiometric concentration of SCN^-, as shown in section 4.6.5. In the reaction between 16-ArN_2^+ and SCN^- in micellar solution, when calculating the yields of SCN^- products we combined the yields of 16-SCN and 16-NCS and noted as 16~SCN, and then referring to the SCN^- standard curve to estimate the interfacial concentration of SCN^- in micellar solution.

Standard curved obtained in aqueous NaX (X = Cl, Br, SCN, I) reference solutions with 1-ArN_2^+

Chemical trapping experiments with 1-ArN_2^+ in aqueous NaX (X = Cl, Br, SCN, I) reference solutions are conceptually exactly the same as doing chemical trapping experiments in micelle systems. Aqueous NaX (X = Cl, Br, SCN, I) stock solutions were prepared at 0.5 ~ 4.0 M. The stock solutions were used to prepare sets of NaX solutions containing incremental amounts of the stock solutions in 1-2 mL volumetric flasks. The solution acidity was adjusted by adding HCl. The pH was measured by using a pH meter. To initiate the dediazoniation reactions, 10-20 μL of freshly prepared stock solutions of 1-ArN_2BF_4 in ice-cold MeCN were added to give a final probe concentration of 4-4.5 x 10^{-3} M. 50-100 μL of cyclohexane were layered on the top of the solutions to prevent the evaporation of volatile 1-ArX and 1-ArOH products (the long chain products, 16-ArX and 16-ArOH, are involatile). The volumetric flasks were sealed with Parafilm and equilibrated at 25 ^oC for 24 hours. Prior to HPLC analysis, the product mixture was diluted 5-fold with MeOH or MeCN to dissolve both the cyclohexane and the aqueous salt solution. Conditions for product separation on the HPLC were the following: an 80% MeOH/20%

H_2O (v/v) mobile phase; flow rate = 0.6 mL/min; detector wavelength λ = 230 nm; the injection volume was 50 μL. Each experiments were repeated three times. In each experiment, concentrations of each products were calculated by referring to the corresponding calibration equations in in section 4.6.4. Yields of each products were calculated from the average of triplicate runs. Normalized yields of 1-ArOH and 1-ArX were used to calculate the standard curves and selectivities. Noted that NaCl, NaBr results were obtained in previous papers.[177]

4.3 RESULTS

To measure the local molarity of anions at the tetradecane/water interface, the concentration of probe molecule 16-N_2^+ needs to be low in the interfacial region to minimize its influence on the surface charge of the interface, otherwise it might induce the formation of an electrical double layer with counterions at the interface.

We assumed that higher stir rate would produces bigger interface, so we measured the yield of 16-ArCl as a function of increasing stir rate. Figure 4-7 shows the relationship between stir rate and percent yield of 16-ArCl. Below 800 rpm, the normalized 16-ArCl% declines and normalized 16-ArOH% increases with increasing stir rate, indicating that as interface area becomes larger, the positive charge introduced by 16-ArN_2^+ has less and less effect on the interfacial Cl^- concentration. Above a stir rate of 1000 rpm, normalized 16-ArCl% is approximately constant, which indicates the interface area is sufficiently large and the probe is sufficiently diluted that it has no significant effect on the electronic properties of the interface. The normalized 16-ArOH% stays unchanged at this condition

as well. In this experiment the NaCl concentration is kept at 1.0 M. All experimental data are included in Table 4-11 and Table 4-12. In all the following experiments the stir rate is set to 1200 rpm to ensure the sparse distribution of probe molecules at the interface.

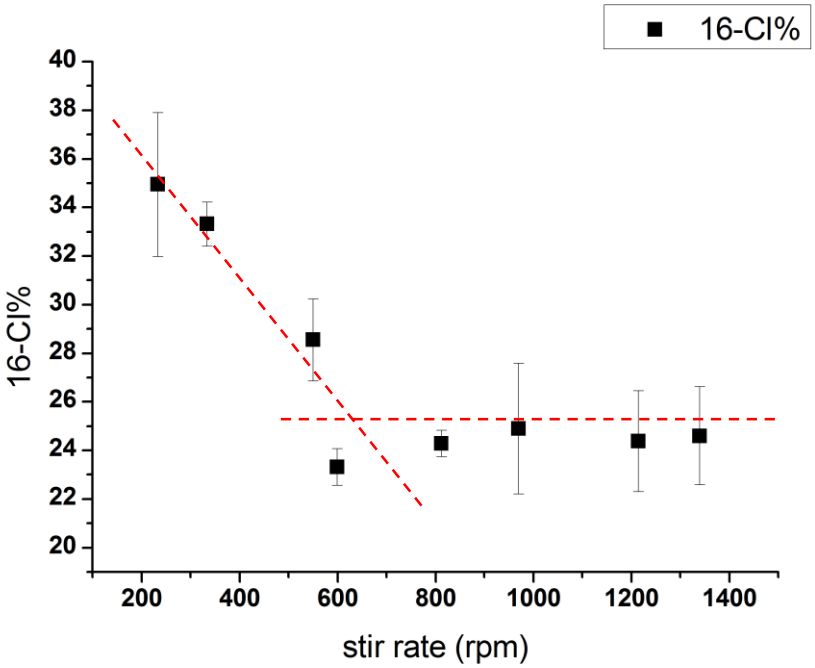

Figure 4-7 16-ArCl yield as a function of stir rate for Cl^- in water/tetradecane(10:1) mixture at ambient temprature. NaCl concentration is 1.0 M. pH=3 with HCl. All the experimental data are included in Table 4-11 and Table 4-12. Red dashed lines are for aiding eyes. All data points are from triplicate runs.

The stoichiometric probe molecule concentration is another important metric because at high local molarity the probe molecules will affect the electronic properties of the interface. Figure 4-8 shows the yields of 16-ArCl with increasing stoichiometric concentration of probe molecule. All the experimental data are included in Table 4-13 and Table 4-14. When the probe concentration is below 5.0×10^{-6} M, 16-ArCl% is approximately constant. At high probe concentrations 16-ArCl% increases significantly

and reaches a plateau above $1.0x10^{-5}$ M. At $1.5x10^{-5}$ M the solution becomes a suspension which indicates the probe saturation.

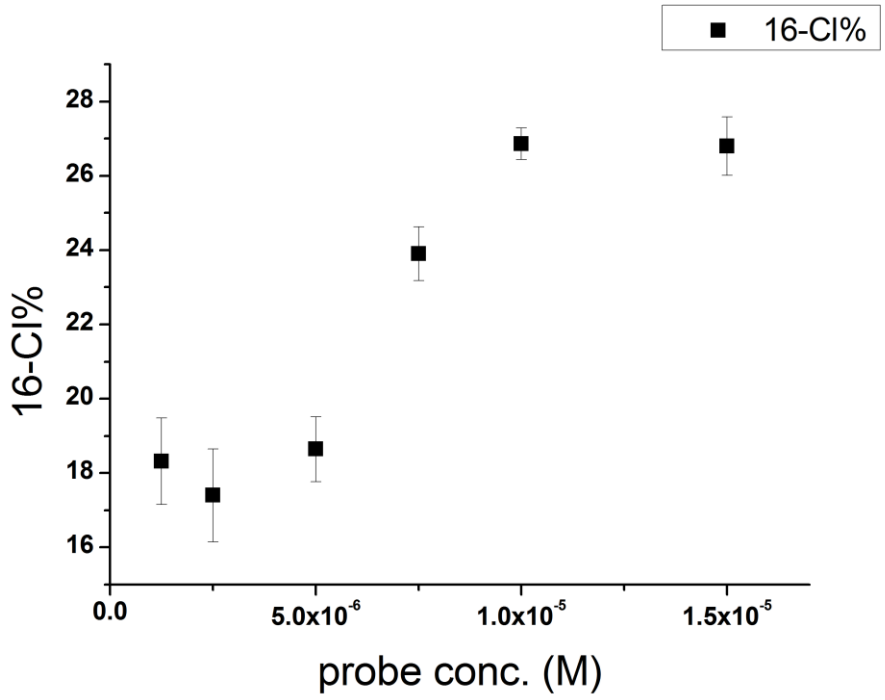

Figure 4-8 16-ArCl yield as a function of probe concentration in water/tetradecane mixture at ambient temperature. NaCl concentration is 1.0 M, stir rate=1200 rpm. The result numbers are in Table 4-13. pH=3 with HCl. All the experimental data are included in Table 4-13 and Table 4-14.

The same control experiment was also performed on 1.0 M NaI as shown in Figure 4-9. All the experimental data are included in Table 4-15 and Table 4-16. The plot profile is the same as that of 1.0 M NaCl solution. We think that the unchanged 16-ArCl% and 16-ArI% below $5.0x10^{-6}$ M suggests that the probe interfacial density is too low to induce any aggregation of anions. Above $5.0x10^{-6}$ M the interfacial charge density is sufficient to organize anions at the interface.

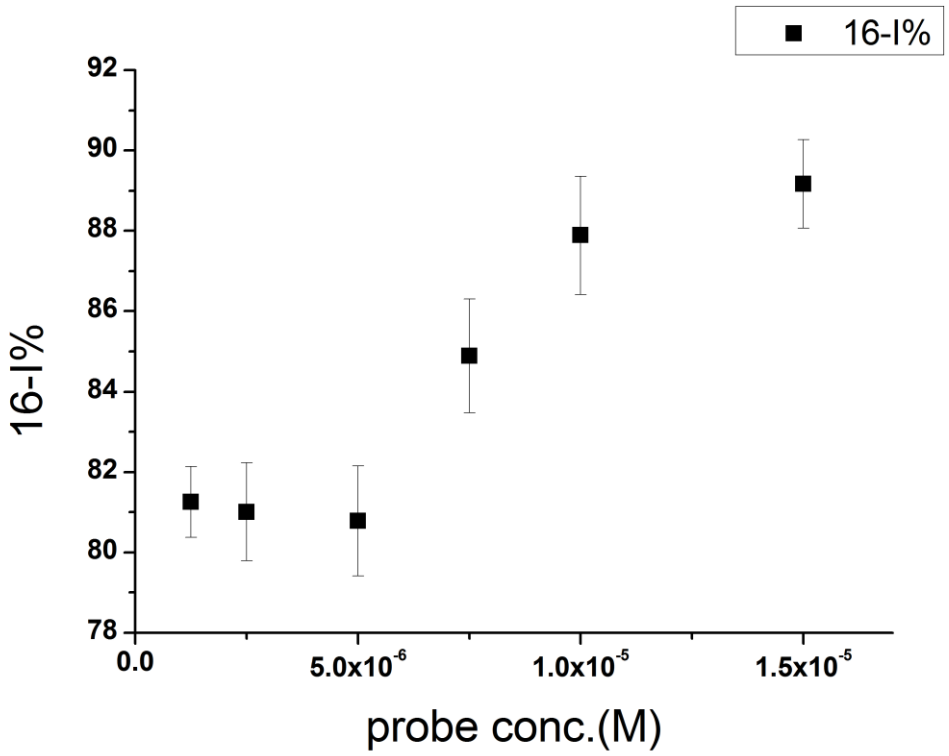

Figure 4-9 16-ArI yield as a function of probe concentration in water/tetradecane mixture at ambient temperature. NaI concentration is 1.0 M. pH=3 with HCl (HI is oxidized easily). All the experimental data are included in Table 4-15 and Table 4-16.

By following the same idea of chemical trapping experiments in micellar solution, the interfacial molarity of Cl^-, Br^-, SCN^-, I^- and water at the water/tetradecane interface were estimated in a mixture system of tetradecane and salt solutions at various concentration, as shown in Figure 4-10. All the experimental data are included in section 4.6.2. As normalized %16-ArX increases with increasing salt concentration, the normalized %16-ArOH decreases. The green line indicates the function f(x) = x which shows the molarity of the added salt in the aqueous phase. The interfacial molarities of all four anions are greater than their bulk concentrations at low concentration of added salts, indicating they

adsorb at the water/tetradecane interface. The increase in the local molarity increment of interfacial concentration is more rapid at low bulk concentration but decreases slower at higher bulk concentration. This trend is especially prominent for I^- but also applies to other ions. As bulk concentration becomes high, the difference between interfacial and bulk concentration gradually becomes small, indicating saturation of the interface.

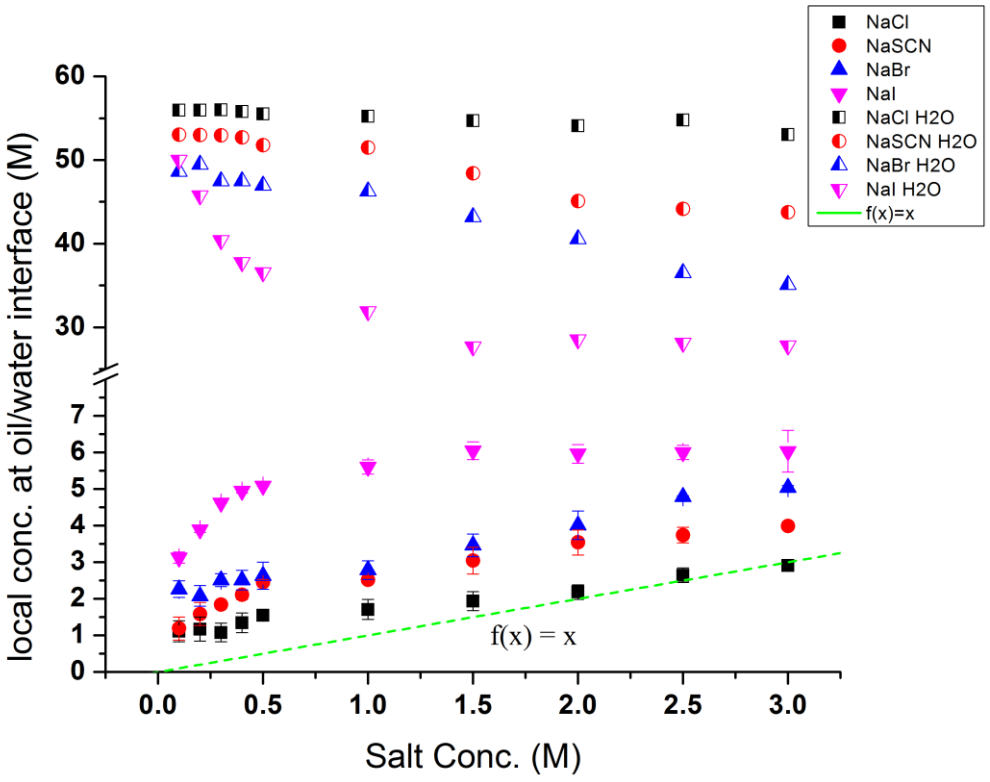

Figure 4-10 Interfacial concentrations of counterions and water molecules vs. added salts concentration at ambient temperature. Function f(x) = x shows the molarity of bulk added salts concentration. All the experimental data are included in section 4.6.2.

Interfacial Cl^- molarity starts at 1.12 M at 0.1 M bulk concentration, and reaches at 2.91 M at 3.0 M bulk concentration; Br^- interfacial molarity starts at 2.26 M at 0.1 M bulk

concentration, and reaches 5.04 M at 3.0 M bulk concentration; SCN^- interfacial molarity starts at 1.19 M at 0.1 M bulk concentration, and reaches 3.99 M at 3.0 M bulk concentration; I^- interfacial molarity starts at 3.13 M at 0.1 M bulk concentration, and reaches 6.04 M at 3.0 M bulk concentration. For the Cl^-, Br^-, SCN^-, the increasing trend of interfacial molarity is close to linearity within the concentration range. I^- is unique because its interfacial molarity shows accelerated growth at low concentrations, and then plateaus. This is the first experimental demonstration that these anions selectively adsorb onto the neat, uncharged H_2O/alkane interfaces.

The interfacial water molarity decreases as the anion concentration increases for all four anions. The interfacial water molarities show the reverse order of the anions, which is common in chemical trapping experiments in micellar solutions in which an increase in the interfacial counterions concentration produces decreasing interfacial water concentration.[53] The anions molarities decrease in the order: I > SCN > Br > Cl and the water molarities follow the reverse order: I < SCN < Br < Cl.

4.4 DISCUSSION

Not much research has been done on ions adsorption onto neat water/oil interfaces. The Jungwirth group[75] used molecular dynamic (MD) simulations to calculate the interfacial concentrations of F^-, Cl^-, Br^- and I^- at the water/decane and water/air interfaces. The simulations show a clear increase in Cl^-, Br^-, I^- concentration at the interface, but not F^-, as shown in Figure 4-11 and Figure 4-12.

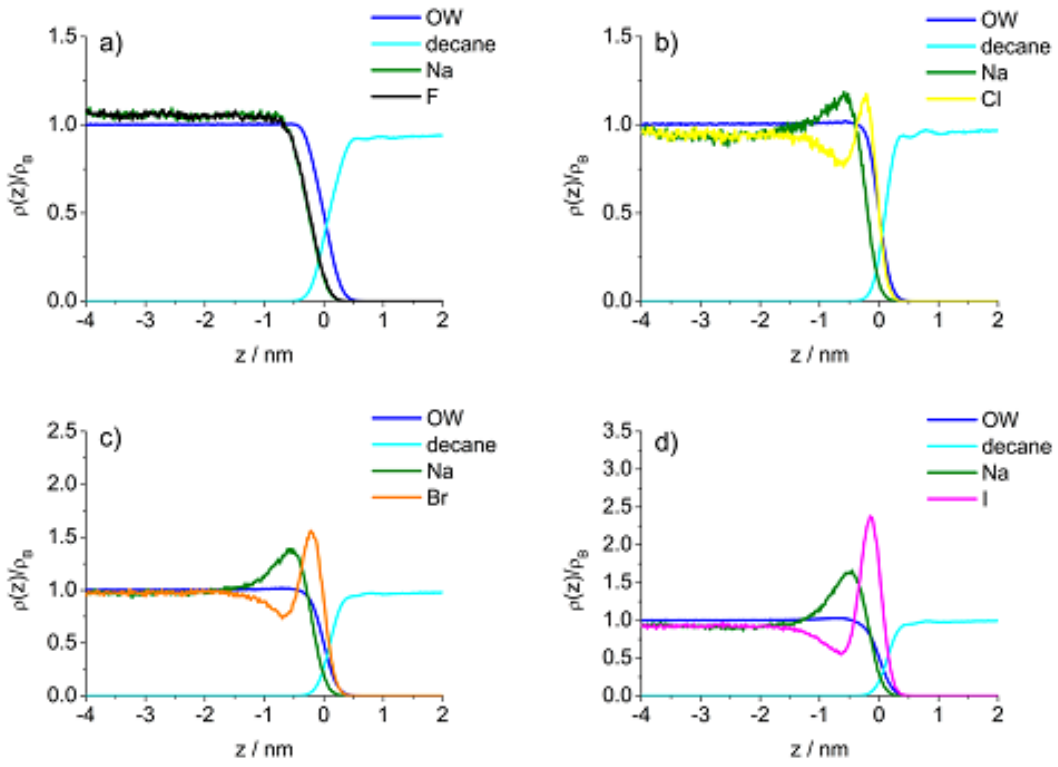

Figure 4-11 Normalized density of Na^+, halides, decane and Oxygen of H_2O at H_2O/decane interface at 298 K calculated from by Jungwirth group paper. [75] [NaX]=1.0 M.

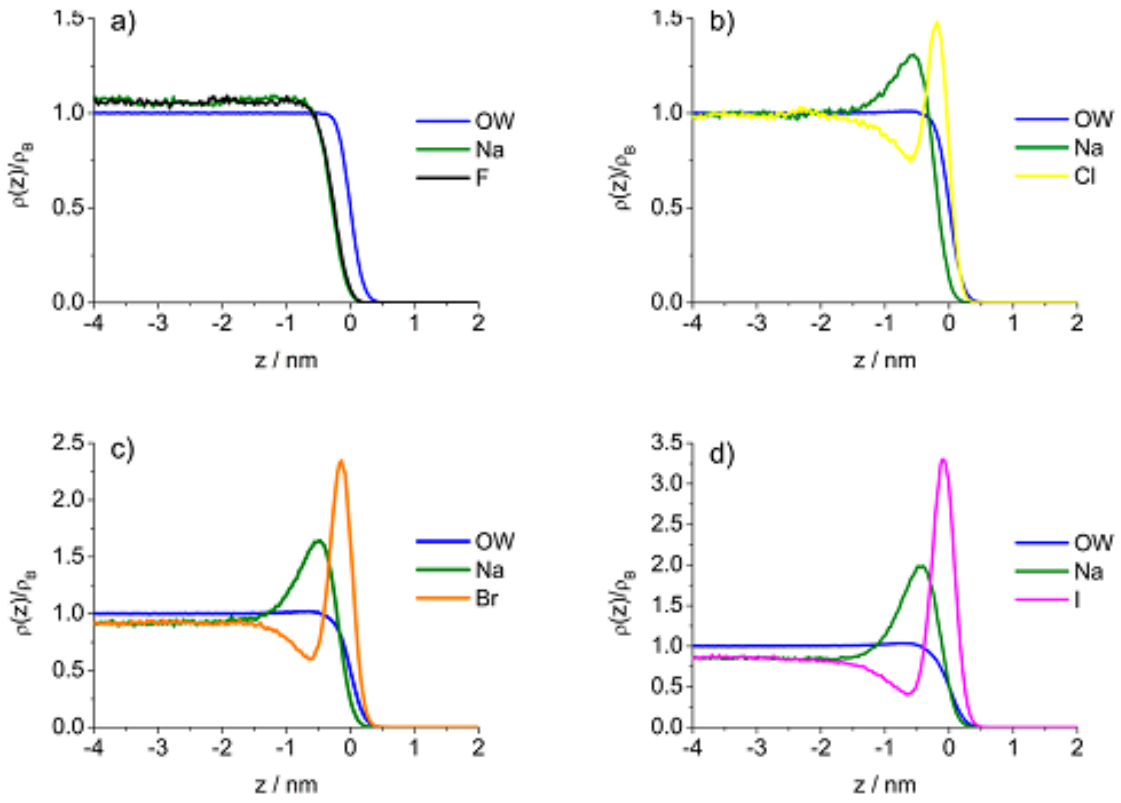

Figure 4-12 Normalized density of Na^+, halides, decane and oxygen of H_2O at H_2O/air interface at 298 K calculated from by Jungwirth et al.[75] [NaX]=1.0 M.

Figure 4-11 and Figure 4-12 are plots of the normalized number density of water oxygen (blue), decane CH_n (cyan), sodium (olive green), and various halides ((a) fluoride (black), (b) chloride (yellow), (c) bromide (orange), and (d) iodide (magenta)) versus the distance *z* to the decane/water interface or air/water interface, respectively. The bulk salts concentrations are all 1.0 M. From these two plots the authors calculated the Cl_{Int} /Cl_{bulk}, Br_{Int} /Br_{bulk} and I_{Int}/I_{bulk} ratios. The comparison between their results and our experimental results are listed in Table 4-1.

	Cl_{Int}/Cl_{bulk}	Br_{Int}/Br_{bulk}	I_{Int}/I_{bulk}
MD, water/decane interface	1.2	1.6	2.5
MD, water/air interface	1.5	2.5	3.5
Chemical trapping, water/tetradecane interface	1.7	2.7	5.6

Table 4-1 Comparison of halides adsorption onto water/oil and water/air interface at 1.0 M bulk salt solution obtained by MD and chemical trapping. [NaX]=1.0 M.

From the table it is easy to see that both our and Jungwirth's results show strong specific ions effect on halides adsorption onto the water/hydrophobic interface. Our interfacial concentration ratios are generally higher than MD results by about 50-100%, but the ions adsorption order is the same: $Cl^- < Br^- < I^-$.

Hemminger's group[72] used x-ray photoelectron spectroscopy to estimate ions percentage in the composition the water/air interfacial layer. The ions percentage is calculated by dividing the number of ions with the total numbers of ions and water molecules at the interface. The results show that bigger and more polarizable anions, especially Br^- and I^-, have more enhanced adsorption onto the interface, as shown in Figure 4-13.

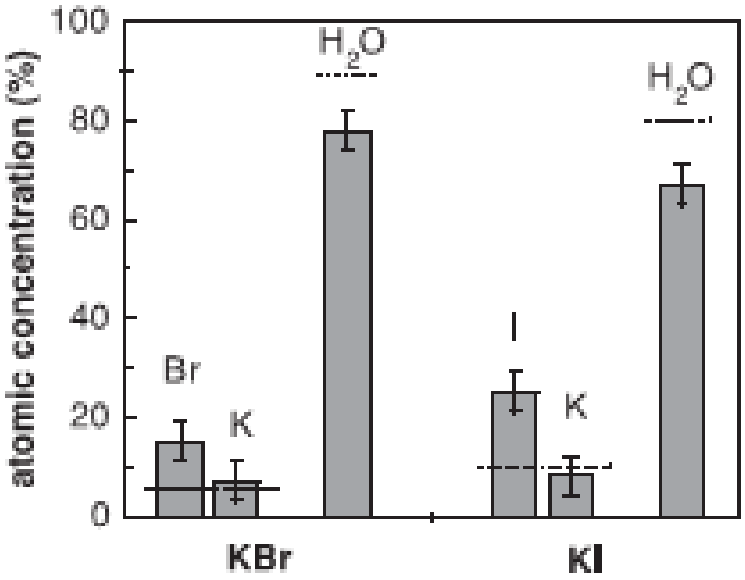

Figure 4-13 Hemminger's result revealing atomic percentage for cations, anions and water molecules at water/air interface at ambient temperature. Both solutions are at 3.0 M concentration.

In Table 4-2 the Br/H_2O ratio and I/H_2O ratio obtained from Hemminger's paper and our experiments are compared. In chemical trapping experiments, the ions/H_2O ratios are directly calculated as the ratio between ions interfacial molarity and H_2O interfacial molarity.

	Br_{interf}/H_2O	I_{interf}/H_2O
X-ray, water/air interface	0.18	0.28
Chemical trapping, water/tetradecane interface	0.14	0.20

Table 4-2 Comparison on ratios of interfacial anions and water molecules between chemical trapping and x-ray photoelectron spectroscopy at ambient temperature. Salts concentrations are all at 3.0 M.

Hemminger's ratios are slightly higher than ours, but the trends are the same. Both of the two experiments imply that Br^- and I^- associate to the interface, and I^- associates stronger than Br^-. The difference between these two experiments are c.a. 30~40%, which is relatively small. To conclude, the results from chemical trapping, MD and x-ray provide similar anions adsorption order at neat hydrophobic/water interfaces.

In related research, people have studied the ion selectivity from the adsorption isotherm perspective. Cremer's group used vibrational sum frequency spectroscopy to detect the vibration intensity of water molecules at vicinity of poly-(N-isopropylacrylamide) (PNIPAM) floating at the water surface.[64] The ions followed a series: NaSCN > $NaClO_4$ > NaI > NaBr > NaCl > NaF. For most of the ions they investigated, except ClO_4^-, a Langmuir isotherm fit the relationship between the relative oscillator strength and the ions concentration well. In Saykally's paper they also found the Langmuir model fit the affinity of the SCN^- at the water/air interface at low bulk ion concentration. The fitting failed at high ion concentration.[71]

Accordingly, we tried to fit our results with the Langmuir model. The assumptions of Langmuir model are that the interface has a fixed space for limited number of molecules, which means once a spot is taken by one molecule, there will be one less free spot. The molecules do not have strong interactions between each other. So the process for one anion to take the "spot" can be described as:

$$Spot_{free} + Anion = Spot \cdots Anion$$

where the $Spot \cdots Anion$ means the spot has been taken by one anion.

The equilibrium constant *K* is defined as:

$$K = \frac{[Spot \cdots Anion]}{[Spot_{free}] * [Anion]}$$

Equation 4-1

Here square brackets mean stoichiometric concentration for each terms. The $[Spot \cdots Anion]$ is proportional to the anions local concentration on interface, because if there are more anions associated to the interface, more spots will be occupied. So

$$\frac{[Spot \cdots Anion]}{[Spot_{free}]} = \frac{S * (Anion)_{interf}}{(TotalArea - S * (Anion)_{interf})} \equiv \frac{\theta}{1-\theta}$$

Equation 4-2

$$\theta = \frac{S * (Anion)_{interf}}{TotalArea} \equiv M * (Anion)_{interf}$$

Equation 4-3

Here $S * (Anion)_{interf}$ equals the area that anions occupy at the interface. *M* is an arbitrary term equal to $\frac{S}{TotalArea}$. The coefficient *S* is the unit area that an anion occupies at the interface. *TotalArea* is the total area of the interface. To simplify last equation, θ is introduced as $\frac{S*(Anion)_{interf}}{TotalArea}$. Solving Equation 4-1 and Equation 4-2 together gives:

$$K = \frac{\theta}{(1-\theta) * [Anion]}$$

$$\theta = \frac{K * [Anion]}{1 + K * [Anion]}$$

Equation 4-4

Combine Equation 4-3 and Equation 4-4,

$$M * (Anion)_{interf} = \frac{K * [Anion]}{1 + K * [Anion]}$$

Equation 4-5

So

$$\frac{1}{(Anion)_{interf}} = \frac{M}{K * [Anion]} + M \equiv a\frac{1}{[Anion]} + b$$

Equation 4-6

Equation 4-6 predicts that $\frac{1}{(Anion)_{interf}}$ and $\frac{1}{[Anion]}$ have a linear relationship if the conditions of Langmuir isotherm are satisfied. The relationships between $\frac{1}{(Anion)_{interf}}$ and $\frac{1}{[Anion]}$ for Cl^-, Br^-, SCN^-, and I^- are plotted in Figure 4-14.

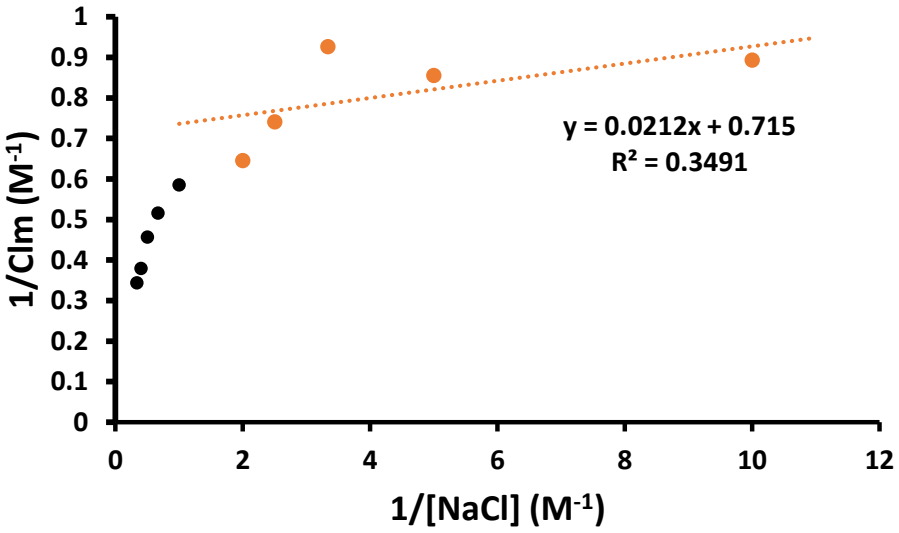

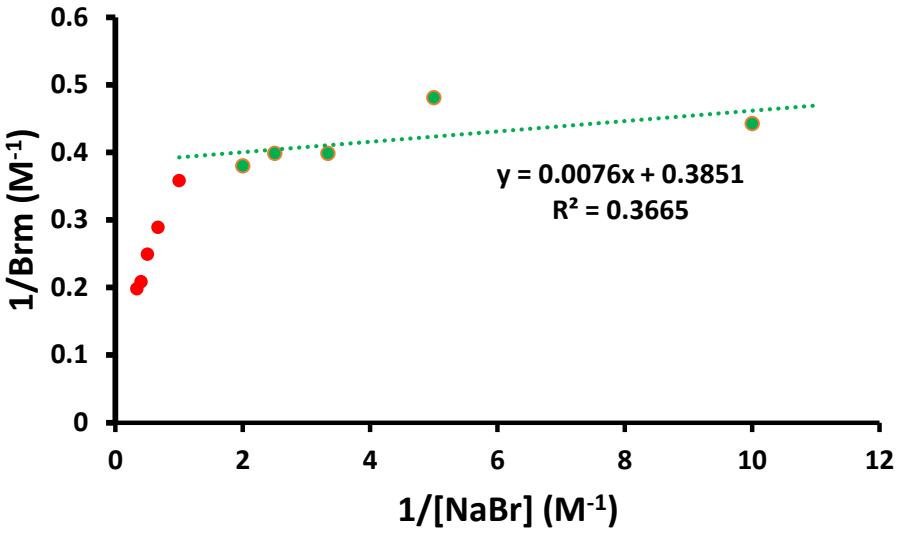
0.6
0.5
0.4
0.3
0.2
0.1
0
1/Brm (M-1)
y = 0.0076x + 0.3851
R² = 0.3665
0
2
4
6
8
10
12
1/[NaBr] (M-1)

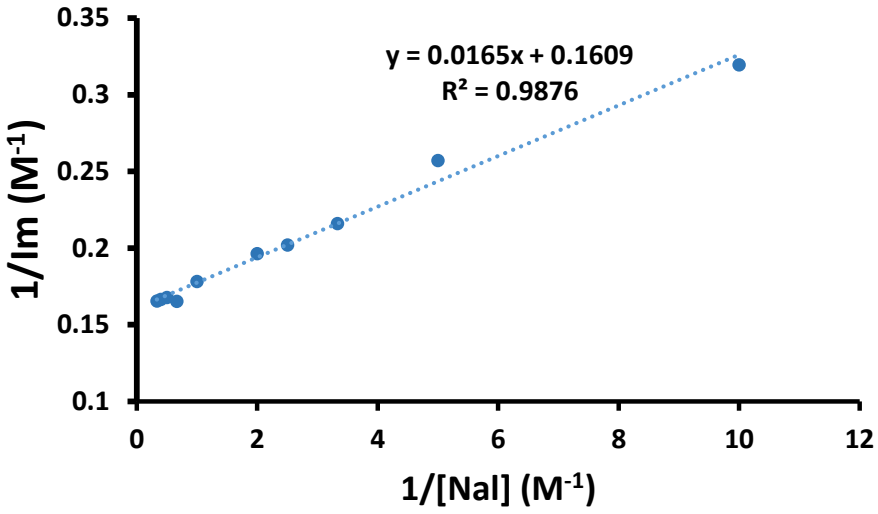
0.35
0.3
0.25
0.2
0.15
0.1
1/Im (M-1)
y = 0.0165x + 0.1609
R² = 0.9876
0
2
4
6
8
10
12
1/[NaI] (M-1)

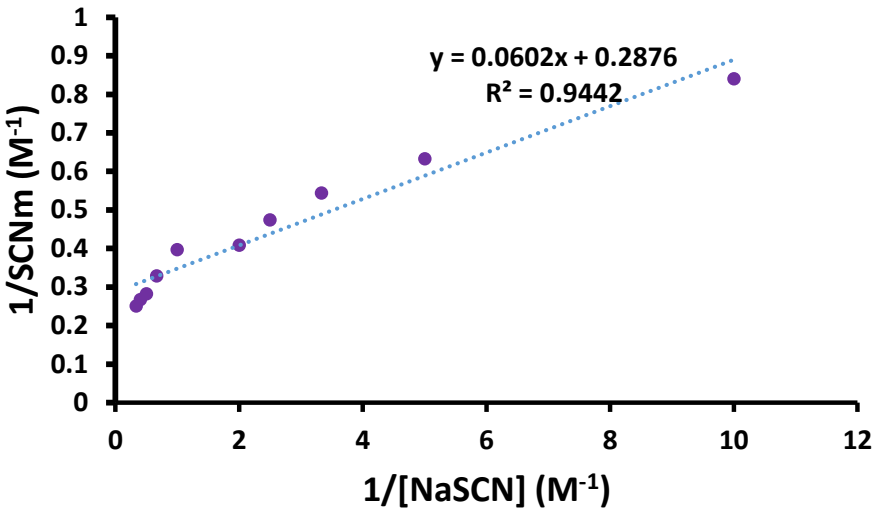

Figure 4-14 Plots of $1/X_m$ against 1/[X] from results of chemical trapping experiments. X = Cl^-, Br^-, I^-, SCN^-. The data points at low concentrations (high 1/[X]) were linearly fitted.

The double reciprocal plot for Cl^- and Br^- is clearly not linear. At higher concentrations (lower 1/[x] values) the interfacial anion molarities deviate significantly from the trend line. It suggests the adsorption of Cl^- and Br^- at high bulk concentration are much higher than the prediction of Langmuir model. SCN^- has similar deviation at a high bulk concentration. This matches with the Saykally group's observation that at higher concentration (> 4 M), the Langmuir modeling breaks down.[71] This might be because that at high concentration there is not only repulsion between interface anions, but also ion pairing between cations and anions. The anions and cations of ion pairs adsorb together at the interface, so the maximum coverage for anions will be close to $\frac{Size\ of\ anions}{Size\ of\ cations} * total\ area$, which depends on the sizes of the cations and anions because cations and anions number ratio is 1:1 for NaX monovalent salt. The anions may adsorb at the interface via interactions between polar ion-pairs and the interface, not by interaction between the anion alone with the interface.

However, MD results in Figure 4-11 show that the distances of cations density peak and anions density peak to the interface is not the same. Anion density peaks are always closer to the interface than that of cations, suggesting the existence of an electronic double layer. So if there are ion pairs formed at the same time at the interface, they probably are oriented with the anions close to the interface.

Onorato and coworkers paper[71] observed that the transition from Langmuir to non-Langmuir conditions appeared to be very sharp at around 4.0 M salt concentration, which also match with our observation here in SCN^- plot. They stated that the sharp transition indicates a structural change at the water/air interface that could come from 3 sources: an interfacial water structure change, or a second set of anion adsorption sites in the interfacial layer, or a disruption of the hydrophobic side of the interface. Even though in my experiments the structural changes of water can not be detected, the decrease of interfacial water molarity, especially for I^-, is very clear. As interfacial water molecules number increases and interfacial anions number increases, the hydration numbers of ions decrease and the anions will be less hydrated.

Saykally's results are consistent with the driving force of adsorption coming from the energetic benefit when big ions adsorb to the interface and decrease the contact area between air and water. Meanwhile, for those hydrophobic ions that don't have strong interactions with water molecules, staying at the interface and interacting with unsatisfied hydrogen bonds is favored from energy perspective rather than disrupting hydrogen bonds between water molecules in the bulk.[71]

Despite a number of observations, the discussion on the intrinsic mechanism of anions adsorption onto water/oil interface is still far from complete. Some physics research groups,

such as Yan Levin and Zhengang Wang group,[178, 179] tried to use physical methods to model ion behavior at the air/water and oil/water interface. By modeling the self-energy of an ion and combining it with nonelectrostatic interactions, Wang predicted specific ion effects on association of halide ions at water/air interface, and the strong adsorption of hydrophobic ions at the interface. Levin developed a model of polarizable ions to interpret interfacial properties of aqueous electrolyte solutions, but it did not pay much attention to the role of image force on the air side of the interface. Alternative explanations are common on the topic, and there is a long way to go before the Hofmeister phenomena at the interfaces is fully understood.

4.5 CONCLUSION

In a stirred mixture of tetradecane and salt solution (NaCl, NaBr, NaSCN, NaI), the interfacial molarities of these anions have been successfully measured at the neat water/tetradecane interface by using a long chain arenediazonium ion 16-ArN_2^+ as a probe. The anions strong adsorption to the interface was directly observed from the reaction products yields, and the corresponding molarities of interfacial anion and water were also obtained. This is the first experimental estimate of anion adsorption to a neat, uncharged water/nonpolar solvent interface has been observed. The order of anion association to the hydrocarbon interface follows a series similar to the Hofmeister Series, and interfacial concentrations were calculated from the experiment data. The anions local concentration has been compared with previously reported literatures and they are in good agreement in terms of the enhancement adsorption amount and anion/water molecule ratio at the

interface. The anions adsorption data was also fit with the classic Langmuir model, and as shown in other previous literatures, at high concentration the adsorption isotherm of Cl^-, Br^- and SCN^- deviate from the model. The deviation could be from the formation of interfacial ion pairs at high salt concentration. Our approach provides a new method to study one of the most basic water/oil interfaces and reveals more details about ions interaction with the interfaces, which is needed to fully interpret the Hofmeister Series.

4.6 SUPPLIMENTARY INFOMATION

4.6.1 Representative HPLC chromatograms

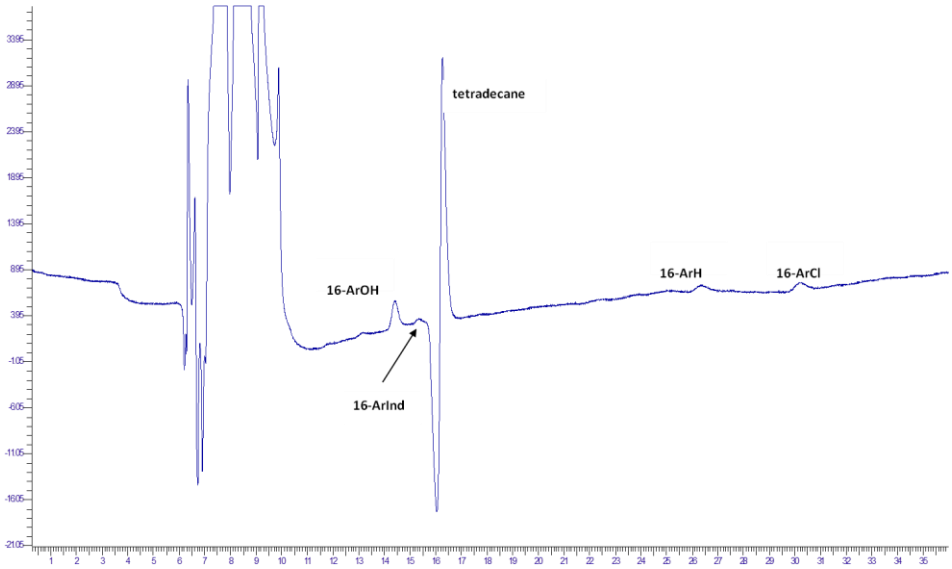

Figure 4-15 HPLC chromatogram of dediazoniation products of chemical trapping experiments in 1.0 M NaCl solution/tetradecane mixture diluted by ~ 4 mL iso-propanol.

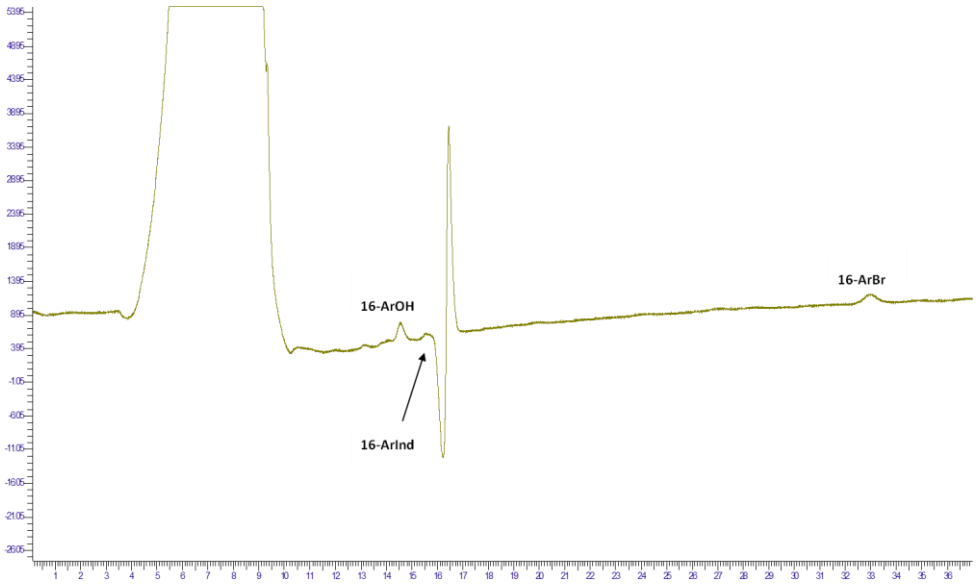

Figure 4-16 HPLC chromatogram of dediazoniation products of chemical trapping experiments in 1.0 M NaBr solution/tetradecane mixture diluted by ~ 4 mL iso-propanol.

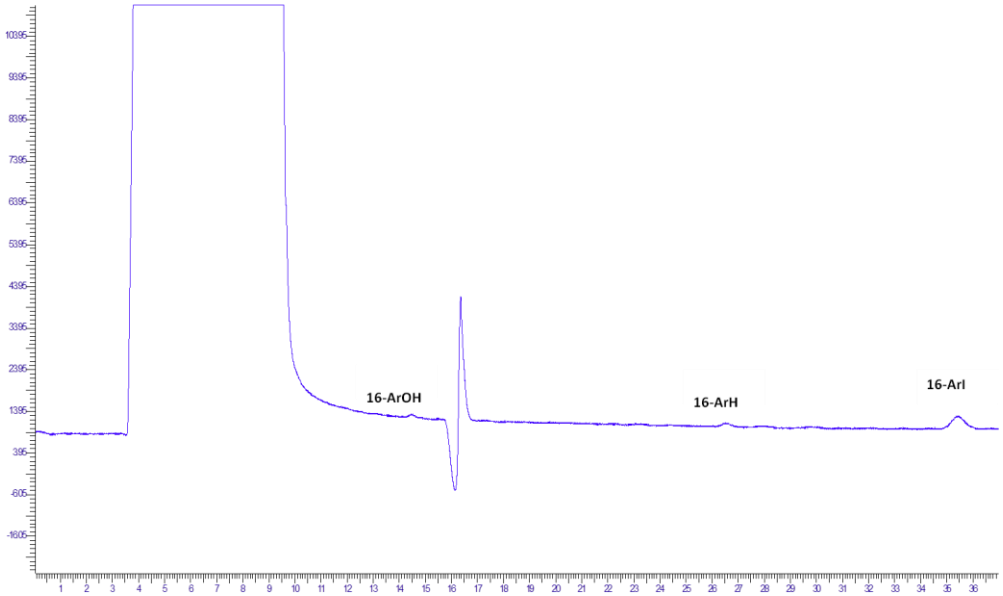

Figure 4-17 HPLC chromatogram of dediazoniation products of chemical trapping experiments in 0.2 M NaI solution/tetradecane mixture diluted by ~ 4 mL iso-propanol.

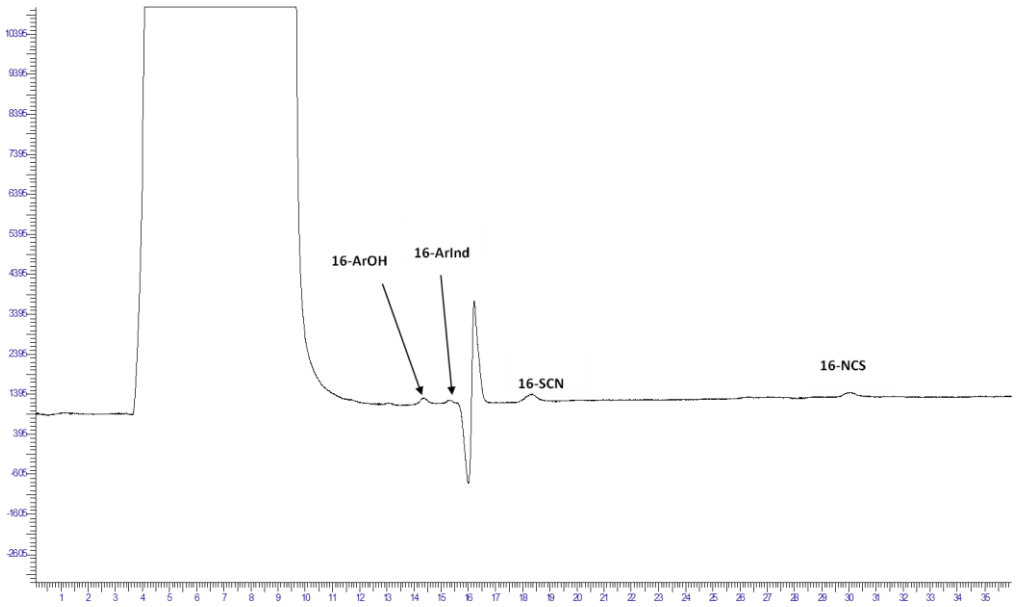

Figure 4-18 HPLC chromatogram of dediazoniation products of chemical trapping experiments in 1.0 M NaSCN solution/tetradecane mixture diluted by ~ 4 mL isopropanol.

4.6.2 Numerical data for Figure 4-10

Table 4-3 Estimated values of Cl_m, H_2O_m, S_w^{Cl} at NaCl solution/tetradecane interface from 0.1 to 3.0 M at 25℃ with [HBr] = 1 mM

[NaCl] M	Cl_m M	Standard Deviation of Cl_m	S_w^{Cl}	H_2O_m	H_2O_m/Cl_m
0.1	1.12	0.29	10.28	55.97	50.20
0.2	1.17	0.33	10.16	55.95	47.72
0.3	1.08	0.25	10.35	55.98	51.88
0.4	1.35	0.37	9.86	55.80	41.46
0.5	1.55	0.07	9.56	55.52	35.92
1.0	1.71	0.27	9.35	55.22	32.29
1.5	1.94	0.26	9.09	54.72	28.20
2.0	2.19	0.20	8.86	54.11	24.75
2.5	2.64	0.20	8.49	54.79	20.71
3.0	2.91	0.10	8.32	53.05	18.26

Table 4-4 Estimated values of Br_m, H_2O_m, S_w^{Br} at NaBr solution/tetradecane interface from 0.1 to 3.0 M at 25℃ with [HCl] = 1 mM

[NaBr] M	Br_m M	Standard Deviation of Br_m	S_w^{Br}	H_2O_m	H_2O_m/Br_m
0.1	2.26	0.29	11.67	48.62	21.47
0.2	2.08	0.33	11.82	49.50	23.79
0.3	2.51	0.25	11.51	47.48	18.89
0.4	2.51	0.27	11.51	47.48	18.89
0.5	2.63	0.07	11.45	46.95	17.83
1.0	2.79	0.27	11.38	46.27	16.61
1.5	3.46	0.24	11.20	43.21	12.48
2.0	4.01	0.20	11.13	40.56	10.11
2.5	4.79	0.20	11.08	36.51	7.63
3.0	5.04	0.10	11.07	35.10	6.96

Table 4-5 Estimated values of I_m, H_2O_m, S_w^I at NaI solution/tetradecane interface from 0.1 to 3.0 M at 25℃ with [HBr] = 1 mM

[NaI] M	I_m M	Deviation	S_w^I	H_2O_m	H_2O_m/I_m
0.1	3.13	0.16	28.55	50.00	15.99
0.2	3.89	0.08	28.12	45.77	11.76
0.3	4.63	0.02	27.70	40.39	8.73
0.4	4.95	0.06	27.52	37.76	7.63
0.5	5.09	0.01	27.44	36.55	7.18
1.0	5.61	0.20	27.14	31.90	5.69
1.5	6.05	0.24	26.89	27.66	4.57
2.0	5.96	0.26	26.94	28.51	4.78
2.5	6.00	0.19	26.92	28.13	4.69
3.0	6.04	0.57	26.90	27.81	4.61

Table 4-6 Estimated values of SCN_m, H_2O_m, S_w^{SCN} at NaSCN solution/tetradecane interface from 0.1 to 3.0 M at 25 C with [HBr] = 1 mM

[NaSCN] M	SCN_m [a] M	Deviation	S_w^{SCN}	H_2O_m	H_2O_m/ SCN_m
0.1	1.19	0.32	35.01	53.04	44.60
0.2	1.58	0.31	33.03	52.98	33.42
0.3	1.84	0.05	32.42	52.95	28.79
0.4	2.11	0.13	31.99	52.69	24.98
0.5	2.45	0.08	31.49	51.75	21.10
1.0	2.52	0.06	31.38	51.48	20.45
1.5	3.04	0.37	30.39	48.41	15.92
2.0	3.54	0.34	29.74	45.07	12.73
2.5	3.74	0.21	29.89	44.15	11.80
3.0	3.99	0.04	30.71	43.74	10.96

a. **SCN_m is calculated from %1-Ar~SCN (%1-Ar~SCN = %1-ArSCN + %1-ArNCS), so it represents the molarity of both 16–SCN product and 16–NCS product.**

Table 4-7 HPLC average peak areas, observed yields and normalized yields for reaction of 16-ArN_2^+ in NaCl solution/tetradecane mixture from 0.1 to 3.0 M at 25 °C. [HBr] = 1 mM[a]

[NaCl] M		Average Peak Areas (μv•s)[c]						Observed Yields (%)							Normalized Yields (%)[d]	
		16-NHAc	16-ArOH	16-Ind	16-H	16-ArCl		16-NHAc	16-ArOH	16-Ind	16-H	16-ArCl	Total		16-ArOH	16-ArCl
0.1		9.22E+03	6.25E+04	9.22E+03	1.98E+04	1.84E+04		5.4%	52.1%	5.5%	16.7%	14.1%	110.4%		83.0%	17.0%
0.2		1.01E+04	6.90E+04	1.08E+04	1.26E+04	1.90E+04		6.0%	57.6%	6.4%	10.6%	14.5%	105.6%		82.4%	17.6%
0.3		1.06E+04	5.39E+04	1.09E+04	1.48E+04	1.50E+04		6.2%	44.9%	6.5%	12.5%	11.5%	94.0%		83.4%	16.6%
0.4		7.32E+03	5.97E+04	1.02E+04	2.02E+04	2.08E+04		4.3%	49.8%	6.0%	17.0%	15.9%	110.0%		80.8%	19.2%
0.5		7.33E+03	4.97E+04	7.23E+03	1.50E+04	1.88E+04		4.3%	41.5%	4.3%	12.7%	14.4%	89.8%		79.0%	21.0%
1.0		5.22E+03	5.63E+04	5.97E+03	1.41E+04	2.23E+04		3.1%	47.0%	3.5%	11.9%	17.0%	94.4%		77.5%	22.5%
1.5		6.46E+03	4.33E+04	1.55E+04	1.66E+04	2.11E+04		3.8%	36.1%	9.2%	14.0%	16.2%	93.3%		75.6%	24.4%
2.0		1.02E+04	4.76E+04	2.02E+04	1.78E+04	2.56E+04		6.0%	39.7%	12.0%	15.0%	19.6%	107.3%		73.6%	26.4%
2.5		3.30E+03	3.77E+04	1.14E+04	1.38E+04	2.39E+04		1.9%	31.4%	6.8%	11.6%	18.3%	96.1%		72.8%	29.8%
3.0		7.36E+03	3.54E+04	2.60E+04	1.44E+04	2.53E+04		4.3%	29.5%	15.4%	12.2%	19.3%	92.9%		69.6%	31.7%

a. Reaction time ca. 24 h to ensure the complete dediazoniation reaction. The concentration of 16-ArN_2BF_4 was around 10^{-6} M due to uneasy precise control on the weight of 16-ArN_2BF_4.

b. Peak areas are average of triplicate injections. Eluting solvents: 65%MeOH/35%*i*-PrOH; Flow rate: 0.4 ml/min; Detector wavelength: 220 nm.

c. % Total = %16-NHAc + %16-ArOH + %16-Ind + %16-ArCl + 2 * %16-ArH

d. % $16\text{-}ArCl_N$ = 100 (%16-ArCl)/(%16-ArOH + %16-ArH + %16-ArCl); % $16\text{-}ArOH_N$ = 100 (%16-ArOH + %16-ArH)/(%16-ArOH + %16-ArH + %16-ArCl).

Table 4-8 HPLC average peak areas, observed yields and normalized yields for reaction of 16-ArN_2^+ in NaBr solution/tetradecane mixture from 0.1 to 3.0 M at 25 °C. [HCl] = 1 mM[a]

[NaBr] M	Average Peak Areas (μv•s)[c]					Observed Yields (%)						Normalized Yields (%)[d]	
	16-NHAc	16-ArOH	16-Ind	16-H	16-Br	16-NHAc	16-ArOH	16-Ind	16-H	16-Br	Total	16-ArOH	16-Br
0.1	6.94E+03	5.14E+04	5.79E+03	1.06E+04	4.71E+04	4.8%	50.4%	4.0%	10.5%	33.1%	113.4%	64.8%	35.2%
0.2	1.40E+04	6.34E+04	6.37E+03	4.41E+03	4.70E+04	9.7%	62.2%	4.4%	4.4%	33.1%	118.2%	66.8%	33.2%
0.3	5.79E+03	5.82E+04	5.75E+03	0	4.94E+04	4.0%	57.1%	4.0%	0.0%	34.8%	99.9%	62.1%	37.9%
0.4	6.71E+03	4.66E+04	6.34E+03	7.99E+03	4.64E+04	4.6%	45.7%	4.4%	7.9%	32.7%	103.3%	62.1%	37.9%
0.5	8.36E+03	4.89E+04	6.62E+03	1.08E+04	5.36E+04	5.8%	48.0%	4.6%	10.7%	37.7%	117.6%	60.9%	39.1%
1.0	7.25E+03	4.51E+04	9.51E+03	6.37E+03	4.92E+04	5.0%	44.2%	6.6%	6.3%	34.6%	103.2%	59.3%	40.7%
1.5	6.48E+03	3.97E+04	8.49E+03	0	4.96E+04	4.5%	38.9%	5.9%	0.0%	34.9%	84.3%	52.7%	47.3%
2.0	4.76E+03	3.58E+04	1.01E+04	0	5.49E+04	3.3%	35.1%	7.0%	0.0%	38.6%	84.1%	47.6%	52.4%
2.5	1.90E+04	2.93E+04	9.92E+03	0	5.94E+04	13.1%	28.8%	6.9%	0.0%	41.8%	90.6%	40.8%	59.2%
3.0	2.41E+04	2.92E+04	1.19E+04	0	6.47E+04	16.7%	28.6%	8.3%	0.0%	45.5%	99.1%	38.6%	61.4%

a. Reaction time ca. 24 h to ensure the complete dediazoniation reaction. The concentration of 16-ArN_2BF_4 was around 10^{-6} M due to uneasy precise control on the weight of 16-ArN_2BF_4.

b. Peak areas are average of triplicate injections. Eluting solvents: 65%MeOH/35%*i*-PrOH; Flow rate: 0.4 ml/min; Detector wavelength: 220 nm.

c. % Total = %16-NHAc + %16-ArOH + %16-Ind + %16-ArBr + 2* %16-ArH

d. % 16-$ArBr_N$ = 100 (%16-ArBr)/(%16-ArOH + %16-ArH + %16-ArBr);% 16-$ArOH_N$ = 100 (%16-ArOH + %16-ArH)/(%16-ArOH + %16-ArH + %16-ArBr).

Table 4-9 HPLC average peak areas, observed yields and normalized yields for reaction of 16-ArN_2^+ in NaI solution/tetradecane mixture from 0.1 to 3.0 M at 25°C. [HBr] = 1 mM[a]

[NaI] M	Average Peak Areas (μv•s)[c]					Observed Yields (%)						Normalized Yields (%)[d]	
	16-NHAc	16-ArOH+	16-Ind	16-H	16-ArI	16-NHAc	16-ArOH+	16-Ind	16-H	16-ArI	Total	16-ArOH	16-ArI
0.1	6.76E+03	1.24E+04	0.00E+00	2.21E+04	9.58E+04	3.8%	10.0%	0.0%	18.1%	50.1%	110.8%	35.9%	64.1%
0.2	0.00E+00	3.73E+03	0.00E+00	2.16E+04	9.43E+04	0.0%	3.4%	0.0%	20.1%	56.3%	97.0%	29.5%	70.5%
0.3	0.00E+00	2.98E+03	0.00E+00	2.07E+04	1.17E+05	0.0%	2.5%	0.0%	17.3%	62.9%	107.6%	24.0%	76.0%
0.4	0.00E+00	3.49E+03	0.00E+00	1.50E+04	1.04E+05	0.0%	3.4%	0.0%	15.0%	66.5%	90.5%	21.7%	78.3%
0.5	0.00E+00	2.75E+03	0.00E+00	1.72E+04	1.19E+05	0.0%	2.4%	0.0%	15.2%	67.2%	102.3%	20.7%	79.3%
1.0	8.66E+03	9.53E+02	0.00E+00	1.62E+04	1.27E+05	5.0%	0.8%	0.0%	13.4%	67.5%	109.3%	17.3%	82.7%
1.5	7.14E+03	0.00E+00	0.00E+00	1.43E+04	1.32E+05	4.2%	0.0%	0.0%	12.2%	71.5%	106.6%	14.5%	85.5%
2.0	7.91E+03	0.00E+00	0.00E+00	1.56E+04	1.37E+05	4.4%	0.0%	0.0%	12.5%	70.5%	112.7%	15.1%	84.9%
2.5	0.00E+00	0.00E+00	0.00E+00	1.64E+04	1.47E+05	0.0%	0.0%	0.0%	12.9%	74.2%	114.4%	14.8%	85.2%
3.0	0.00E+00	0.00E+00	0.00E+00	1.54E+04	1.40E+05	0.0%	0.0%	0.0%	12.8%	74.5%	108.9%	14.6%	85.4%

a. Reaction time ca. 24 h to ensure the complete dediazoniation reaction. The concentration of 16-ArN_2BF_4 was around 10^{-6} M due to uneasy precise control on the weight of 16-ArN_2BF_4.

b. Peak areas are average of triplicate injections. Eluting solvents: 65%MeOH/35%*i*-PrOH; Flow rate: 0.4 ml/min; Detector wavelength: 220 nm.

c. % Total = %16-NHAc + %16-ArOH + %16-Ind + %16-ArI + 2* %16-ArH

d. % 16-ArI_N = 100 (%16-ArI)/(%16-ArOH + %16-ArH + %16-ArI);% 16-$ArOH_N$ = 100 (%16-ArOH + %16-ArH)/(%16-ArOH + %16-ArH + %16-ArI).

Table 4-10 HPLC average peak areas, observed yields and normalized yields for reaction of 16-ArN_2^+ in NaSCN solution/tetradecane mixture from 0.1 to 3.0 M at 25°C. [HBr] = 1 mM[a]

[NaSCN] M	Average Peak Areas (μv•s)[c]						Observed Yields (%)						Normalized Yields (%)[d]	
	16-NHAc	16-ArOH+	16-Ind	16-SCN	16-H	16-NCS	16-NHAc	16-ArOH+	16-Ind	16-H	16(SCN)	Total	16-$ArOH_N$	16-$(SCN)_N$
0.1	6.55E+03	1.65E+04	4.11E+04	2.83E+04	2.03E+04	2.80E+04	3.8%	13.7%	24.3%	18.1%	24.1%	106.6%	56.0%	44.0%
0.2	7.04E+03	1.40E+04	3.82E+04	3.78E+04	2.09E+04	2.14E+04	4.0%	11.4%	22.1%	23.7%	28.2%	109.0%	50.3%	49.7%
0.3	6.45E+03	1.40E+04	1.81E+04	3.98E+04	1.93E+04	2.71E+04	4.2%	12.9%	11.9%	28.4%	34.9%	95.8%	47.0%	53.0%
0.4	3.21E+03	1.65E+04	1.87E+04	4.30E+04	1.46E+04	2.60E+04	2.2%	16.2%	13.1%	32.7%	39.4%	89.8%	43.8%	56.2%
0.5	1.20E+04	3.05E+04	1.38E+04	5.62E+04	4.74E+03	3.58E+04	7.6%	27.5%	8.8%	39.1%	47.4%	98.3%	40.1%	59.9%
1.0	5.79E+03	2.77E+04	9.57E+03	5.90E+04	8.12E+03	3.69E+04	3.7%	25.1%	6.2%	41.4%	50.0%	97.5%	39.4%	60.6%
1.5	5.83E+03	2.29E+04	9.72E+03	6.36E+04	7.78E+03	3.73E+04	3.8%	21.1%	6.4%	45.3%	54.2%	96.0%	34.4%	65.6%
2.0	7.61E+03	1.42E+04	1.47E+04	7.03E+04	1.16E+04	2.49E+04	4.7%	12.5%	9.1%	47.5%	53.1%	101.1%	30.0%	70.0%
2.5	8.20E+03	1.09E+04	1.62E+04	6.53E+04	1.05E+04	1.59E+04	5.6%	10.5%	11.1%	48.5%	52.4%	92.1%	28.3%	71.7%
3.0	0	1.36E+04	1.06E+04	6.95E+04	8.33E+03	3.11E+04	0.0%	13.6%	7.6%	53.8%	61.9%	88.2%	26.3%	73.7%

a. Reaction time ca. 24 h to ensure the complete dediazoniation reaction. The concentrations of 16-ArN_2BF_4 were around 10^{-6} M but vary in each experiments.

b. Peak areas are average of triplicate injections. Eluting solvents: 65%MeOH/35%*i*-PrOH; Flow rate: 0.4 ml/min; Detector wavelength: 220 nm.

c. % Total = %16-NHAc + %16-ArOH + %16-Ind + %16-ArSCN + %16-ArNCS + 2* %16-ArHd. % 16-$ArSCN_N$ = 100 (%16-ArSCN + %16-ArNCS)/(+ %16-ArOH + %16-ArH + %16-ArSCN + %16-ArNCS); % 16-$ArOH_N$ = 100 (%16-ArOH + %16-ArH)/(%16-ArOH + %16-ArH + %16-ArSCN + %16-ArNCS).

4.6.3 Results for control experiments in 1.0 M NaCl & NaI solution

Table 4-11 Results for control experiment in 1.0 M NaCl solution with increasing stirring speed. [HCl] = 1 mM. Each run was repeated 3 times.

Probe conc. (M)	Stirring rate (rpm)	%16-OH_N	%16-Cl_N	Standard deviation of %16-Cl_N	Cl_m (M)	S_w^{Cl}	H_2O_m	H_2O_m/ Cl_m
5.10E-06	233	65.1%	34.9%	2.97%	3.36	8.05	50.55	15.04
	334	70.2%	29.8%	4.98%	2.64	8.50	52.84	20.04
	550	71.5%	28.5%	1.68%	2.46	8.63	53.36	21.67
	599	76.7%	23.3%	0.75%	1.82	9.23	55.00	30.29
	812	75.7%	24.3%	0.54%	1.93	9.10	54.74	28.31
	970	75.1%	24.9%	2.69%	2.01	9.03	54.57	27.19
	1215	75.6%	24.4%	3.63%	1.94	9.09	54.72	28.19
	1340	75.4%	24.6%	2.02%	1.97	9.07	54.66	27.79

Table 4-12 HPLC average peak areas, observed yields and normalized yields for reaction of 16-ArN_2^+ in stir rate controlling experiment in NaCl solution/tetradecane mixture at 1.0 M at 25°C. [HCl] = 1 mM. Each run was repeated 3 times.

[probe] (M)	Stirring speed (rpm)	Average Peak Areas (mv s)[c]				Observed Yields (%)					Normalized Yields (%)			
		16-ArOH	16-Ind	16-H	16-Cl	16-ArOH	16-Ind	16-H	16-Cl	Total	16-ArOH_N	16-Cl_N		St. dev. of 16-Cl_N
5.10E-06	233	2.05E+05	6.22E+04	6.86E+04	1.60E+05	40.2%	8.7%	13.6%	28.8%	91.3%	65.1%	34.9%		2.97%
	334	2.20E+05	6.14E+04	7.78E+04	1.38E+05	43.2%	8.6%	15.4%	24.9%	92.1%	70.2%	29.8%		4.98%
	550	2.24E+05	5.57E+04	8.45E+04	1.34E+05	43.8%	7.8%	16.8%	24.1%	92.5%	71.5%	28.5%		1.68%
	599	2.47E+05	5.02E+04	6.30E+04	1.03E+05	48.4%	7.0%	12.5%	18.5%	86.4%	76.7%	23.3%		0.75%
	812	2.01E+05	1.37E+05	5.79E+04	9.09E+04	39.4%	19.2%	11.5%	16.3%	86.4%	75.7%	24.3%		0.54%
	970	2.74E+05	4.67E+04	5.83E+04	1.20E+05	53.7%	6.5%	11.6%	21.7%	93.4%	75.1%	24.9%		2.69%
	1215	2.73E+05	2.35E+04	7.46E+04	1.22E+05	53.5%	3.3%	14.8%	22.0%	93.6%	75.6%	24.4%		3.63%
	1340	3.26E+05	3.84E+04	3.56E+04	1.29E+05	64.0%	5.4%	7.1%	23.2%	99.6%	75.4%	24.6%		2.02%

Table 4-13 Results for control experiment in 1.0 M NaCl solution with increasing probe concentration. [HCl] = 1 mM. Each run was repeated 3 times.

Probe conc. (M)	probe relative conc. to cmc	%Norm. H2O	Norm. %16-ArCl	Standard deviation of %16-ArCl	Cl_m (M)	S_w^{Cl}	H_2O_m	H_2O_m/ Cl_m
1.25E-06	25%	81.7%	18.3%	1.2%	1.25	10.02	55.90	44.66
2.50E-06	50%	82.6%	17.4%	1.3%	1.16	10.19	55.96	48.39
5.00E-06	100%	81.4%	18.6%	0.9%	1.29	9.96	55.86	43.44
7.50E-06	150%	76.1%	23.9%	0.7%	1.88	9.15	54.86	29.14
1.00E-05	200%	73.1%	26.9%	0.4%	2.25	8.80	53.94	23.96
1.50E-05	300%	73.2%	26.8%	0.8%	2.24	8.81	53.96	24.05

Table 4-14 HPLC average peak areas, observed yields and normalized yields for reaction of 16-ArN_2^+ in probe concentration controlling experiment in NaCl solution/tetradecane mixture at 1.0 M at 25°C. [HCl] = 1 mM. Each run was repeated 3 times.

[probe] (M)		Average Peak Areas (mv s)[c]					Observed Yields (%)						Normalized Yields (%)[e]			Std. dev. of 16-Cl_N
		16-ArOH	16-Ind	16-H	16-Cl		16-ArOH	16-Ind	16-H	16-Cl	Total		16-$ArOH_N$	16-Cl_N		
1.25E-06		1.43E+04	1.48E+03	4.57E+03	4.63E+03		57.2%	4.2%	18.5%	17.0%	115.4%		81.7%	18.3%		1.2%
2.50E-06		3.48E+04	4.54E+03	4.31E+03	8.98E+03		69.7%	6.5%	8.7%	16.5%	110.1%		82.6%	17.4%		1.3%
5.00E-06		6.70E+04	8.64E+03	5.96E+03	1.82E+04		67.1%	6.2%	6.0%	16.7%	101.9%		81.4%	18.6%		0.9%
7.50E-06		8.58E+04	1.91E+04	8.90E+03	3.25E+04		57.2%	9.1%	6.0%	19.9%	98.2%		76.1%	23.9%		0.7%
1.00E-05		1.27E+05	2.13E+04	1.59E+04	5.76E+04		63.6%	7.6%	8.1%	26.4%	113.8%		73.1%	26.9%		0.4%
1.50E-05		1.73E+05	4.23E+04	2.85E+04	8.05E+04		57.7%	10.0%	9.6%	24.6%	111.6%		73.2%	26.8%		0.8%

Table 4-15 Results for control experiment in 1.0 M NaI solution with increasing probe concentration. [HCl] = 1 mM. Each run was repeated 3 times.

Probe conc. (M)	probe relative conc.	%Norm. H2O	Norm. %16-ArI	Standard deviation of %16-ArI	I_m(M)	S_w^I	H_2O_m	H_2O_m/ I_m
1.25E-06	25%	18.7%	81.3%	0.89%	5.39	27.27	33.89	6.29
2.50E-06	50%	19.0%	81.0%	1.22%	5.35	27.29	34.23	6.40
5.00E-06	100%	19.2%	80.8%	1.37%	5.32	27.31	34.54	6.50
7.50E-06	150%	15.1%	84.9%	1.42%	5.96	26.94	28.57	4.79
1.00E-05	200%	12.1%	87.9%	1.47%	6.45	26.66	23.71	3.67
1.50E-05	300%	10.8%	89.2%	1.10%	6.67	26.54	21.49	3.22

Table 4-16 HPLC average peak areas, observed yields and normalized yields for reaction of 16-ArN_2^+ in probe concentration controlling experiment in NaI solution/tetradecane mixture at 1.0 M at 25°C. [HCl] = 1 mM. Each run was repeated 3 times.

probe conc. (M)	Average Peak Areas (mv s)[c]			Observed Yields (%)				Normalized Yields (%)		Std. dev. of 16-I_N
	16-ArOH	16-H	16-I	16-ArOH	16-H	16-I	Total[d]	16-$ArOH_N$	16-I_N	
1.25E-06	0.00E+00	1.95E+04	1.41E+05	0.0%	12.2%	87.8%	95.14%	18.7%	81.3%	0.89%
2.50E-06	9.02E+03	3.23E+04	2.75E+05	2.9%	10.2%	86.9%	91.84%	19.0%	81.0%	1.22%
5.00E-06	2.32E+04	6.58E+04	6.05E+05	3.3%	9.5%	87.2%	99.82%	19.2%	80.8%	1.37%
7.50E-06	2.02E+04	9.75E+04	9.58E+05	1.9%	9.1%	89.1%	101.69%	15.1%	84.9%	1.42%
1.00E-05	0.00E+00	1.09E+05	1.24E+06	0.0%	8.1%	91.9%	93.25%	12.1%	87.9%	1.47%
1.50E-05	0.00E+00	1.44E+05	1.86E+06	0.0%	7.2%	92.8%	90.78%	10.8%	89.2%	1.10%

4.6.4 Calibration curves

Table 4-17 Calibration curves for long-chain dediazonation products.[a]

Reaction Product	Calibration Equation[b]	R^2
16-ArI[d]	$\mathbf{y}=1.542\times10^{11}\mathbf{x}$	1.0000
16-ArCl[c]	$\mathbf{y}=1.087\times10^{11}\mathbf{x}$	1.0000
16-ArAc[c]	$\mathbf{y}=9.338\times10^{10}\mathbf{x}$	1.0000
16-ArOH[c]	$\mathbf{y}=10.00\times10^{10}\mathbf{x}-28660$	0.9998
16-ArH[c]	$\mathbf{y}=9.883\times10^{10}\mathbf{x}+14590$	1.0000
16-ArInd[c]	$\mathbf{y}=1.404\times10^{11}\mathbf{x}+249000$	0.9980
16-ArBr[c]	$\mathbf{y}=1.393\times10^{11}\mathbf{x}+14530$	1.0000
16-SCN	$\mathbf{y}=1.295\times10^{11}\mathbf{x}$	0.99908
16-NCS	$\mathbf{y}=3.864\times10^{11}\mathbf{x}$ [e]	0.9996

a. HPLC Eluting solvent: 35%/65% v/v, *i*-PrOH/MeOH (except 16-Ind: 40%/60%, v/v). Flow rate: 0.4 ml/min. Detector wavelength: 220 nm. Injection volume: 100 μL.
b. Units: **y**-peak area (in μv·s), **x**-concentration (in molarity), and R^2 (correlation coefficient).
c. Zhang, Y. L.; Romsted, L. S.; Zhuang, L. Z.; de Jong, S. *Langmuir* **2013**, *29*, 534.
d. Measured by Changyao Liu
e. This is the calibration curve of 1-NCS under HPLC conditions: 35%/65% v/v, *i*-PrOH/ MeOH. Flow rate: 0.4 ml/min. Detector wavelength: 220 nm. Injection volume: 100 μL. 16-NCS is hard to obtain and I used 1-NCS calibration curve to represent that of 16-NCS. They share the same functional group and should have the same response to the same wavelength UV lights.

Table 4-18 Calibration curves for short-chain dediazonation products.[a]

Reaction Product	Calibration Equation[b]	R^2
1-ArI[d]	$\mathbf{y}=5.436\times10^{10}\mathbf{x}$	0.9998
1-ArCl[c]	$\mathbf{y}=1.178\times10^{10}\mathbf{x}$	0.9996
1-ArAc[c]	$\mathbf{y}=3.965\times10^{9}\mathbf{x}$	1.0000
1-ArOH[c]	$\mathbf{y}=1.300\times10^{10}\mathbf{x}$	0.9995
1-ArBr[c]	$\mathbf{y}=2.321\times10^{10}\mathbf{x}+14530$	0.9998
1-ArSCN	$\mathbf{y}=3.118\times10^{10}\mathbf{x}$	0.99879
1-ArNCS	$\mathbf{y}=4.307\times10^{10}\mathbf{x}$	0.99975

a. HPLC Eluting solvent: 80%/20% v/v, MeOH/H_2O. Flow rate: 0.6 ml/min. Detector wavelength: 230 nm. Injection volume: 50 μL.
b. Units: **y**-peak area (in μv·s), **x**-concentration (in molarity), and R^2 (correlation coefficient).
c. Zhang, Y. L.; Romsted, L. S.; Zhuang, L. Z.; de Jong, S. *Langmuir* **2013**, *29*, 534.
d. Measured by Changyao Liu

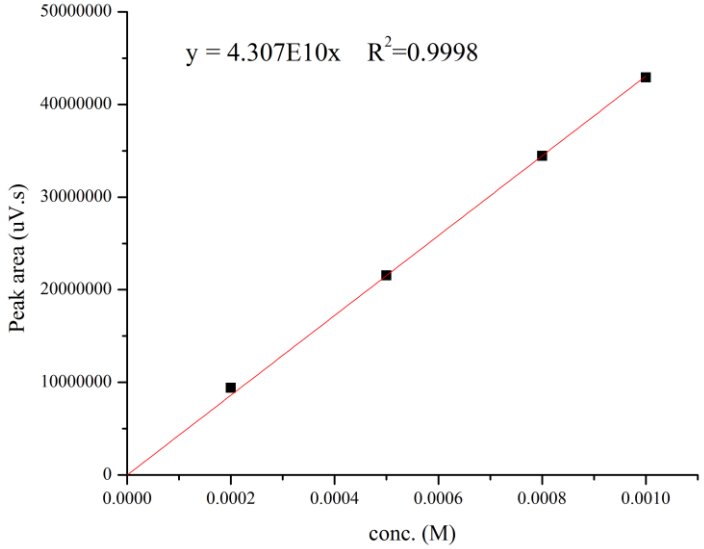

Figure 4-19 Calibration curve for 1-ArNCS.

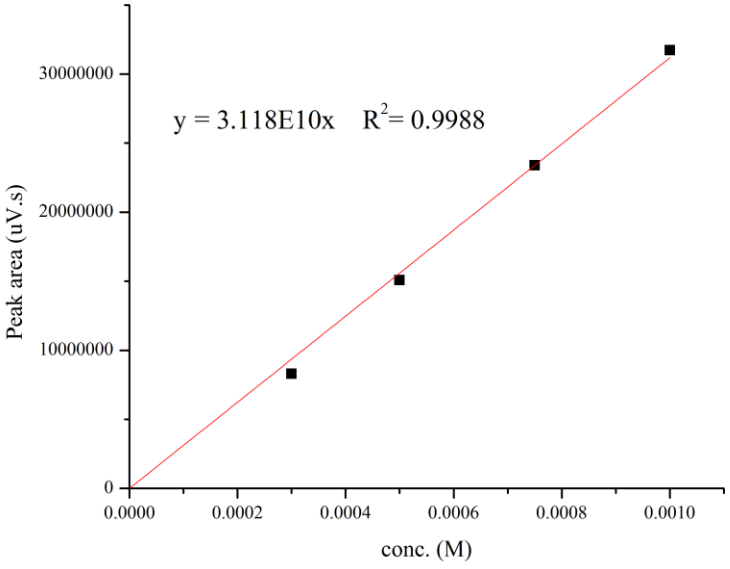

Figure 4-20 Calibration curve for 1-ArSCN.

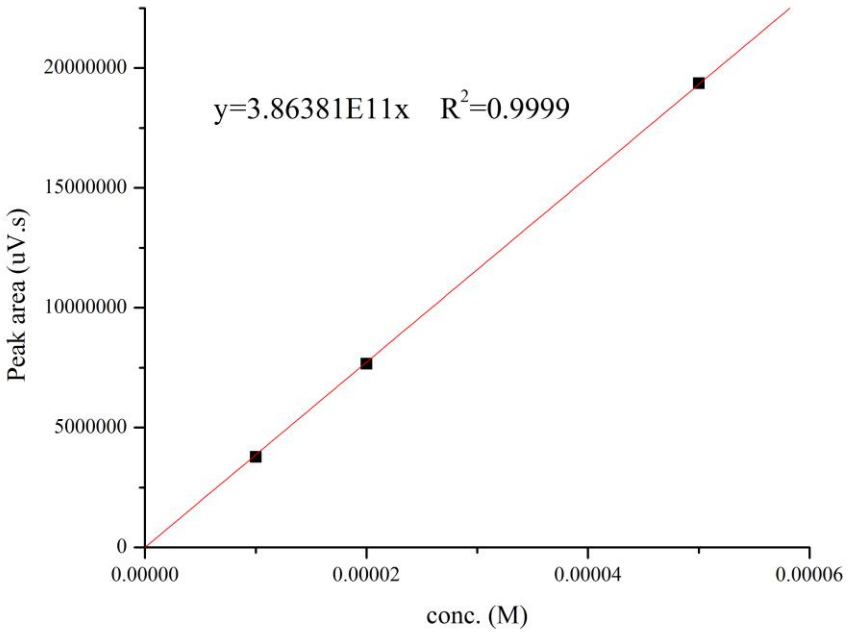

Figure 4-21 Calibration curve for 16-ArNCS.

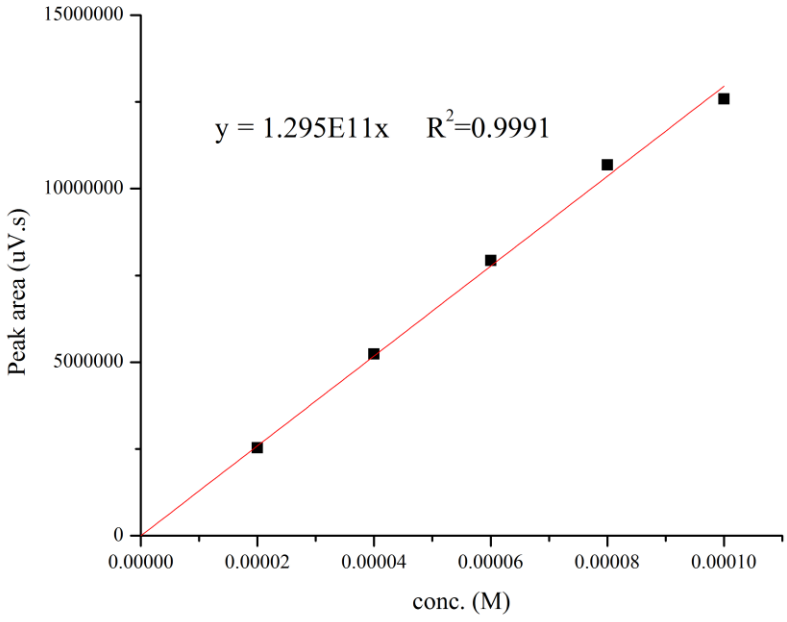

Figure 4-22 Calibration curve for 16-ArSCN.

4.6.5 Standard curves for chemical trapping method

Figure 4-23 Dediazoniation product yields from reaction of 5 × 10^{-3} M 1-ArN_2BF_4 with SCN^- (%1-Ar~SCN = %1-ArSCN + %1-ArNCS) in aqueous NaSCN solutions at room temperature. Standard curve for %1-Ar~SCN against NaSCN (M) is fitted by the equation: %1-Ar~SCN = 40.844 $[NaSCN]^{0.4264}$

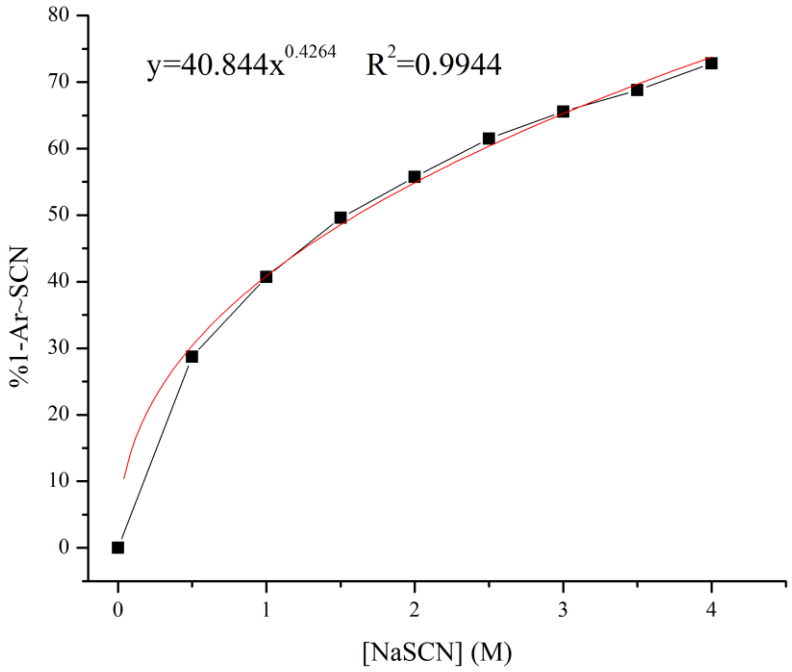

Figure 4-24 Selectivity of the dediazoniation reaction towards SCN^- compared to H_2O, S_w^{SCN}, for reactions in NaSCN aqueous solutions at room temperature. S_w^{SCN} against NaSCN concentration is fitted by the equation: $S_w^{SCN} = 37.84\ [NaSCN]^{-0.216}$.

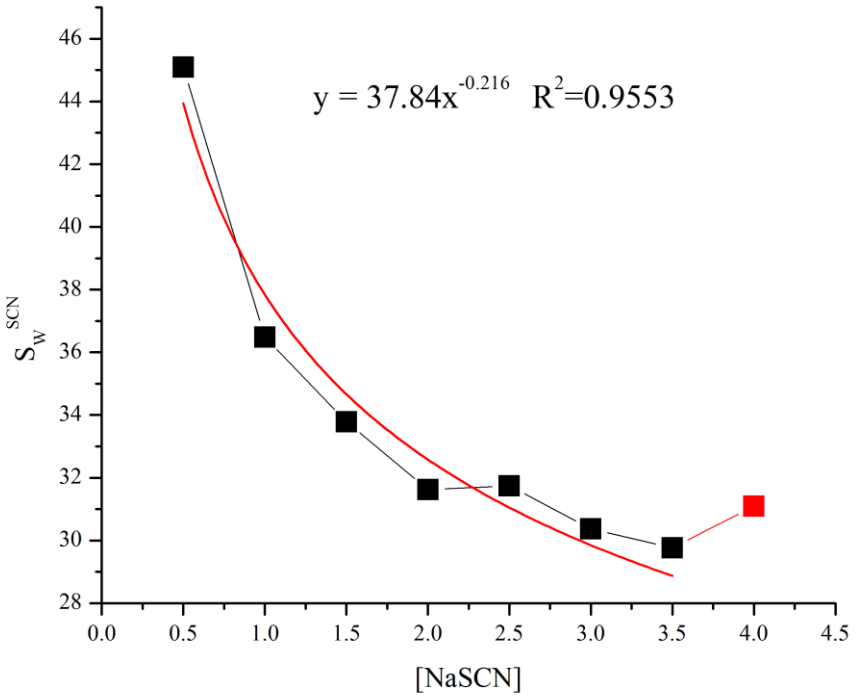

Figure 4-25 Dediazoniation product yields from reaction of 5 × 10^{-3} M 1-ArN_2BF_4 with I^- (%1-ArI) in aqueous NaI solutions at room temperature. Standard curve for %1-ArI against NaI (M) is fitted by the equation: %1-ArI = 39.05 $[NaI]^{0.4328}$

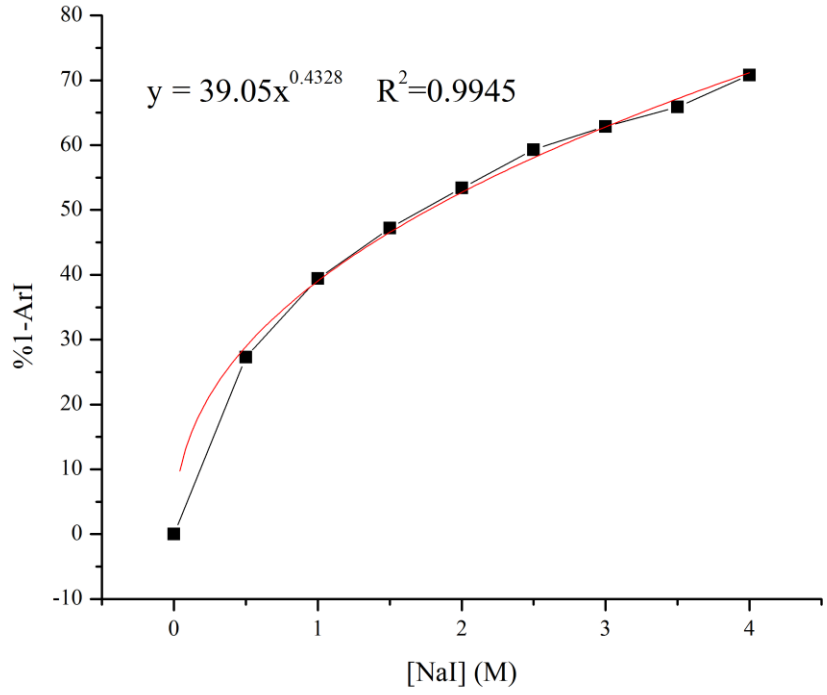

Figure 4-26 Selectivities of the dediazoniation reaction towards I^- compared to H_2O, S_w^I, for reactions in NaI aqueous solutions at room temperature. S_w^I against NaI concentration is fitted by the equation: $S_w^I = 34.62\ [NaI]^{-0.118}$.

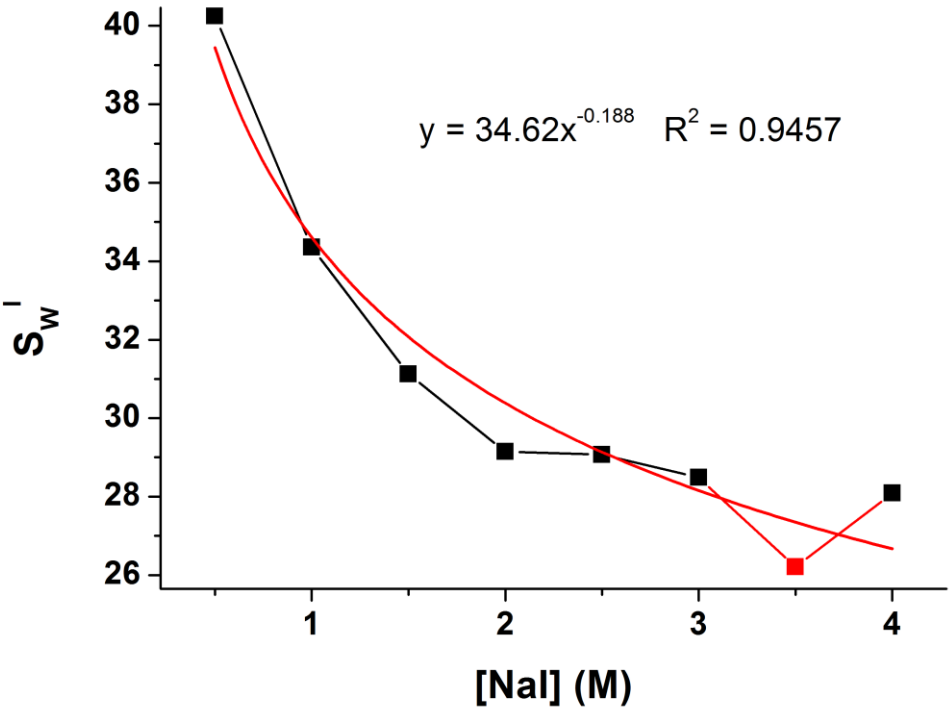

REFERENCES

1. Kunz, W.; Henle, J.; Ninham, B. W. 'Zur Lehre von der Wirkung der Salze' (about the science of the effect of salts): Franz Hofmeister's historical papers. *Curr. Opin. Colloid Interface Sci.* **2004,** *9* (1-2), 19-37.

2. Pegram, L. M.; Wendorff, T.; Erdmann, R.; Shkel, I.; Bellissimo, D.; Felitsky, D. J.; Record, M. T. Why Hofmeister effects of many salts favor protein folding but not DNA helix formation. *Proceedings of the National Academy of Sciences of the United States of America* **2010,** *107* (17), 7716-7721.

3. Manet, S.; Karpichev, Y.; Bassani, D.; Kiagus-Ahmad, R.; Oda, R. Counteranion Effect on Micellization of Cationic Gemini Surfactants 14-2-14: Hofmeister and Other Counterions. *Langmuir* **2010,** *26* (13), 10645-10656.

4. Lo Nostro, P.; Ninham, B. W. Hofmeister Phenomena: An Update on Ion Specificity in Biology. *Chem. Rev.* **2012,** *112* (4), 2286-2322.

5. Duignan, T. T.; Parsons, D. F.; Ninham, B. W. Collins's rule, Hofmeister effects and ionic dispersion interactions. *Chem. Phys. Lett.* **2014,** *608*, 55-59.

6. Jungwirth, P.; Cremer, P. S. Beyond Hofmeister. *Nature Chemistry* **2014,** *6* (4), 261-263.

7. Zhang, Y. J.; Cremer, P. S. Chemistry of Hofmeister Anions and Osmolytes. *Annual Review of Physical Chemistry, Vol 61* **2010,** *61*, 63-83.

8. Cacace, M. G.; Landau, E. M.; Ramsden, J. J. The Hofmeister series: salt and solvent effects on interfacial phenomena. *Quarterly Reviews of Biophysics* **1997,** *30* (3), 241-277.

9. Ferreira, G. S. S.; Perigo, D. M.; Politi, M. J.; Schreier, S. Effect of anions from the Hofmeister series and urea on the binding of the charged and uncharged forms of the local anesthetic tetracaine to zwitterionic micelles. *Photochem. Photobiol.* **1996,** *63* (6), 755-761.

10. Leberman, R. The Hofmeister Series and Ionic-Strength. *FEBS Lett.* **1991,** *284* (2), 293-294.

11. Salis, A.; Pinna, M. C.; Bilanicova, D.; Monduzzi, M.; Lo Nostro, P.; Ninham, B. W. Specific anion effects on glass electrode pH measurements of buffer solutions: Bulk and surface phenomena. *J. Phys. Chem. B* **2006,** *110* (6), 2949-2956.

12. Salis, A.; Bhattacharyya, M. S.; Monduzzi, M. Specific Ion Effects on Adsorption of Lysozyme on Functionalized SBA-15 Mesoporous Silica. *J. Phys. Chem. B* **2010,** *114* (23), 7996-8001.

13. Toth, K.; Sedlak, E.; Sprinzl, M.; Zoldak, G. Flexibility and enzyme activity of NADH oxidase from Thermus thermophilus in the presence of monovalent cations of Hofmeister series. *Biochimica Et Biophysica Acta-Proteins and Proteomics* **2008,** *1784* (5), 789-795.

14. Pinna, M. C.; Bauduin, P.; Touraud, D.; Monduzzi, M.; Ninham, B. W.; Kunz, W. Hofmeister effects in biology: Effect of choline addition on the salt-induced super activity of horseradish peroxidase and its implication for salt resistance of plants. *J. Phys. Chem. B* **2005,** *109* (34), 16511-16514.

15. Craig, V. S. J. Bubble coalescence and specific-ion effects. *Curr. Opin. Colloid Interface Sci.* **2004,** *9* (1-2), 178-184.

16. Murgia, S.; Portesani, F.; Ninham, B. W.; Monduzzi, M. Interaction of sodium ions with cationic surfactant interfaces. *Chemistry-a European Journal* **2006,** *12* (30), 7889-7898.

17. Vacha, R.; Siu, S. W. I.; Petrov, M.; Bockmann, R. A.; Barucha-Kraszewska, J.; Jurkiewicz, P.; Hof, M.; Berkowitz, M. L.; Jungwirth, P. Effects of Alkali Cations and Halide Anions on the DOPC Lipid Membrane. *J. Phys. Chem. A* **2009,** *113* (26), 7235-7243.

18. Alkschbirs, M. I.; Percebom, A. M.; Loh, W.; Westfahl, H.; Cardoso, M. B.; Sabadini, E. Effects of some anions of the Hofmeister series on the rheology of cetyltrimethylammonium-salicylate wormlike micelles. *Colloids and Surfaces a-Physicochemical and Engineering Aspects* **2015,** *470*, 1-7.

19. Ninham, B. W.; Lo Nostro, P. *Molecular forces and self assembly in colloid, nano sciences and biology* [Online]; Cambridge University Press,: Cambridge, U.K. ; New York, 2010; pp. 1 online resource (xvi, 365 p.). http://app.knovel.com/web/toc.v/cid:kpMFSAICN3.

20. Kunz, W. *Specific ion effects*; World Scientific: Hackensack, NJ, 2010. p xxi, 325 p.

21. Suresh, S. J.; Kapoor, K.; Talwar, S.; Rastogi, A. Internal structure of water around cations. *J. Mol. Liq.* **2012,** *174*, 135-142.

22. Dill, K. A.; Truskett, T. M.; Vlachy, V.; Hribar-Lee, B. Modeling water, the hydrophobic effect, and ion solvation. *Annu. Rev. Biophys. Biomol. Struct.* **2005,** *34*, 173-199.

23. Zavitsas, A. A. Properties of water solutions of electrolytes and nonelectrolytes. *J. Phys. Chem. B* **2001,** *105* (32), 7805-7817.

24. Kuzmin, V. L. Charge Models of Water-Molecules and the Dipole Quadrupole Theory of Surface-Potential. *Colloid J.* **1994,** *56* (5), 593-603.

25. Okamoto, Y.; Mikami, T.; Yoshii, N.; Okazaki, S. A molecular analysis of the vibrational energy relaxation mechanism of the CN- ion in water based upon path integral influence functional theory combined with a dipole expansion of the solute-solvent interaction. *J. Mol. Liq.* **2007,** *134* (1-3), 34-39.

26. Middleton, S. R.; Pallas, N. R.; Mingins, J.; Pethica, B. A. Thermodynamics of Ionized Monolayers: Surface Manometry on Very Low Density Spread Monolayers of Sodium Octadecyl Sulfate at the Air/Water Interface and Analysis of Ionic Double Layer Contributions to the Isotherms. *Journal of Physical Chemistry C* **2011,** *115* (16), 8056-8063.

27. Tavares, F. W.; Bratko, D.; Blanch, H. W.; Prausnitz, J. M. Ion-specific effects in the colloid-colloid or protein-protein potential of mean force: Role of salt-macroion van der Waals interactions. *J. Phys. Chem. B* **2004,** *108* (26), 9228-9235.

28. Zhou, H.; Preston, M. A.; Tilton, R. D.; White, L. R. Calculation of the electric polarizability of a charged spherical dielectric particle by the theory of colloidal electrokinetics. *J. Colloid Interface Sci.* **2005,** *285* (2), 845-856.

29. Bostrom, M.; Deniz, V.; Franks, G. V.; Ninham, B. W. Extended DLVO theory: Electrostatic and non-electrostatic forces in oxide suspensions. *Adv. Colloid Interface Sci.* **2006,** *123*, 5-15.

30. Valle, R. P.; Huang, C. L.; Loo, J. S. C.; Zuo, Y. Y. Increasing Hydrophobicity of Nanoparticles Intensifies Lung Surfactant Film Inhibition and Particle Retention. *Acs Sustainable Chemistry & Engineering* **2014,** *2* (7), 1574-1580.

31. Collins, K. D. Ion hydration: Implications for cellular function, polyelectrolytes, and protein crystallization. *Biophys. Chem.* **2006,** *119* (3), 271-281.

32. Ninham, B. W.; Duignan, T. T.; Parsons, D. F. Approaches to hydration, old and new: Insights through Hofmeister effects. *Curr. Opin. Colloid Interface Sci.* **2011,** *16* (6), 612-617.

33. Millero, F. J. Chem. Rev. 1971, 71, 147

34. Zavitsas, A. A. Ideal Behavior of Water Solutions of Strong Electrolytes and Non-electrolytes at High Concentrations. *J. Solution Chem.* **2010,** *39* (3), 301-317.

35. Collins, K. D. Ions from the Hofmeister series and osmolytes: effects on proteins in solution and in the crystallization process. *Methods* **2004,** *34* (3), 300-311.

36. Samoilov, O. Y. Discuss. Faraday Soc. 1957, 24, 141

37. Beck, T. L. A Local Entropic Signature of Specific Ion Hydration. *J. Phys. Chem. B* **2011,** *115* (32), 9776-9781.

38. Collins, K. D.; Neilson, G. W.; Enderby, J. E. Ions in water: Characterizing the forces that control chemical processes and biological structure. *Biophys. Chem.* **2007,** *128* (2-3), 95-104.

39. Salis, A.; Ninham, B. W. Models and mechanisms of Hofmeister effects in electrolyte solutions, and colloid and protein systems revisited. *Chem. Soc. Rev.* **2014,** *43* (21), 7358-7377.

40. Bostrom, M.; Tavares, F. W.; Finet, S.; Skouri-Panet, F.; Tardieu, A.; Ninham, B. W. Why forces between proteins follow different Hofmeister series for pH above and below pI. *Biophys. Chem.* **2005,** *117* (3), 217-224.

41. Ninham, B. W.; Yaminsky, V. Ion binding and ion specificity: The Hofmeister effect and Onsager and Lifshitz theories. *Langmuir* **1997,** *13* (7), 2097-2108.

42. Bostrom, M.; Ninham, B. W. Why pH titration in lysozyme suspensions follow a Hofmeister series. *Colloids and Surfaces a-Physicochemical and Engineering Aspects* **2006,** *291* (1-3), 24-29.

43. Roque, A.; Pina, F.; Alves, S.; Ballardini, R.; Maestri, M.; Balzani, V. Micelle effect on the 'write-lock-read-unlock-erase' cycle of 4 '-hydroxyflavylium ion. *J. Mater. Chem.* **1999,** *9* (9), 2265-2269.

44. Andrews, B. A.; Haywood, K. Effect of Ph, Ion Type and Ionic-Strength on Partitioning of Proteins in Reverse Micelle Systems. *J. Chromatogr. A* **1994,** *668* (1), 55-60.

45. Almgren, M.; Linse, P.; Vanderauweraer, M.; Deschryver, F. C.; Gelade, E.; Croonen, Y. Fluorescence Quenching by Counterions in Ionic Micelle Solution - the Effect of Ion Migration. *J. Phys. Chem.* **1984,** *88* (2), 289-295.

46. Doughty, D. A. Effect of Co-Ion on the Preferential Interaction Parameter and Micelle Aggregation Number - Sodium Dodecyl-Sulfate in Aqueous Sodium-Halide. *J. Phys. Chem.* **1983,** *87* (25), 5286-5290.

47. Koelsch, P.; Motschmann, H. Varying the counterions at a charged interface. *Langmuir* **2005,** *21* (8), 3436-3442.

48. Heyda, J.; Vincent, J. C.; Tobias, D. J.; Dzubiella, J.; Jungwirth, P. Ion Specificity at the Peptide Bond: Molecular Dynamics Simulations of N-Methylacetamide in Aqueous Salt Solutions. *J. Phys. Chem. B* **2010,** *114* (2), 1213-1220.

49. Kadam, Y.; Singh, K.; Marangoni, D. G.; Ma, J. H.; Aswal, V. K.; Bahadur, P. Induced micellization and micellar transitions in aqueous solutions of non-linear block copolymer Tetronic (R) T904. *J. Colloid Interface Sci.* **2010,** *351* (2), 449-456.

50. Lagi, M.; Lo Nostro, P.; Fratini, E.; Ninham, B. W.; Baglioni, P. Insights into Hofmeister mechanisms: Anion and degassing effects on the cloud point of dioctanoylphosphatidylcholine/water systems. *J. Phys. Chem. B* **2007,** *111* (3), 589-597.

51. Murgia, S.; Monduzzi, M.; Ninham, B. W. Hofmeister effects in cationic microemulsions. *Curr. Opin. Colloid Interface Sci.* **2004,** *9* (1-2), 102-106.

52. Mittal, K. L.; American Chemical Society. *Micellization, solubilization, and microemulsions : [proceedings]*; Plenum Press: New York, 1977.

53. Geng, Y.; Romsted, L. S.; Menger, F. Specific ion pairing and interfacial hydration as controlling factors in gemini micelle morphology. Chemical trapping studies. *JACS* **2006,** *128* (2), 492-501.

54. Oda, R.; Huc, I.; Schmutz, M.; Candau, S. J.; MacKintosh, F. C. Tuning bilayer twist using chiral counterions. *Nature* **1999,** *399* (6736), 566-569.

55. Johans, C.; Behrens, M. A.; Bergquist, K. E.; Olsson, U.; Manzanares, J. A. Potential Determining Salts in Microemulsions: Interfacial Distribution and Effect on the Phase Behavior. *Langmuir* **2013,** *29* (51), 15738-15746.

56. Takata, Y.; Miyayama, T.; Nagahashi, T.; Hyono, A.; Ohshima, H. Micelle Formation Effect on Electroacoustics in an Aqueous Surfactant Solution: Colloid Vibration Current and Ion Vibration Current. *Journal of Oleo Science* **2009,** *58* (11), 557-563.

57. Cui, D.; Ou, S. C.; Patel, S. Protein Denaturants at Aqueous-Hydrophobic Interfaces: Self-Consistent Correlation between Induced Interfacial Fluctuations and Denaturant Stability at the Interface. *J. Phys. Chem. B* **2015,** *119* (1), 164-178.

58. Hornby, J. A. T.; Codreanu, S. G.; Armstrong, R. N.; Dirr, H. W. Molecular recognition at the dimer interface of a class Mu glutathione transferase: Role of a hydrophobic interaction motif in dimer stability and protein function. *Biochemistry* **2002,** *41* (48), 14238-14247.

59. Walder, R.; Schwartz, D. K. Dynamics of protein aggregation at the oil-water interface characterized by single molecule TIRF microscopy. *Soft Matter* **2011,** *7* (17), 7616-7622.

60. Sottmann, T.; Strey, R.; Chen, S. H. A small-angle neutron scattering study of nonionic surfactant molecules at the water-oil interface: Area per molecule, microemulsion domain size, and rigidity. *J. Chem. Phys.* **1997,** *106* (15), 6483-6491.

61. Janusz, W.; Sedlak, A.; Matysek-Nawrocka, M. Experimental Study of the Co-adsorption of Cadmium and Citrate Ions onto a TiO2 (Anatase)/Electrolyte Solution Interface. *Adsorption Science & Technology* **2008,** *26* (8), 599-612.

62. Touhami, A.; Alexander, M.; Kurylowicz, M.; Gram, C.; Corredig, M.; Dutcher, J. R. Probing protein conformations at the oil droplet-water interface using single-molecule force spectroscopy. *Soft Matter* **2011,** *7* (21), 10274-10284.

63. Luo, G. M.; Malkova, S.; Yoon, J.; Schultz, D. G.; Lin, B. H.; Meron, M.; Benjamin, I.; Vanysek, P.; Schlossman, M. L. Ion distributions near a liquid-liquid interface. *Science* **2006,** *311* (5758), 216-218.

64. Chen, X.; Yang, T.; Kataoka, S.; Cremer, P. S. Specific ion effects on interfacial water structure near macromolecules. *JACS* **2007,** *129* (40), 12272-12279.

65. Wick, C. D.; Dang, L. X. Recent advances in understanding transfer ions across aqueous interfaces. *Chem. Phys. Lett.* **2008,** *458* (1-3), 1-5.

66. Schnell, B.; Schurhammer, R.; Wipff, G. Distribution of hydrophobic ions and their counterions at an aqueous liquid-liquid interface: A molecular dynamics investigation. *J. Phys. Chem. B* **2004,** *108* (7), 2285-2294.

67. Jungwirth, P.; Tobias, D. J. Specific ion effects at the air/water interface. *Chem. Rev.* **2006,** *106* (4), 1259-1281.

68. Jungwirth, P.; Tobias, D. J. Molecular structure of salt solutions: A new view of the interface with implications for heterogeneous atmospheric chemistry. *J. Phys. Chem. B* **2001,** *105* (43), 10468-10472.

69. Ishiyama, T.; Morita, A. Molecular dynamics study of gas-liquid aqueous sodium halide interfaces. I. Flexible and polarizable molecular modeling and interfacial properties. *Journal of Physical Chemistry C* **2007,** *111* (2), 721-737.

70. Ishiyama, T.; Morita, A. Molecular dynamics study of gas-liquid aqueous sodium halide interfaces. II. Analysis of vibrational sum frequency generation spectra. *Journal of Physical Chemistry C* **2007,** *111* (2), 738-748.

71. Onorato, R. M.; Otten, D. E.; Saykally, R. J. Adsorption of thiocyanate ions to the dodecanol/water interface characterized by UV second harmonic generation. *Proceedings of the National Academy of Sciences of the United States of America* **2009,** *106* (36), 15176-15180.

72. Ghosal, S.; Hemminger, J. C.; Bluhm, H.; Mun, B. S.; Hebenstreit, E. L. D.; Ketteler, G.; Ogletree, D. F.; Requejo, F. G.; Salmeron, M. Electron spectroscopy of aqueous solution interfaces reveals surface enhancement of halides. *Science* **2005,** *307* (5709), 563-566.

73. Shamay, E. S.; Richmond, G. L. Ionic Disruption of the Liquid-Liquid Interface. *Journal of Physical Chemistry C* **2010,** *114* (29), 12590-12597.

74. McFearin, C. L.; Richmond, G. L. The Role of Interfacial Molecular Structure in the Adsorption of Ions at the Liquid-Liquid Interface. *Journal of Physical Chemistry C* **2009,** *113* (50), 21162-21168.

75. Vazdar, M.; Pluharova, E.; Mason, P. E.; Vacha, R.; Jungwirth, P. Ions at Hydrophobic Aqueous Interfaces: Molecular Dynamics with Effective Polarization. *Journal of Physical Chemistry Letters* **2012,** *3* (15), 2087-2091.

76. Chou, T. H. Current Application of Lipid- and Surfactant-based Vesicles for Cosmeceuticals: A Review. *Current Pharmaceutical Biotechnology* **2015,** *16* (12), 1035-1044.

77. Knoche, M. Organosilicone Surfactant Performance in Agricultural Spray Application - a Review. *Weed Research* **1994,** *34* (3), 221-239.

78. Wauer, R. R.; Rogalski, M.; Schwerecke, A.; Schmalisch, G. Endotracheal Application of an Exogenic Surfactant for Prophylaxis and Therapy of Neonatal Respiratory-Distress Syndrome - Literature-Review. *Zeitschrift Fur Klinische Medizin-Zkm* **1991,** *46* (13), 985-992.

79. Bunton, C. A.; Nome, F.; Quina, F. H.; Romsted, L. S. Ion Binding and Reactivity at Charged Aqueous Interfaces. *Acc. Chem. Res.* **1991,** *24* (12), 357-364.

80. Hamilton, A. D. *Supramolecular control of structure and reactivity*; Wiley: Chichester ; New York, 1996. p x, 339 p.

81. Zana, R.; Xia, J. *Gemini surfactants synthesis, interfacial and solution-phase behavior, and applications* [Online]; Marcel Dekker,: New York, 2004; pp. viii, 331 p. http://marc.crcnetbase.com/isbn/9780203913093.

82. Franks, F.; SpringerLink (Online service). *Water A Comprehensive Treatise Aqueous Solutions of Amphiphiles and Macromolecules* [Online]; Springer US : Imprint: Springer,: Boston, MA, 1975; pp. XXI, 839 p. http://dx.doi.org/10.1007/978-1-4684-2958-9.

83. Preston, W. C, Some correlating principles of detergent action, J. Phys. Colloid Chem., 52, 84-96 (1948).

84. Holmberg, K. *Surfactants and polymers in aqueous solution*; 2nd ed.; John Wiley & Sons: Chichester, West Sussex, England ; Hoboken, NJ, 2003. p xvi, 545 p.

85. Malliaris, A.; Lemoigne, J.; Sturm, J.; Zana, R. Temperature-Dependence of the Micelle Aggregation Number and Rate of Intramicellar Excimer Formation in Aqueous Surfactant Solutions. *J. Phys. Chem.* **1985,** *89* (12), 2709-2713.

86. Brady, J. E.; Evans, D. F.; Warr, G. G.; Grieser, F.; Ninham, B. W. Counterion Specificity as the Determinant of Surfactant Aggregation. *J. Phys. Chem.* **1986,** *90* (9), 1853-1859.

87. Malliaris, A.; Binanalimbele, W.; Zana, R. Fluorescence Probing Studies of Surfactant Aggregation in Aqueous-Solutions of Mixed Ionic Micelles. *J. Colloid Interface Sci.* **1986,** *110* (1), 114-120.

88. Kalyanasundaram, K. Photochemistry in Microheterogeneous Systems; Academic Press, Orlando, FL, 1987.

89. Bravo-Diaz, C.; Romsted, L. S.; Liu, C. Y.; Losada-Barreiro, S.; Pastoriza-Gallego, M. J.; Gao, X.; Gu, Q.; Krishnan, G.; Sanchez-Paz, V.; Zhang, Y. L.; Dar, A. A. To Model Chemical Reactivity in Heterogeneous Emulsions, Think Homogeneous Microemulsions. *Langmuir* **2015,** *31* (33), 8961-8979.

90. Kwetkat, K. SOFT (Eng. Ed.) 2002, 128, 38

91. Sugihara, G.; Nakamura, A. A.; Nakashima, T. H.; Araki, Y. I.; Okano, T.; Fujiwara, M. An electroconductivity study on degree of counterion binding or dissociation of a-sulfonatomyristic acid methyl ester micelles in water as a function of temperature. *Colloid. Polym. Sci.* **1997,** *275* (8), 790-796.

92. Evans, H.C., Alkyl Sulphates. Part I. Critical Micelle Concentrations of the Sodium Salts. J.Chem. Soc., 1956: p. 579-586.

93. Walter, A.; Yeagle, P. L.; Siegel, D. P. Diacylglycerol and Hexadecane Increase Divalent Cation-Induced Lipid Mixing Rates between Phosphatidylserine Large Unilamellar Vesicles. *Biophys. J.* **1994,** *66* (2), 366-376.

94. Lear, J. D.; Gratkowski, H.; Adamian, L.; Liang, J.; DeGrado, W. F. Position-dependence of stabilizing polar interactions of asparagine in transmembrane helical bundles. *Biochemistry* **2003,** *42* (21), 6400-6407.

95. Ruzza, A. A.; Froehner, S. J.; Minatti, E.; Nome, F.; Zanette, D. Quantitative Treatment of Ketal Hydrolysis in Aqueous-Solutions Containing Polymer Surfactant Complexes Using a Pseudophase Kinetic-Model. *J. Phys. Chem.* **1994,** *98* (47), 12361-12366.

96. Harwell, J. H.; Hoskins, J. C.; Schechter, R. S.; Wade, W. H. Pseudophase Separation Model for Surfactant Adsorption - Isomerically Pure Surfactants. *Langmuir* **1985,** *1* (2), 251-262.

97. Mittal, K. L.; Lindman, B.; Bothorel, P. *Surfactants in solution*; Plenum Press: New York, 1984. p v.

98. Geng, Y. Ph. D., Rutgers, The State University of New Jersey, 2003.

99. Romsted, L. S. Do amphiphile aggregate morphologies and interfacial compositions depend primarily on interfacial hydration and ion-specific interactions? The evidence from chemical trapping. *Langmuir* **2007,** *23* (2), 414-424.

100. Chaudhuri, A.; Loughlin, J. A.; Romsted, L. S.; Yao, J. H. Arenediazonium Salts - New Probes of the Interfacial Compositions of Association Colloids .1. Basic Approach, Methods, and Illustrative Applications. *JACS* **1993,** *115* (18), 8351-8361.

101. Zollinger, H. *Diazo chemistry I : aromatic and heteroaromatic compounds*; VCH: Weinheim ; New York, 1994. p xiii, 453 p.

102. C. Swain, J. Sheats, K. Harbison. Evidence for phenyl cation as an intermediated in reactions of benzenediazonium salts in solution. J. Am. Chem. Soc., 1975, 97 (4), pp 783–790

103. Garti, N. Progress in stabilization and transport phenomena of double emulsions in food applications. *Food Science and Technology-Lebensmittel-Wissenschaft & Technologie* **1997,** *30* (3), 222-235.

104. Okochi, H.; Nakano, M. Preparation and evaluation of w/o/w type emulsions containing vancomycin. *Advanced Drug Delivery Reviews* **2000,** *45* (1), 5-26.

105. Lee, J. S.; Kim, J. W.; Han, S. H.; Chang, H. S.; Kang, H. H.; Lee, O. S.; Oh, S. G.; Suh, K. D. The stabilization of L-ascorbic acid in aqueous solution and water-in-oil-in-water double emulsion by controlling pH and electrolyte concentration. *Journal of Cosmetic Science* **2004,** *55* (1), 1-12.

106. Fingas, M.; Fieldhouse, B. Water-in-Oil Emulsions: Formation and Prediction. *Handbook of Oil Spill Science and Technology* **2015**, 225-270.

107. Myers, D. *Surfactant science and technology*; VCH: New York, NY, 1988. p xiii, 351 p.

108. Romsted, L. S.; Bravo-Diaz, C. Modeling chemical reactivity in emulsions. *Curr. Opin. Colloid Interface Sci.* **2013,** *18* (1), 3-14.

109. Priebe, J. P.; Satnami, M. L.; Tondo, D. W.; Souza, B. S.; Priebe, J. M.; Micke, G. A.; Costa, A. C. O.; Fiedler, H. d.; Bunton, C. A.; Nome, F. The Chameleon-like Nature of Zwitterionic Micelles: The Intrinsic Relationship of Anion and Cation Binding in Sulfobetaine Micelles. *J. Phys. Chem. B* **2008,** *112* (46), 14373-14378.

110. Drinkel, E.; Souza, F. D.; Fiedler, H. D.; Nome, F. The chameleon effect in zwitterionic micelles: Binding of anions and cations and use as nanoparticle stabilizing agents. *Curr. Opin. Colloid Interface Sci.* **2013,** *18* (1), 26-34.

111. Tondo, D. W.; Leopoldino, E. C.; Souza, F. D.; Micke, G. A.; Costa, A. C. O.; Fiedler, H. D.; Bunton, C. A.; Nome, F. Synthesis of a New Zwitterionic Surfactant Containing an Imidazolium Ring. Evaluating the Chameleon-like Behavior of Zwitterionic Micelles. *Langmuir* **2010,** *26* (20), 15754-1576.

112. Priebe, J. P.; Souza, F. D.; Silva, M.; Tondo, D. W.; Priebe, J. M.; Micke, G. A.; Costa, A. C. O.; Bunton, C. A.; Quina, F. H.; Fiedler, H. D.; Nome, F. The Chameleon-Like Nature of Zwitterionic Micelles: Effect of Cation Binding. *Langmuir* **2012,** *28* (3), 1758-1764.

113. de Souza, T. P.; Chaimovich, H.; Fahr, A.; Schweitzer, B.; Neto, A. A.; Cuccovia, I. M. Interfacial concentrations of chloride and bromide in zwitterionic micelles with opposite dipoles: Experimental determination by chemical trapping and a theoretical description. *J. Colloid Interface Sci.* **2012,** *371*, 62-72.

114. Lowry, T. H.; Richardson, K. S. *Mechanism and Theory in Organic Chemistry*; 3rd ed.; Harper and Row: New York, 1987.

115. Ninham, B. W.; Lo Nostro, P. *Molecular Forces and Self Assembly in Colloid, Nano Sciences and Biology*; Cambridge University Press: Cambridge, 2010.

116. Pereira, R. D.; Zanette, D.; Nome, F. Application of the Pseudophase Ion-Exchange Model to Kinetics in Microemulsions of Anionic Detergents. *J. Phys. Chem.* **1990,** *94* (1), 356-361.

117. Chaimovich, H.; Bonilha, J. B. S.; Zanette, D.; Cuccovia, I. M. Analysis of the Effect of Micelles and Vesicles on the Reactivity of Nucleophiles Derived from the Dissociation of Weak Acids. In *Surfactants in Solution*, Mittal, K. L.; Lindman, B., Eds.; Plenum Press: New York, 1984; Vol. 2, pp 1121-1138.

118. Scarpa, M. V.; Maximiano, F. A.; Chaimovich, H.; Cuccovia, I. M. Interfacial Concentrations of Chloride and Bromide and Selectivity for Ion Exchange in Vesicles Prepared with Dioctadecyldimethylammonium Halides, Lipids, and Their Mixtures. *Langmuir* **2002,** *18*, 8817-8823.

119. Romsted, L. S.; Bravo-Diaz, C. Modeling chemical reactivity in emulsions. *Curr. Opin. Colloid Interface Sci.* **2013,** *18* (1), 3-14.

120. Gu, Q.; Bravo-Diaz, C.; Romsted, L. S. Using the pseudophase kinetic model to interpret chemical reactivity in ionic emulsions: determining antioxidant partition constants and interfacial rate constants. *J. Colloid Interface Sci.* **2013,** *accepted*.

121. Palaprat, G.; Ganachaud, F.; Mauzac, M.; Hemery, P. Cationic polymerization of 2,4,6,8-tetramethylcyclotetrasiloxane processed by tuning the pH of the miniemulsion. *Polymer* **2005,** *46* (25), 11213-11218.

122. Golding, M.; Wooster, T. J. The influence of emulsion structure and stability on lipid digestion. *Curr. Opin. Colloid Interface Sci.* **2010,** *15* (1-2), 90-101.

123. Choi, S. J.; Decker, E. A.; Henson, L.; Popplewell, L. M.; McClements, D. J. Influence of Droplet Charge on the Chemical Stability of Citral in Oil-in-Water Emulsions. *J. Food Sci.* **2010,** *75* (6), C536-C540.

124. Kaminski, W.; Kwapinski, W. Applicability of liquid membranes in environmental protection. *Pol. J. Environ. Stud.* **2000,** *9* (1), 37-43.

125. Halpern, M. E. *Phase Transfer Catalysis*. ACS: Washington, DC, 1997; p 314.

126. Holmberg, K. Reactions in Organized Surfactant Systems. In *Microemulsions*, Stubenrauch, C., Ed.; John Wiley and Sons: Chitchester, 2009.

127. Rosen, M. J. *Surfactants and Interfacial Phenomena*; 3rd ed.; John Wiley & Sons: New York, 2004. p 464.

128. Sanchez-Paz, V.; Pastoriza-Gallego, M. J.; Losada-Barreiro, S.; Bravo-Diaz, C.; Gunaseelan, K.; Romsted, L. S. Quantitative determination of *alpha*-tocopherol distribution in a tributyrin/Brij 30/water model food emulsion. *J. Colloid Interface Sci.* **2008,** *320* (1), 1-8.

129. Zuman, P.; Patel, R. *Techniques in Organic Reaction Kinetics*; John Wiley & Sons: New York, 1984. p 340.

130. Brown, K. C.; Doyle, M. P. Reduction of Arenediazonium Salts by Hydroquinone. Kinetics and Mechanism for the Electron-Transfer Step. *J. Org. Chem.* **1988,** *53*, 3255-3261.

131. Silberberg, M. *Chemistry*; 6th ed.; McGraw-Hill: Boston, 2011.

132. Jencks, W. P.; Regenstein, J. In *Handbook of Biochemistry*, Sorber, S. A., Ed.; The Chemical Rubber Co.: Cleveland, 1970, pp J187-J226.

133. Romsted, L. S. Quantitative Treatment of Benzimidazole Deprotonation Equilibria in Aqueous Micellar Solutions of Cetyltrimethylammonium Ion (CTAX, X^- = Cl^-, Br^-, and NO_3^-) Surfactants. 1. Variable Surfactant Concentration. *J. Phys. Chem.* **1985,** *89* (23), 5107-5113.

134. He, Z. M.; Oconnor, P. J.; Romsted, L. S.; Zanette, D. Specific Counterion Effects on Indicator Equilibria in Micellar Solutions of Decyl Phosphate and Lauryl Sulfate Surfactants. *J. Phys. Chem.* **1989,** *93* (10), 4219-4226.

135. Martin, R. B. Fe^{3+} and Al^{3+} Hydrolysis Equilibria. Cooperativity in Al^{3+} Hydrolysis Reactions. *J. Inorg. Biochem.* **1991,** *44* (2), 141-147.

136. Priebe, J. P.; Souza, B. S.; Micke, G. A.; Costa, A. C. O.; Fiedler, H. D.; Bunton, C. A.; Nome, F. Anion-Specific Binding to *n*-Hexadecyl Phosphorylcholine Micelles. *Langmuir* **2010,** *26* (2), 1008-1012.

137. Urabe, T.; Tanaka, M.; Kumakura, S.; Tsugoshi, T. Study on chemical speciation in aluminum chloride solution by ESI-Q-MS. *J. Mass Spectrom.* **2007,** *42* (5), 591-597.

138. Bottero, J. Y. C., J. M.;Fiessinger, F.;Poirier, J. E. . Studies of hydrolyzed aluminum chloride solutions. 1. Nature of aluminum species and composition of aqueous solutions. *J. Phys. Chem.* **1980,** *84* (22), 2933-2939.

139. Bostrom, M.; Craig, V. S. J.; Albion, R.; Williams, D. R. M.; Ninham, B. W. Hofmeister effects in pH measurements: Role of added salt and co-ions. *J. Phys. Chem. B* **2003,** *107* (13), 2875-2878.

140. Kunz, W.; Lo Nostro, P.; Ninham, B. W. Hofmeister phenomena. *Curr. Opin. Colloid Interface Sci.* **2004,** *9* (1-2), Vii-Vii.

141. Lund, M.; Jungwirth, P. Patchy proteins, anions and the Hofmeister series. *Journal of Physics-Condensed Matter* **2008,** *20* (49).

142. Vlachy, N.; Jagoda-Cwiklik, B.; Vacha, R.; Touraud, D.; Jungwirth, P.; Kunz, W. Hofmeister series and specific interactions of charged headgroups with aqueous ions. *Adv. Colloid Interface Sci.* **2009,** *146* (1-2), 42-47.

143. Schwierz, N.; Horinek, D.; Netz, R. R. Anionic and Cationic Hofmeister Effects on Hydrophobic and Hydrophilic Surfaces. *Langmuir* **2013,** *29* (8), 2602-2614.

144. Manet, S.; Karpichev, Y.; Dedovets, D.; Oda, R. Effect of Hofmeister and Alkylcarboxylate Anionic Counterions on the Krafft Temperature and Melting Temperature of Cationic Gemini Surfactants. *Langmuir* **2013,** *29* (11), 3518-3526.

145. Lee, K. Y. C.; Lipp, M. M.; Zasadzinski, J. A.; Waring, A. J. Effects of lung surfactant specific protein SP-B and model SP-B peptide on lipid monolayers at the air-water interface. *Colloids and Surfaces a-Physicochemical and Engineering Aspects* **1997,** *128* (1-3), 225-242.

146. Post, A.; Nahmen, A. V.; Schmitt, M.; Ruths, J.; Riegler, H.; Sieber, M.; Galla, H. J. Pulmonary Surfactant Protein-C Containing Lipid Films at the Air-Water-Interface as a Model for the Surface of Lung Alveoli. *Molecular Membrane Biology* **1995,** *12* (1), 93-99.

147. Flores, S. C.; Chen, X.; Kherb, J.; Cremer, P. S. Sum frequency vibrational spectroscopy study of the interaction of Hofmeister ions with hydrophilic surfaces. *Abstracts of Papers of the American Chemical Society* **2011,** *241*.

148. Flores, S. C.; Kherb, J.; Cremer, P. S. Direct and Reverse Hofmeister Effects on Interfacial Water Structure. *Journal of Physical Chemistry C* **2012,** *116* (27), 14408-14413.

149. Flores, S. C.; Kherb, J.; Konelick, N.; Chen, X.; Cremer, P. S. The Effects of Hofmeister Cations at Negatively Charged Hydrophilic Surfaces. *Journal of Physical Chemistry C* **2012,** *116* (9), 5730-5734.

150. Kherb, J.; Flores, S. C.; Cremer, P. S. Role of Carboxylate Side Chains in the Cation Hofmeister Series. *J. Phys. Chem. B* **2012,** *116* (25), 7389-7397.

151. Kunz, W.; Lo Nostro, P.; Ninham, B. W. The present state of affairs with Hofmeister effects. *Curr. Opin. Colloid Interface Sci.* **2004,** *9* (1-2), 1-18.

152. Bostrom, M.; Williams, D. R. M.; Ninham, B. W. Influence of Hofmeister effects on surface pH and binding of peptides to membranes. *Langmuir* **2002,** *18* (22), 8609-8615.

153. Sun, X. D.; Arntfield, S. D. Molecular forces involved in heat-induced pea protein gelation: Effects of various reagents on the rheological properties of salt-extracted pea protein gels. *Food Hydrocolloids* **2012,** *28* (2), 325-332.

154. Romsted, L. S.; Zhang, J. B. Determining antioxidant distributions in macroemulsions: A kinetic method. *Abstracts of Papers of the American Chemical Society* **2001,** *222*, U315-U315.

155. Romsted, L. S. Specific Ion-Pair/Hydration Model for the Sphere-To-Rod Transitions of Aqueous Cationic Micelles. The Evidence from Chemical Trapping. *Recent Trends in Surface and Colloid Science* **2012,** *12*, 171-198.

156. Williams, R. J.; Phillips, J. N.; Mysels, K. J. Trans. Faraday Soc. 1955, 51, 728.

157. Evans, H.C., Alkyl Sulphates. Part I. Critical Micelle Concentrations of the Sodium Salts. J.Chem. Soc., 1956: p. 579-586.

158. Zana, R. Critical micellization concentration of surfactants in aqueous solution and free energy of micellization. *Langmuir* **1996,** *12* (5), 1208-1211.

159. Reekmans, S.; Bernik, D.; Gehlen, M.; Vanstam, J.; Vanderauweraer, M.; Deschryver, F. C. Change in the Micellar Aggregation Number or in the Size Distribution - a Dynamic Fluorescence Quenching Study of Aqueous Cetyltrimethylammonium Chloride. *Langmuir* **1993,** *9* (9), 2289-2296.

160. Wattebled, L.; Laschewsky, A.; Moussa, A.; Habib-Jiwan, J. L. Aggregation numbers of cationic oligomeric surfactants: A time-resolved fluorescence quenching study. *Langmuir* **2006,** *22* (6), 2551-2557.

161. Tehrani-Bagha, A. R.; Karnbratt, J.; Lofroth, J. E.; Holmberg, K. Cationic ester-containing gemini surfactants: Determination of aggregation numbers by time-resolved fluorescence quenching. *J. Colloid Interface Sci.* **2012,** *376*, 126-132.

162. Gehlen, M. H. Fluorescence Quenching in Clusters of Reverse Micelles. *Chem. Phys. Lett.* **1993,** *212* (3-4), 362-366.

163. Boens, N.; Luo, H. W.; Vanderauweraer, M.; Reekmans, S.; Deschryver, F. C.; Malliaris, A. Simultaneous Analysis of Fluorescence Decay Curves for the One-Step Determination of the Mean Aggregation Number of Aqueous Micelles. *Chem. Phys. Lett.* **1988,** *146* (3-4), 337-342.

164. C.A.Bunton , Catal.Rev. Sci. Eng,(1979) 1,20.

165. Gulaboski, R.; Riedl, K.; Scholz, F. Standard Gibbs energies of transfer of halogenate and pseudohalogenate ions, halogen substituted acetates, and cycloalkyl carboxylate anions at the water backslash nitrobenzene interface. *PCCP* **2003,** *5* (6), 1284-1289.

166. Lissi, E.; Abuin, E.; Ribot, G.; Valenzuela, E.; Chaimovich, H.; Araujo, P.; Aleixo, R. M. V.; Cuccovia, I. M. Ion-Exchange between Normal-Alkyl Carboxylates and Bromide at the Surface of Cetyltrimethylammonium Micelles. *J. Colloid Interface Sci.* **1985,** *103* (1), 139-144.

167. Thalody, B.; Warr, G. G. The selective binding of carboxylate ions at cationic surfactant solution/air interfaces. *J. Colloid Interface Sci.* **1997,** *188* (2), 305-312.

168. Anacker, E. W.; Underwood, A. L. Organic Counterions and Micellar Parameters - N-Alkyl Carboxylates. *J. Phys. Chem.* **1981,** *85* (17), 2463-2466.

169. Texter, J. *Reactions and synthesis in surfactant systems* [Online]; Marcel Dekker,: New York, 2001; pp. xii, 909 p. http://marc.crcnetbase.com/isbn/9780203908662.

170. Private communication with them. 2014

171. Medda, L.; Barse, B.; Cugia, F.; Bostrom, M.; Parsons, D. F.; Ninham, B. W.; Monduzzi, M.; Salis, A. Hofmeister Challenges: Ion Binding and Charge of the BSA Protein as Explicit Examples. *Langmuir* **2012,** *28* (47), 16355-16363.

172. Peruzzi, N.; Ninham, B. W.; Lo Nostro, P.; Baglioni, P. Hofmeister Phenomena in Nonaqueous Media: The Solubility of Electrolytes in Ethylene Carbonate. *J. Phys. Chem. B* **2012,** *116* (49), 14398-14405.

173. Salis, A.; Cugia, F.; Parsons, D. F.; Ninham, B. W.; Monduzzi, M. Hofmeister series reversal for lysozyme by change in pH and salt concentration: insights from electrophoretic mobility measurements. *PCCP* **2012,** *14* (13), 4343-4346.

174. Gao, X.; Bravo-Diaz, C.; Romsted, L. S. Interpreting Ion-Specific Effects on the Reduction of an Arenediazonium Ion by t-Butylhydroquinone (TBHQ) Using the Pseudophase Kinetic Model in Emulsions Prepared with a Zwitterionic Sulfobetaine Surfactant. *Langmuir* **2013,** *29* (16), 4928-4933.

175. Moore, F. G.; Richmond, G. L. Integration or segregation: How do molecules behave at oil/water interfaces? *Acc. Chem. Res.* **2008,** *41* (6), 739-748.

176. Scheu, R.; Chen, Y. X.; Subinya, M.; Roke, S. Stern Layer Formation Induced by Hydrophobic Interactions: A Molecular Level Study. *JACS* **2013,** *135* (51), 19330-19335.

177. Zhang, Y. L.; Romsted, L. S.; Zhuang, L. Z.; de Jong, S. Simultaneous Determination of Interfacial Molarities of Amide Bonds, Carboxylate Groups, and Water by Chemical Trapping in Micelles of Amphiphiles Containing Peptide Bond Models. *Langmuir* **2013,** *29* (2), 534-544.

178. dos Santos, A. P.; Diehl, A.; Levin, Y. Surface Tensions, Surface Potentials, and the Hofmeister Series of Electrolyte Solutions. *Langmuir* **2010,** *26* (13), 10778-10783.

179. Wang, R.; Wang, Z. G. Continuous Self-Energy of Ions at the Dielectric Interface. *Phys. Rev. Lett.* **2014,** *112* (13).

180. Dasent, W.E., Inorganic energetics: an introduction, 2nd Ed. Cambridge, 1982, Chap. 5.

181. E. Pretsch, P. Buhlmann, C. Affolter. Structure Determination of Organic Compounds Tables of Spectral Data. *Springer-Verlag Berlin Heidelberg*, 2009.